GEOMETRY OPTIMIZATION OF A FRANCIS TURBINE FOR EFFICIENCY, CAVITATION AND EROSION USING COMPUTATIONAL FLUID DYNAMICS

ING. RUBEN DARIO APONTE NUÑEZ

UNIVERSIDAD DEL VALLE

MECHANICAL ENGINEERING SCHOOL

SANTIAGO DE CALI

2018

GEOMETRY OPTIMIZATION OF A FRANCIS TURBINE FOR EFFICIENCY, CAVITATION AND EROSION USING COMPUTATIONAL FLUID DYNAMICS

Research work for Master Engineering degree

Presented by

ING. RUBEN DARIO APONTE NUÑEZ

Advisor:

SARA AIDA RODRÍGUEZ PULECIO, Ph.D.

Co – Advisor:

JAIR ALEXANDER LADINO OSPINA, M.Sc.

UNIVERSIDAD DEL VALLE

MECHANICAL ENGINEERING SCHOOL

SANTIAGO DE CALI

2018

CONTENTS

RESUMEN

En los últimos años, la aplicación de modelos numéricos computacionales basados en dinámica computacional de fluidos (CFD por sus siglas en inglés) a problemas industriales ha venido incrementándose; hoy la CFD se utiliza para optimizar y desarrollar equipos y procesos en muchos tipos de industria incluida la industria energética. La principal ventaja de las soluciones con CFD está en la obtención de las condiciones de funcionamiento y el análisis de flujos internos y externos, que experimentalmente es muy difícil y costoso de lograr. En este documento se presentan los resultados de la investigación del proyecto de maestría en ingeniería con énfasis en Ingeniería Mecánica en donde se obtuvo la geometría que minimiza el desgaste erosivo por partícula dura y cavitación, para los diferentes regímenes de operación manteniendo la eficiencia, de la turbina Francis de 10MW de la central hidroeléctrica Amaime. Para lograrlo se implementó una metodología de laboratorio virtual simplificado (SLV por sus siglas en ingles), que consiste en el uso de Dinámica Computacional de Fluidos y de una técnica de optimización. Primero se realizó la simulación de la geometría actual de la turbina para caracterizar y verificar, con datos experimentales, que el modelo representa las condiciones actuales de operación; esto requirió generar geometrías CAD 3D por medio de planos e ingeniería inversa usando escaneo tridimensional de elementos complejos de la turbina como los alabes. Segundo, se optimizó la geometría de los alabes del rodete, alabes directrices, tapas y laberintos mediante el uso combinado de diseño de experimentos factoriales, redes neurales artificiales y técnicas de optimización por algoritmo genético. Finalmente, se realizó un análisis de resistencia mecánica por medio de simulaciones de elementos finitos para verificar resistencia estática, fatiga y resonancia para los diferentes componentes de la turbina ya optimizados. El desarrollo de este proyecto permitió la publicación de dos artículos en revistas de alto impacto Q1, un artículo adicional que se sometió para publicación y participación en tres simposios de ingeniería y dos congresos internacionales; los tres artículos reúnen los resultados completos de este trabajo y dan cumplimiento al 100% de los objetivos propuestos.

Palabras claves: Desgaste. Erosión. Cavitación. Dinámica Computacional de Fluidos. Optimización. Diseño de Experimentos. Algoritmos Genéticos. Redes Neurales Artificiales.

ABSTRACT

In recent years, the application of numerical computational models based on computational fluid dynamics (CFD) to industrial problems has been increasing; Today CFD is used to optimize and develop equipment and processes in many types of industry including the energy industry. The main advantage of the solutions with CFD is in the obtaining of the operating conditions and the analysis of internal and external flows, which experimentally is very difficult and expensive to achieve. This document presents the results of the research project of a master's degree in engineering with an emphasis in mechanical engineering where the geometry that minimizes the erosive wear by hard particle and cavitation for the different operating regimes maintaining the efficiency of the 10MW Francis turbine of the Amaime hydroelectric plant was obtained. To achieve this, a Simplified Virtual Laboratory (SVL) methodology was implemented, consisting of the use of Computational Fluid Dynamics and an optimization technique. First, the simulation of the current geometry of the turbine was carried out to characterize and verify, with experimental data, that the model represents the current operating conditions; this required to generate 3D CAD geometries by means of planes and reverse engineering using three-dimensional scanning of complex elements of the turbine such as blades. Second, it was required to optimize the geometry of the runner blades, guide vanes, covers and labyrinths by the combined use of factorial design of experiments, artificial neural networks (ANN) and optimization techniques by genetic algorithms. Finally, an analysis of mechanical resistance was carried out by means of finite element simulations to verify static resistance, fatigue and resonance for the different components of the turbine already optimized. The development of this project allowed the publication of two articles in high impact factor journals Q1, an additional article that was submitted for publication and participation in three engineering symposiums and two international congresses; the three articles gather the full results of this work and comply with 100% of the proposed objectives.

Keywords: Wear. Erosion. Cavitation. Computational Fluid Dynamics. Optimization. Design of Experiments. Genetic Algorithms. Artificial Neural Networks.

1. INTRODUCTION

1.1. Problem overview

The Amaime hydroelectric power plant is located in the department of Valle del Cauca and has two generation groups for a total of 20MW power generation. A summary of main characteristics of turbines is in Table 1 and a picture of one of the turbines is included in Figure 1. The plant works with two run-of-the-river horizontal Francis turbines since 2011, that is to say, this plant works only with the instant flow provided by the Amaime River and for that reason, desanders are required to avoid high concentrations of suspended solids in the water that can enter to the turbines generating irregular operation. Precisely, 5 months after the start of the operation, this condition generated that the turbines showed wear problems in some areas caused by erosion, manifested by the increase in temperature of the thrust bearing, loss of working capacity and low efficiency. The increase in temperature was due to the increase in pressure between the generator side cover and the runner caused by the wear on the seal labyrinths as shown in Figure 2, which presents increases in the clearance of 300% with respect to the initial clearance [1]. This wear is due to the high concentration of solid particles in the water, these particles traveling at high velocity impact the components causing wear. They also generate wear on the runner and guide vanes. Additionally, due to the gradient of pressures that are generated inside the turbine vortexes can appear and could lead to the appearance of the phenomenon of cavitation wear.

Table 1. Characteristics of turbines from Amaime hydraulic power plant of EPSA.

Inlet piping	Length: 4,865 m Net Head: 195.98 m
Nominal Speed	720 rpm
Capacity	10 MW (each unit)
Design Flow Rate	6 m3/s

Due to the premature wear losses that occurred in the hydroelectric power plant, repair costs for the first year of operation exceeded USD $400.000 and the efficiency of the machine decreased by 25% due to severe wear [1].

To solve this problem, some solutions have been presented by foreign companies with high costs and no local employment generation, which makes it relevant to look for local alternatives. On the other hand, the University of Valle has several research groups, which has allowed it to acquire the skills that could help the industry to solve this type of situations, through comprehensive analysis of the problem, the use of analytical and numerical approaches and optimizations using numerical modeling. The local metalworking industry also has the capacity to manufacture the components of the turbine but they haven’t the sufficient knowledge to define geometries that are competitive and efficient.

Figure 1. Francis turbine of the Amaime hydroelectric plant of EPSA.

Figure 2. Wear in the runner and gaps between cap and runner.

According to this, the goal of numerical modeling is to reduce the cost of design by avoiding the construction of several prototypes, which must be tested to determine if they fulfill the required parameters. When the designs don't use virtual models, if the prototype geometries don't accomplish these parameters, they must be redefined and re-constructed to verify if the design parameters are met, and this process is repeated until the appropriate geometry is obtained. With a simplified virtual model these additional prototype construction costs are significantly reduced because the preliminary physical models are no longer physically built.

Therefore, this project develops an optimization methodology that couple the computational fluid dynamics models with an optimization algorithms and existing geometries to solve problems such those present at the Amaime hydroelectric plant.

This research Project was part of the global Project called "Integral design of strategies to control the erosive wear in turbines", developed by EPSA E.S.P. - Celsia, Colciencias and The Universidad del Valle under the project number 110656237170. The results of this work have been included in three research articles, the first one titled *"Analysis of economic impact from erosive wear by hard particles in a run-of-the-river hydroelectric plant"* published on July 2016 on the journal *Energy [2]*, the second *"Computational study of the particle size effect on a jet erosion wear device"* published on January 2017 on the journal *Wear [3]*, and finally *"Minimizing erosive wear through a CFD multi-objective optimization methodology for different operating points of a Francis turbine"* which was submitted in the journal *Energy*. Additionally, the results allowed to the project team to publish the article "*Failure analysis of a run-of-the-river hydroelectric power plant*" [1] where the developed CFD analysis were used to explain tribological aspects of the failure.

1.2. Objectives

1.2.1. Main Objective

Find the geometry that minimizes the erosive wear of the 10MW Francis turbine from the Amaime hydroelectric power plant using computational fluid dynamics and multi-point and multi-objective optimization methodologies.

1.2.2. Specific Goals

- Define the initial state of the turbine by means of CFD simulations and experimental data measured on field.

- Implement multi-point and multi-objective minimization strategies to minimize erosion wear and cavitation while keeping the efficiency close to its design value.

- Get a new design of runner, guide vanes, covers and labyrinths by means of geometry optimization.

- Verify the behavior of mechanical components of the turbine with the new conditions of geometry and loads.

1.3. Thesis Scheme

This thesis is a collection of 3 academic articles, which have been published on indexed international journals and some have been presented at international conferences.

There is a coherence between the objectives of this thesis and the academic papers written and published, which can be observed and understood in Figure 3.

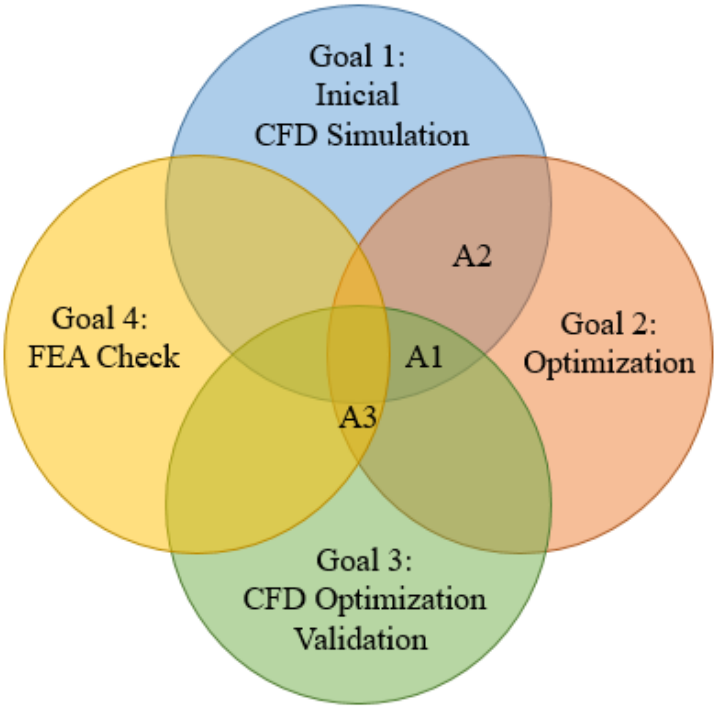

Figure 3. Correlation between the proposed objectives and the coverage of the developed academic articles.

Where, A1, A2 and A3 refers to academic articles developed as follows:

A1: Analysis of economic impact from erosive wear by hard particles in a run-of-the-river hydroelectric plant
L.A Terán, R.D. Aponte, J. Muñoz-Cubillos, C.V. Roa, J.J. Coronado, J.A. Ladino, F.J. Larrahondo, S.A. Rodríguez

In this paper the CFD model of Amaime Francis turbine was characterized. The validation of the model was performed comparing experimental efficiency tests of the turbine and the results obtained via CFD. It was also introduced and presented the erosion model implemented and the qualitative results of the areas where erosive wear occurs in the turbine components. Finally, a correlation between the power generated, the concentration of solids in the water and the associated wear rate was presented along with a wear costs analysis, which allowed to obtain an operating rule that minimizes the costs of operation generating profitability in power production.

This paper was submitted and approved by Elsevier International Magazine *Energy* in July 2016, in which the author's main contribution is the numerical verification of the computational model, the implementation of the erosion model and turbines operating

rule according to flow rate and available concentration. The paper has at today 8 citations.

A2: Computational study of the particle size effect on a jet erosion wear device
R.D. Aponte, L.A Terán, J.A. Ladino, F.J. Larrahondo, J.J. Coronado, S.A. Rodríguez

In this paper, a CFD model of a jet erosion tribometer was made to characterize wear by hard particle of the stainless steel ASTM A743 grade CA6NM, which is the material used in some of the internal components of Amaime Francis turbine (runner, guide vanes) and to find the relation between the size of the sand particles contained in the water, the impact angle and the obtained wear. For this, experimental results and data fitting techniques were used to obtain the constants of the erosion model.

This article was submitted and approved by Elsevier international magazine *Wear* in January 2017 and presented at the Wear of Materials Conference 2017 in April 2017, in which the author's main contribution is the numerical verification of the erosion model for the conditions on the tribometer and the adjustment of erosion model constants based on experimental data reported in the literature. The paper has at today 5 citations.

A3: Minimizing erosive wear through a CFD multi-objective optimization methodology for different operating points of a Francis turbine
R.D. Aponte, L.A Terán, J.A. Ladino, F.J. Larrahondo, J.J. Coronado, S.A. Rodríguez

This paper presents the optimization methodology to obtain the geometry that minimizes the erosive and cavitation wear of the internal components of the Amaime Francis turbine (runner, guide vanes, covers and labyrinths), maintaining the efficiency near the initial values. This study was made using factorial design of experiments, genetic algorithms and artificial neural networks. A structural verification of the optimized components was also performed, which includes static stress and displacement verification, a modal analysis and fatigue checks using stationary and transient models.

This article was submitted to Elsevier International Magazine *Energy* in July 2018 in which the author has as the main contribution the parameterization of the geometries, implement optimization methodology and the structural verification of the components of the turbine.

1.4. Background

Wear on a Francis turbine is due to different flow phenomena, such as pressure gradient in the boundary layer at runner inlet causing horseshoe vortex, the relative velocity of the fluid which causes that the immersed particles diverge from the fluid streamlines and impact the walls of the turbine, also, the erosion due to cavitation by operating the turbine in partial load has a large impact on the turbine performance. These wear problems can

be controlled by geometric aspects of the turbine like shape, length, number and thickness of the runner blades and guide vanes. Once a hydroelectric plant is built, a control in the operating conditions of variables like partial load, overload and changes in the geometrical aspects mentioned above can minimize overall wear. Although the effect of geometry modification on turbines wear have been studied using CFD and optimization techniques, in the literature there are no optimization studies that simultaneously minimize erosive wear keeping the actual turbine efficiency for a range set points of the turbine such as partial load and best efficiency point (BEP).

One of the first studies on wear analysis using CFD simulations was made by Neopane [4] in 2010, where he performed a two-phase CFD study of a Francis turbine where not only evaluates the different hydraulic characteristics of the turbine, but also takes into account the effect of erosive wear by hard particles immersed in the water. As a result of this research he concluded that operating the turbine at maximum load not only generates low efficiency but also high turbulence and inlet relative velocities greater than the output of the runner generating swirling flows. With respect to erosion wear, he found that implemented CFD model agrees with experimental tests and that the erosion rate increases when the turbine is operated outside the BEP. However, in this investigation no optimization method was performed, only the modeling of the current operating conditions was performed. Later, Lain *et al.* [5] in 2012, presented a methodology to simulate Francis turbines; i.e., the general consideration prior to simulation itself, source of errors in simulations, geometry and mesh generation, how to perform steady state and transient simulation and finally abnormal operations conditions in Francis turbines such as partial load, erosion wear, cavitation, head losses and fatigue.

On the other hand, more complex design optimization process for hydraulic turbine components has focused on efficiency and has had different approaches over the years. One of the first research carried out for the optimum design of turbomachinery was made by Pierret *et al.* [6] in 1999. In his work, the geometric parameters of the turbine runner blades were defined and used with a numerical model that contained an approximate prediction results of the Navier - Stokes equations to obtain the aerodynamic performance of the runner. These results were stored in a database trained by an ANN, which reduces the simulation time, manifesting itself in a decrease in the time of the design process. Later, Derakhshan *et al.* [7] in 2011 used a multi-objective optimization method based on ANN and genetic algorithms and software to solve the Navier - Stokes 3D equations. The objective of this research was to increase the overall efficiency of the turbine at BEP by changing the profile of the runner blades keeping the net head as a constrain. The maximum efficiency error calculated by this numerical method was 0.22% compared to the measured experimental data. As a result of the optimization process, a 1,8% efficiency increase was obtained with respect to the initial geometry. Enomoto *et al.* [8] in 2012, used multi-objective optimization base on evolutionary method and CFD to obtain a new geometry of the runner that improved the efficiency of a turbine for different points of operation, achieving an increase of efficiency for the entire operating range. Also, they analyzed the vibration instability that occurs in the turbine and concluded that this occurs when the turbine is overloaded, that is, when the

turbine operates above the BEP. In 2012, Flores *et al.* [9] made a complete design of a large Francis turbine, using local and global optimization of spiral case geometries, stay vanes, guide vanes, runner and draft tube for a different expected hydraulic characteristics (runner speed profiles, vortex between blades, torch in the draft tube, cavitation, hydraulic losses). These processes used blade design tools, automatic meshing and a numerical Navier - Stokes equations solver and genetic algorithms. In addition, it introduced the use of HPC (High Performance Computing) clusters as a mean to perform simulations in a shorter time and to observe transient behavior in each parts of the turbine. The local optimization was sequential and contributed to the overall optimization results. Recently, in a research of our investigation group GIFS, Terán *et al.* [10] in 2016, used computational fluid dynamics in the development of a new geometry that increase the efficiency of a 500 kW Francis turbine (designed and built more than a hundred years ago) to a value close to the values in recent turbines. Due to the complexity of the geometry, they implemented a methodology that combines a factorial design of experiments, ANN and optimization by genetic algorithm. Modifications were made in the runner blades and covers and managed to reduce vortex on the runner blade keeping to the minimum the phenomenon of main cavitation causing wear at the outlet of the runner. Finally, with the modifications obtained and after carrying out CFD simulations they got an increase in efficiency of 14.77% at best efficiency point and managed to increase production to 16.4% due to the modifications. Also, they performed mechanical strength check of the turbine components, using finite element analysis (FEA) and checking static resistance, fatigue and modal check for the optimized components of the turbine. One of the conclusions of these work was the need of selection of new materials for the turbine, like stainless steel ASTM A743 grade CA6NM.

With the objective of evaluating erosion wear in the runner of the turbine, Thapa *et al.* [11] in 2012 made an optimization study by means of "KHOJ" software and CFD simulations of the runner blade that allowed to reduce the vortex and relative speeds in this one, which allowed the phenomenon of erosion to diminish. The CFD results showed that the shape of the runner blade has a significant effect on the velocity distribution and therefore on erosion, reducing this effect by 33% with respect to the original model. Recently, Celebioglu *et al.* [12] in 2018, presented a CFD based rehabilitation methodology involving the state of the art redesign of a turbine for better performance (efficiency and cavitation) at design and off-design conditions. This was made by direct design optimization of several CFD aided designs and as result of this a 3% efficiency gain was achieved.

1.5. General Methodology

The overall methodology implemented in this project, which is developed in the 3 academic articles that cover this work, can be summarized in the flow chart of Figure 4. The first step is to perform a validation of the parameterized CAD model using CFD and

compare it with experimental data obtained in tests of efficiency performed on the turbine. The result of this process was reflected in Articles 1 and 3. The coefficients of the model of erosion wear for the material used in the CFD analysis were published in the paper 2.

Finally, in Article 3 was described how the initial population contained in a database is obtained using a design of experiments, then the database enters into the loop of the optimization process that uses an ANN and a Genetic Algorithm. Once the optimization process is finished, a mechanical check of the optimum geometry is performed, which if it is satisfactory will end the optimization process, otherwise, the objective function needs to be redefined and the optimization process begins again.

The academic articles described above are presented in the final sections.

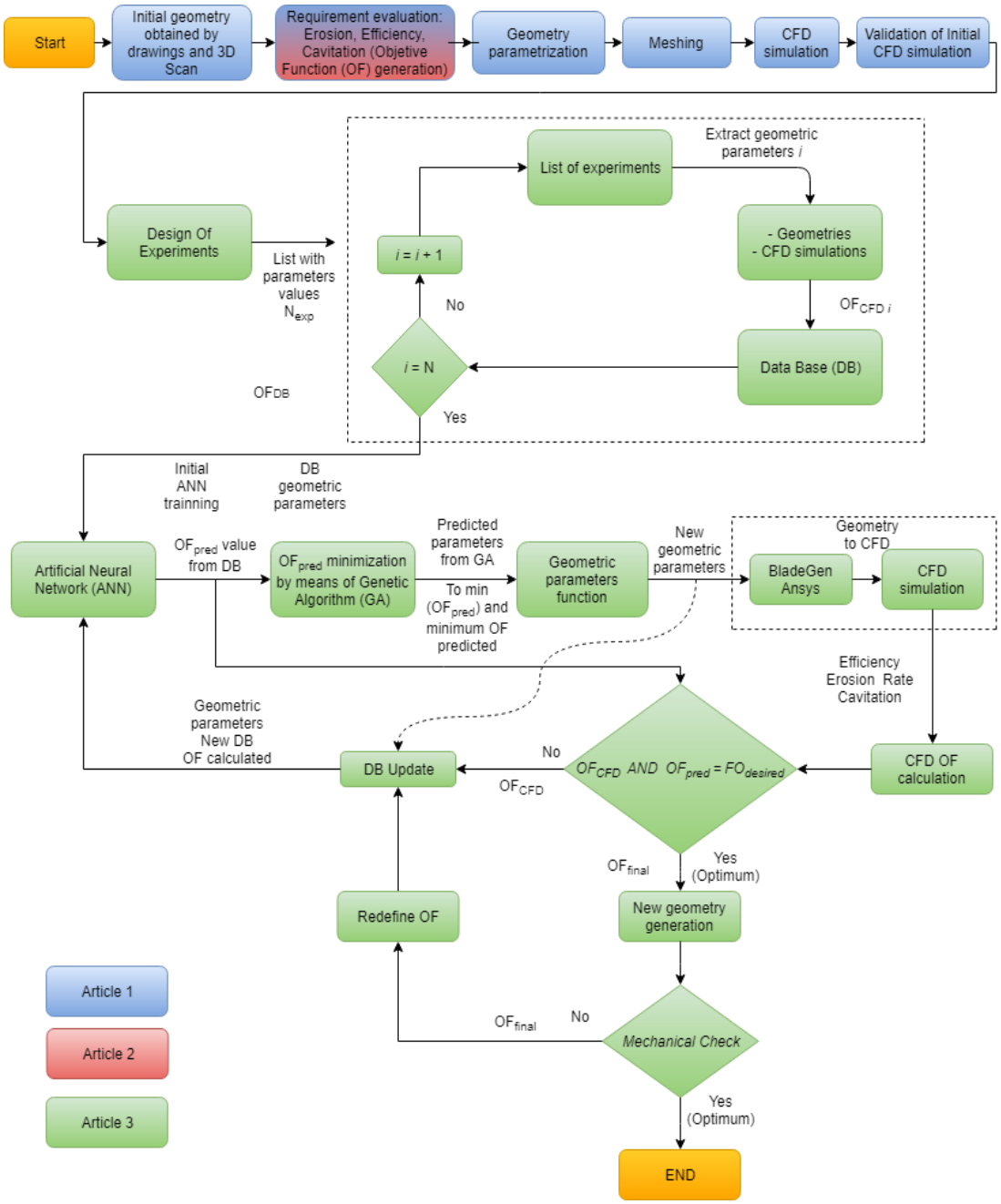

Figure 4. Flow chart for the implemented methodology.

2. CONCLUSIONS

- In this research it was possible to establish a methodology for the CFD simulation of Francis turbines considering the effects of erosion on its performance.
- The main hydraulic characteristics of a Francis turbine (efficiency, power, turbulence) were validated for different operating points and the effects on these when the turbine operates outside the BEP.
- Relevant parameters for the CFD simulation of erosive wear by hard particle in Francis turbines such as mesh size and quality, characteristics of the solid phase (factor, shape, size, hardness, concentration, velocity) were found.
- It was possible to validate the Tabakoff-Grant erosion model for the interaction between the sand immersed in the fluid and the steel of the turbines (CA6NM stainless steel).
- It was possible to find, through CFD simulations, the areas commonly affected within a Francis turbine because of erosive wear by hard particles.
- The use of experimental design, artificial neural networks and genetic algorithms allowed to configure a multi-point and multi-objective optimization process to obtain geometries of the internal components of a Francis turbine (guide vanes, runner and labyrinths) able to reduce the wear by hard particle without significantly affecting its hydraulic performance.
- A mechanical verification of the optimized components was carried out, presenting these safety factors that validate the reliability of the turbine.

REFERENCES

[1] L. Teran et al., "Failure analysis of a run-of-the-river hydroelectric power plant," Engineering Failure Analysis, vol. 68, pp. 87-100, 2016.

[2] L. Teran et al., "Analysis of economic impact from erosive wear by hard particles in a run-of-the-river hydroelectric plant," Energy, vol. 113, pp. 1188-1201, 2016.

[3] R. Aponte, L. Teran, J. Ladino, F. Larrahondo, J. Coronado, and S. Rodríguez, "Computational study of particle size effect on jet erosion wear device," Wear, 2017.

[4] H. P. Neopane, "Sediment erosion in hydro turbines," Faculty of Engineering Science and Technology, NTNU, 2010.

[5] S. Lain, M. Garcia, F. Avellan, B. Quintero, and S. Orrego, F. E. U. EAFIT, Ed. Simulación numérica de turbinas Francis. 2011.

[6] P. S. y. V. D. Braembussche, "Turbomachinery blading design using NavierStokes solver and artificial neural network," ASME Journal of Turbomachinery, vol. 121, pp. 326–332, 1999.

[7] S. Derakhshan and A. Mostafavi, "Optimization of GAMM Francis turbine runner," World Acad. Sci. Eng. Technol, vol. 59, pp. 717-723, 2011.

[8] Y. Enomoto, S. Kurosawa, and H. Kawajiri, "Design optimization of a high specific speed Francis turbine runner," in IOP Conference Series: Earth and Environmental Science, 2012, vol. 15, no. 3, p. 032010: IOP Publishing.

[9] E. Flores, L. Bornard, L. Tomas, J. Liu, and M. Couston, "Design of large Francis turbine using optimal methods," in IOP Conference Series: Earth and Environmental Science, 2012, vol. 15, no. 2, p. 022023: IOP Publishing.

[10] L. Teran, F. Larrahondo, and S. Rodríguez, "Performance improvement of a 500-kW Francis turbine based on CFD," Renewable Energy, vol. 96, pp. 977-992, 2016.
[11] B. S. Thapa, B. Thapa, M. Eltvik, K. Gjosater, and O. G. Dahlhaug, "Optimizing runner blade profile of Francis turbine to minimize sediment erosion," in IOP Conference Series: Earth and Environmental Science, 2012, vol. 15, no. 3, p. 032052: IOP Publishing.
[12] K. Celebioglu, S. Aradag, E. Ayli, and B. Altintas, "Rehabilitation of Francis Turbines of Power Plants with Computational Methods," Hittite Journal of Science & Engineering, vol. 5, no. 1, pp. 37-48, 2018.

3. ARTICLE 1: ANALYSIS OF ECONOMIC IMPACT FROM EROSIVE WEAR BY HARD PARTICLES IN A RUN-OF-THE-RIVER HYDROELECTRIC PLANT

Energy 113 (2016) 1188–1201

Contents lists available at ScienceDirect

Energy

journal homepage: www.elsevier.com/locate/energy

Analysis of economic impact from erosive wear by hard particles in a run-of-the-river hydroelectric plant

L.A. Teran [a], R.D. Aponte [a], J. Muñoz-Cubillos [a], C.V. Roa [a], J.J. Coronado [a], J.A. Ladino [a], F.J. Larrahondo [b], S.A. Rodríguez [a, *]

[a] Research Group of Fatigue and Surfaces, School of Mechanical Engineering, Universidad Del Valle, Cali, Colombia
[b] EPSA E.S.P. A CELSIA Company, Colombia

ARTICLE INFO

Article history:
Received 16 January 2016
Received in revised form
19 June 2016
Accepted 14 July 2016

Keywords:
Francis turbines
Computational fluid dynamics
Erosive wear
Wear costs

ABSTRACT

Small-scale hydroelectric plants, primarily run-of-the-river designs, are regularly subjected to hard particle wear and cavitation erosion due to the wide range of operating points. Depending on the severity of the operating conditions and erosion damage experienced by the machine throughout its service life, the operating companies of these facilities will be impacted. The impact will be technical, operational, logistical, and economic. A small-scale generation plant located in Amaime River in Colombia, is one such case, where severe wear occurs in the turbine components, with a consequent reduction of efficiency. In this study, the analysis of the erosion damage has been expanded and supplemented by computational fluid dynamics (CFD). From this approach, correlations between the wear rate and power output were obtained. Likewise and in conjunction with the computer estimates, a methodology to analyse the costs associated with wear based on historical data of operation was developed, creating a strategy of operation based on a stopping criterion that depends primarily on sediment concentration, turbinated flow, and wear level. The methodology optimizes the use of generators, which takes into consideration the revenue generation and the costs associated with operation and maintenance of pieces under conditions of intrinsic erosion wear in the facility.

1. Introduction

Controlling wear is a major challenge when designing and operating a hydraulic turbine under severe sediment conditions and operating in potential cavitation regimes, which is the case of many small run-of-the-river plant generators in the South American Andes [1,4] and the Himalayas [2,3]. A particular case is the Amaime hydroelectric plant in southwestern Colombia [4].

The water used by this plant has been repeatedly affected by high concentrations of sediment as a result of deforestation, mining, and flash flooding. The intake of the plant has a desander, that is unable to remove particles smaller than 150 μm, which, as reported in Ref. [2], may be the primary cause of damage; this has been verified in a parallel work reported by the authors in Ref.[4], where severe wear corresponding to hard particle erosion was found, causing premature efficiency loss and machine repairs that incur significant economic losses to the operating company.

With the aim to evaluate the hard particle erosion in hydraulic components of reaction turbines, several authors have performed simulations of computational fluid dynamics (CFD) to characterize the wear phenomenon. Eltvik et al. [5] performed a simplified CFD analysis of a Francis turbine in a hydraulic generation plant in Peru, where it was found that wear significantly depends on the operating conditions of the turbine, fluid velocity, and the size and shape of the particles. Thapa et al. [6] used CFD analysis to evaluate optimum blade profiles of a Francis runner derived from optimization results from a *custom-made* code at both efficiency and performance against erosion. They showed that optimized geometries of the runner reduced the rate of wear at the point of maximum efficiency by 39.5% but at the cost of a reduction in efficiency from 95% to 90%.

Moreover, on the topic of wear influence on economics, the first study on the economic impact of tribology estimated that economic losses in England (1966) were 515 million British pounds, which corresponds to 0.5% of the gross domestic product (GDP) [7,8]. Later, these data were corrected [7], where it was concluded that

* Corresponding author.
E-mail address: sara.rodriguez@correounivalle.edu.co (S.A. Rodríguez).

http://dx.doi.org/10.1016/j.energy.2016.07.072
0360-5442/

the losses actually correspond to 1.5% of the GDP in England in 1966. Subsequently, a similar exercise was conducted in the USA, which concluded that wear losses reached 180 billion dollars in 1984 (6% of the GDP) [9]. The cost reduction that could be achieved by implementing the existing industry knowledge in tribology and materials science has been estimated at 20% [10]. Although, other authors have also conducted similar studies, and a detailed summary can be found in Ref. [11], more recent works in this area are not available in literature.

In the context of hydraulic turbines, Pradhan [12] developed a trading strategy that reduces the operating and maintenance costs of a turbine; this strategy uses historical operating data and keeps track of the efficiency and concentration of the river. Additionally, Castro [13] developed criteria for extended range operations, which are outside the operating limits recommended by the turbine manufacturer, such that the maximum economic benefit is achieved by taking into account variables such as operating income, future price of water reservoirs, machine start-up, wear costs as well as the consequent loss of efficiency by estimating the cost at these points of operation using the method of nonlinear programming optimization.

Some works have shown that the most important costs in the power generation are caused by wear of mechanical equipment and the corresponding increase in maintenance cost of the turbines [14–16]. On the other hand, there is not a common practice of how to calculate these costs. Most of the companies have some estimate of the costs, but these were seldom based on large investigations [15]. However, electrical companies and turbine operators are in agreement that these losses should be quantified.

This work combines both computational strategies and operating data analysis to determine the wear behaviour of a Francis turbine with a focus on developing operation strategies that can produce the maximum benefit from the generating plant subjected to technical and economic restrictions imposed on operating the plant due to erosive wear, which considers the wear and associated costs, such as maintenance costs, stop costs, and costs associated with a loss in equipment efficiency. This approach based on an economic and technical approach has not been reported in the literature yet and could be replicated in other facilities for the benefit and profit of the operator company.

2. Materials and methods

2.1. Obtaining the experimental process variables

Experimental data regarding the turbine flow, power generated, water level in the forebay tank and outlet flume, penstock pressure, and draft tube pressure were acquired by a data acquisition system of the plant at a rate of one sample per second. Torque was also measured at the turbine shaft by mounting strain gauges configured in a full *Wheatstone* bridge; these data were acquired wirelessly using TorqueTrak 10 K telemetry equipment from the manufacturer *Binsfeld* that captures signals of deformation and converts them into voltages between 0 and 10 V. In addition, the historical sediment concentration was measured every two hours using the Imhoff cone method.

2.2. Numerical simulation of the turbine

CFD simulations were performed in a steady-state, incompressible and turbulent flow, with Multiple Reference Frame approach for rotor-stator interaction (Frozen Rotor Model). Simulations were developed with the aim to: *i*) determine the characteristic performance curve of the turbine, *ii*) identify areas prone to cavitation and hard particle erosion wear at typical operating conditions, *iii*) numerically estimate the erosive wear rate on the turbine, and *iv)* visualize flow behaviour in the turbine and extract valuable information that cannot be measured directly via experimentation. In this process, simplified geometric simulations that allow to analyse the wear efficiently and match them with simulations of the complete geometry were developed. The simulation platform was CFX (ANSYS Inc), which is a widely used and validated platform for turbomachinery analysis [6,17,18]. The Francis turbine simulations were based on the methodology used in Ref. [19].

2.2.1. Pre-processing

The simulation geometry was rebuilt from the manufacturing drawings, on-site measurements, and 3D scanning, particularly for critical hydrodynamic parts, such as the runner blades. Complete model simulations of the turbine as well as a simplified version were developed.

The discretization and meshing resulted in a highly structured nonconformal mesh, which was developed by the blocks methodology of ICEM-CFD (ANSYS Inc). Domain couplings were performed using the algorithm GGI (*general grid interface*). The resulting mesh density was defined in a prior grid independence study according to the methodology used in Ref. [17]. This analysis was based on independent integral variables, such as power, mechanical efficiency, hydraulic head and wear rate. The mesh used for the analysis of this paper reports deviations of approximately 2% against finner mesh for both simulations of the complete turbine and its simplified equivalent. Fig. 1 shows a plot of the mesh convergence that was achieved in a mesh with 4.5 million nodes for the simplified model.

According to [17] and particularly for studying wear rate, there are differences between grid independence in a model that analyses only flow variables and the case of erosion, where the dispersed phase (sediments) interacts with the solid surface of the turbines (fluid-structure interaction); as a result of such interaction, the erosion rate is estimated by prediction models, such as either the Finnie model or the Tabakoff and Grant model [20]. Therefore, according to the methodology described in Ref. [17] and according to the recommendations given in Ref. [20], a special validation of the mesh was performed to obtain reliable wear values, which depend on the number of embedded particles in the fluid, that in this case was defined in 400.000 particles after a convergence analysis, and the mesh refinement in the areas of interest. The final mesh has an average value y+ of 102.3 for the areas of interest, such as the runner and guide vanes, and remained essentially constant

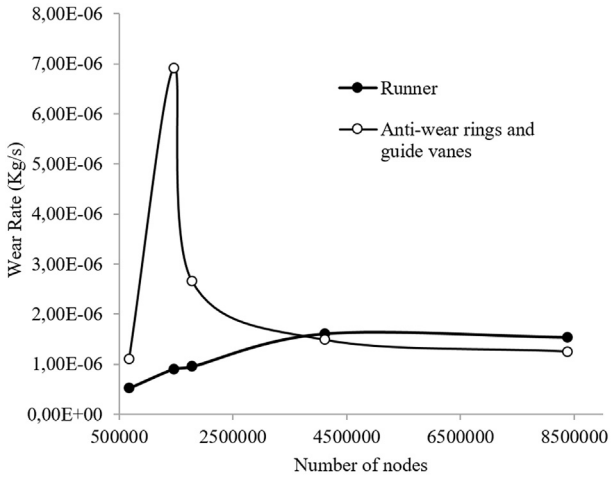

Fig. 1. Mesh convergence simplified model.

Table 1
Definition of simulation and the models used.

	Complete Model	Simplified Model
Simulation Type	Stationary	
Stator rotor coupling	*Frozen rotor* [20]	
Number of elements	3.799.850	6.883.573
Number of particles	400.000	
Turbulence model	*Shear Stress Transport* [21]	
Wall functions	*Low-Re Wall formulation (automatic near wall treatment)*	
Average y+	102.3	
Convergence criterion	RMS 10^{-4}	
Erosion model	Tabakoff and Grant [20]	

for the entire set of simulations developed for this work as describe in Table 1. Fig. 2 shows a sample of the type of mesh used in the complete turbine and simplified turbine simulations. In the simplified model, a section of the turbine was analysed, this model included the guide vanes, runner, and the labyrinth seals, which are the turbine areas where the erosion phenomena are severe and need to be analysed. Simplified domain size corresponds to the best ratio between the number of guide vanes and the number of runner blades.

The boundary conditions were obtained from experimental tests on the turbine without wear (1176 h of operation after full reconstruction of the geometry). The applied conditions are presented in Table 2. In the case of the simplified model, the boundary conditions correspond to the result of the velocity profile at the inlet of the guide vanes and the pressure distribution at the outlet of the runner obtained from the complete turbine simulation. ANSYS CFX-Solver [3,5,18–20], which is based on finite volume discretization, was used to obtain the solution of the flow.

2.2.2. Erosive wear simulation

The erosion simulation was developed in a simplified domain due to computing resource issues. Validation of the results were conducted by comparing the erosion results in the simplified domain against the full simulation of the turbine for a characteristic flow configuration at the point of maximum efficiency and at partial load of 3 MW, maintaining invariant density mesh conditions.

The model used to simulate erosion is based on a phase dispersed of solid particles (sediment) that is immersed in a continuous phase (water); its evolution is Lagrangian. The dispersed phase is one way and fully coupled to the fluid according to [22]. The erosion model used in this work was developed by Tabakoff and Grant [20,23], where the dimensionless erosion rate E is defined by:

$$E = k_1 f(\gamma) V_p^2 \cos^2\gamma \left[1 - R_T^2\right] + f(V_{PN}) \tag{1}$$

$$f(\gamma) = [1 + k_2 k_{12} \sin(\gamma \frac{\pi/2}{\gamma_0})]^2 \tag{2}$$

$$R_T = 1 - k_4 V_p \sin\gamma \tag{3}$$

$$f(V_{PN}) = k_3 (V_p \sin\gamma)^4 \tag{4}$$

$$k_2 \begin{cases} 1.0 \; if \; \gamma \le 2\gamma_0 \\ 0.0 \; if \; \gamma > 2\gamma_0 \end{cases} \tag{5}$$

where E is the dimensionless mass obtained from the relationship between the mass loss due to erosion and particle mass, V_P is the impact velocity of the particle, γ is the angle of impact, γ_0 is the angle of maximum erosion, and k_1, k_{12}, k_3, *and* k_4, are model constants dependent on the particle properties (hardness, shape) and the surface material. The values of the constants define the reference speeds V_1, V_2, and V_3:

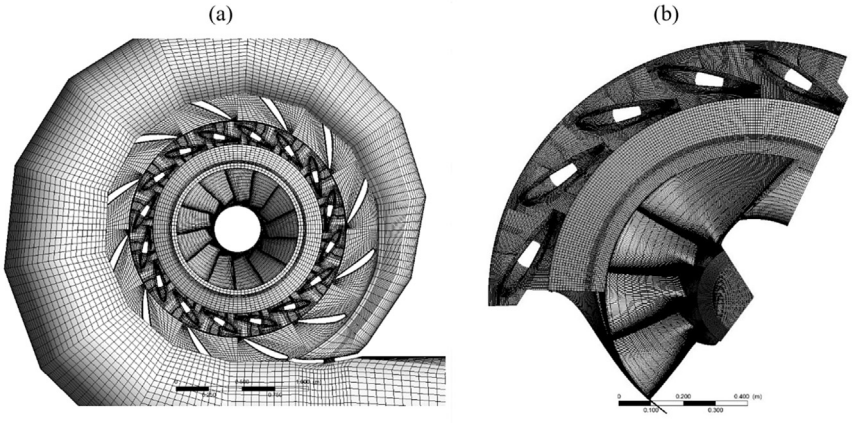

Fig. 2. (a) Mesh of the model of the complete turbine and (b) mesh of the simplified model.

Table 2
Turbine boundary conditions for each point of the simulated operation.

Power (MW) spinning at 720 rpm	Input mass flow (kg/s)	Output pressure (Pa) type opening	Input particle mass flow (kg/s), simplified model, concentration 10 ml/l
3	2043.85	46,311	13.76
5	3033.10	47,274	20.43
7	4037.85	48,252	27.17
9	5084.70	49,035	34.24
10	5623.08	49,587	37.18
10,4	5842.42	49,669	39.29

Table 3
Adjustment constants for the Tabakoff and Grant model for sand-13Cr-4Ni stainless steel interactions.

Constant	Value
k12	3.52
V1	2375.14
V2	153.17
V3	19.16
γ_0	45°

$$V_1 = \frac{1}{\sqrt{k_1}} \quad V_2 = \frac{1}{\sqrt[4]{k_3}} \quad V_3 = \frac{1}{k_4} \tag{6}$$

The erosion rate of an arbitrary surface is calculated by:

$$E_r = E * \dot{N} * m_P \tag{7}$$

where E_r is the rate of erosion due to a particle, E is the dimensionless mass loss, m_p is the average particle mass, and $\dot{N}$ is the rate of the number of particles, which refers to how the discretization of the particles immersed in the fluid is performed, therefore $\dot{N}$ is a representative value of the concentration of particles or deposits in the medium [22].

Thus, the overall rate of erosion of the surface is given by the contribution to erosion generated by all particles. Likewise, locally, the erosion rate density that represents the wear distribution per unit area can be reconstructed [20].

Finally, the pattern of erosion of Grant and Tabakoff given by CFX is modified for the characteristic sediment of the Amaime installation and its interaction with the steel of the turbine. The interaction type is sand [4], and 13Cr-4Ni steel which is considered equivalent to ASTM A743 CA6NM steel. Using the experimental data reported in Ref. [24], the model of Eqs. (1)–(5) was adjusted by least squares. The constants are shown in Table 3. The resulting adjustment curve is shown in Fig. 3 and compared with experimental data from Romo [24] and Shivamurthy [25] for sand-CA6NM interaction. Additionally, we present the curve that is obtained using the constants for AISI 304 steel reported by Ref. [20], which has been used in the analysis of erosive wear due to its wide use in industrial applications [26]. As shown, the settings used in this work are practically bounded between the data given by these authors for this particular interaction, whereas for AISI 304 steel, the data fall outside the range of wear rates corresponding to CA6NM steel. The use of constants corresponding to AISI 304 not only leads to unreliable estimates of the wear rate but also increases the uncertainty regarding the improvement in erosion geometry changes based on simulations with these constants, where it can be seen that the critical angles and relative wear rate also differs between angles.

3. Results

3.1. Operation histograms by generated power

According to operational data recorded in the Amaime plant for the two generation groups in the period from May 2013 to October 2014 and taking into account the outages for preventive and corrective maintenance, the operating frequency for the generated power is shown in Fig. 4, where the power of the maximum frequency was the maximum power generation, i.e., 10 MW (design point); this corresponds to the rainy season, in which the river provides more water than the maximum turbinable flow.

The greatest difference in the frequency distribution for the two groups is that group 1 was stopped for repairs from April 2013 to August 2014; however, the two groups operated simultaneously for three-month in the review period.

This chart identifies two higher operating frequency points (3 MW and 10 MW), which will be important later for continuing multi-parameter optimization, i.e., it is required to improve the turbine operating conditions at these two points to effectively reduce wear rates.

3.2. Numerical simulation of the turbine

The simulation results and their comparison with the experimental data are presented in Table 4; the efficiency curves and numerical and experimental powers reconstructed for the turbine without wear condition are shown in Fig. 5.

As shown, the simulations are consistent with the experimental results with low error primarily near to the turbine design point (maximum efficiency). The greatest differences are for low flow, which are caused by transient phenomena, such as vortex rope in the discharge tube [19] due to dynamic flow behaviour, and also due to the mesh resolution to predict flow patterns in areas with high pressure gradients, which occurs in the case of the flow

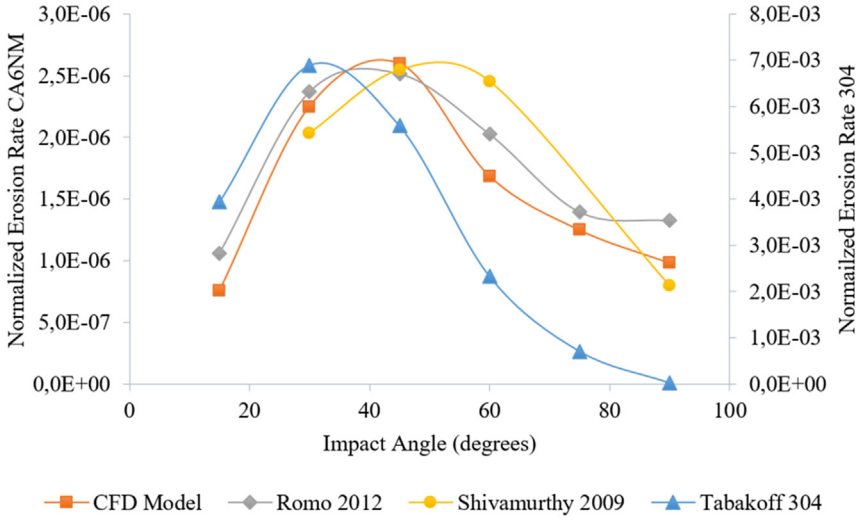

Fig. 3. Normalized erosion rate vs. impact angle.

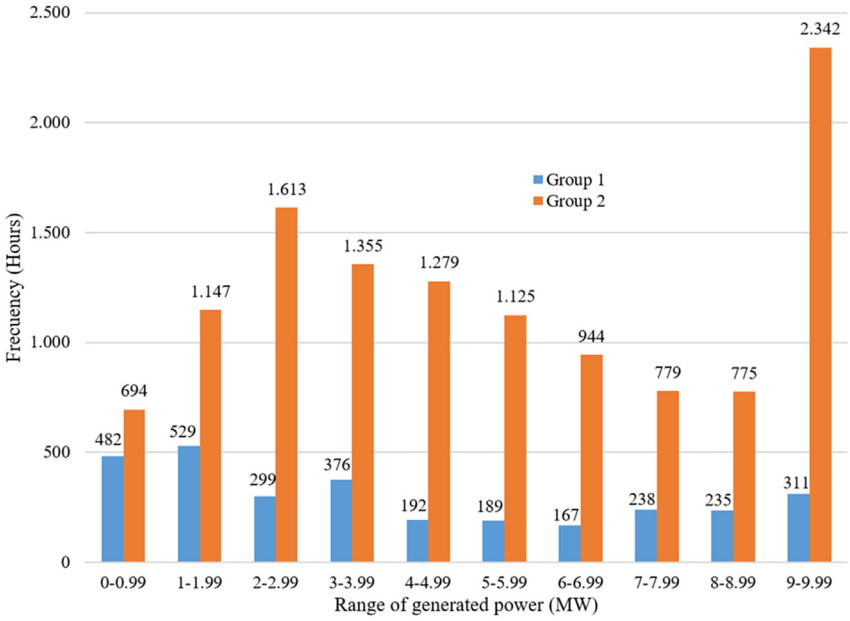

Fig. 4. Distribution of the operating frequency vs. the generated power from May 2013 to October 2014.

Table 4
Experimental and numerical results for the turbine simulations for unworn conditions.

Flow (m^3/s)	Actual turbine mechanical power (MW)	Simulated turbine mechanical power (MW)	Error (%)	Actual net height (m)	Simulated net height (m)	Error (%)
5.86	10.44	10.33	1.06%	198.30	200.37	1.04%
5.64	10.05	10.06	0.10%	198.73	201.37	1.33%
5.1	9.06	9.09	0.39%	200.06	202.78	1.36%
4.05	7.06	6.97	1.36%	202.16	202.11	0.02%
3.04	5.08	5.05	0.57%	203.70	204.72	0.50%
2.05	3.15	3.02	4.23%	204.94	203.84	0.54%

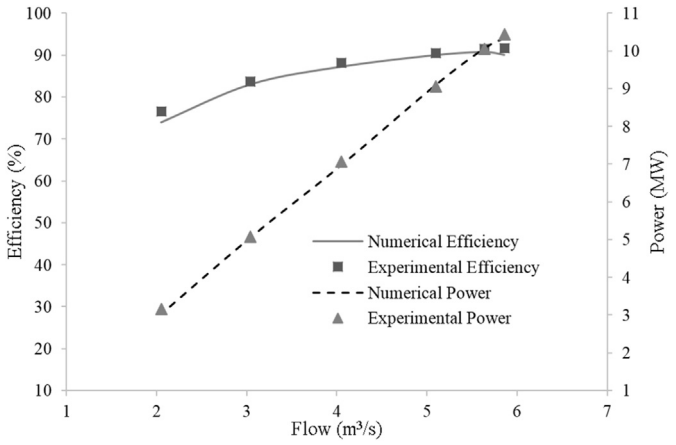

Fig. 5. Comparison of experimental and numerical power and efficiency.

around the blades when the turbine is operating outside the designed range. Indeed, according to the experimental data, the point of maximum efficiency is 10.4 MW at 91.6% efficiency; this value is the maximum rated turbine operation when the flow is available; however, the turbine can reach up to 11 MW.

Fig. 6 shows representative flow patterns in the turbine, particularly the streamlines around the runner blades in the case of operation at the (a) optimal point and for the (b) partial load. In the case of partial load, large recirculation zones with high curvature in the streamlines are observed. This behaviour is due to the flow separation (boundary layer) in the vicinity of the surface of the runner blades, which is primarily caused by large adverse pressure gradients experienced by local flows as a result of a high angle of attack of the flow current on the blades [27]. This hydrodynamic effect explains the reduced efficiency, which is also evidenced in the experimental data. It should also be noted, at the point of maximum efficiency, there is recirculation, but it is less drastic, which means that efficiency, at least at the point of maximum efficiency, can likely be improved.

Moreover, Fig. 7 shows, starting from an iso-surface in a 100-kPa pressure field, the flow behaviour at the exit of the runner (inlet in draft tube) for both the (a) optimal operating point and the (b) partial-load. As seen in the case of the partial load, the existence of the vortex rope is clear in the operating regime, whereas at the point of maximum efficiency, there is no appreciable presence of this phenomenon.

Regarding the wear results, Fig. 8 shows the density erosion rate on the surfaces of the anti-wear rings analysed in a previous study by the authors [28], which indicates the distribution and wear trend on such surfaces. High wear regions predicted by CFD match areas where the greatest wear occurred in the actual areas. The position of the guide vane marked by wear on the ring corresponds to a power output of 10 MW, which is the optimum operating point and the highest frequency of operation according to Fig. 4. As is also shown in Fig. 9, we can observe the range of the angles of attack of the particles on the surface in these areas, where impact angles are considered grazing angles, including values of 38°; these angles

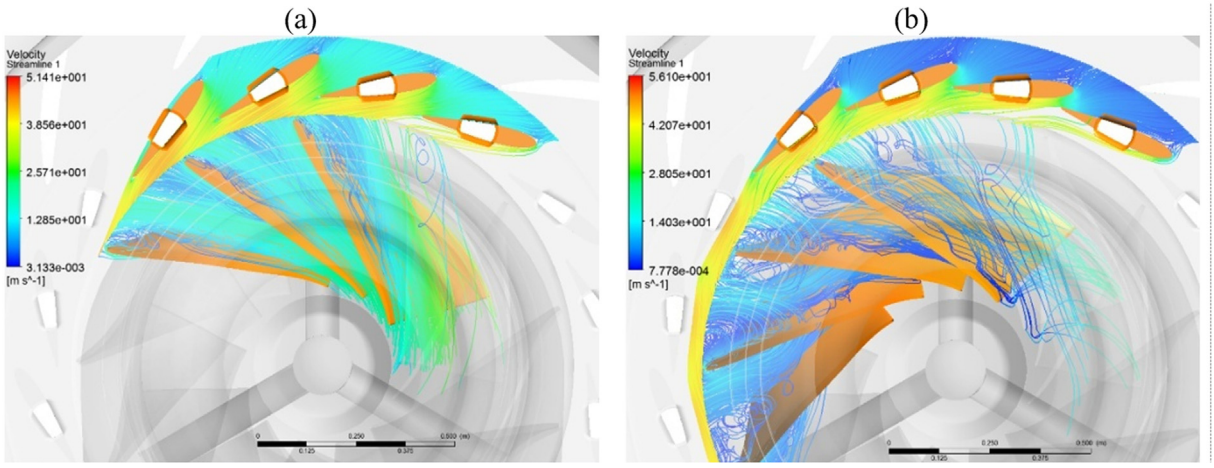

Fig. 6. Streamlines around the guide vanes and the runner: (a) optimal operating points (10.44 MW of power, efficiency of 91.6%) and (b) partial-load operation (5.08 MW of power, efficiency of 83.5%).

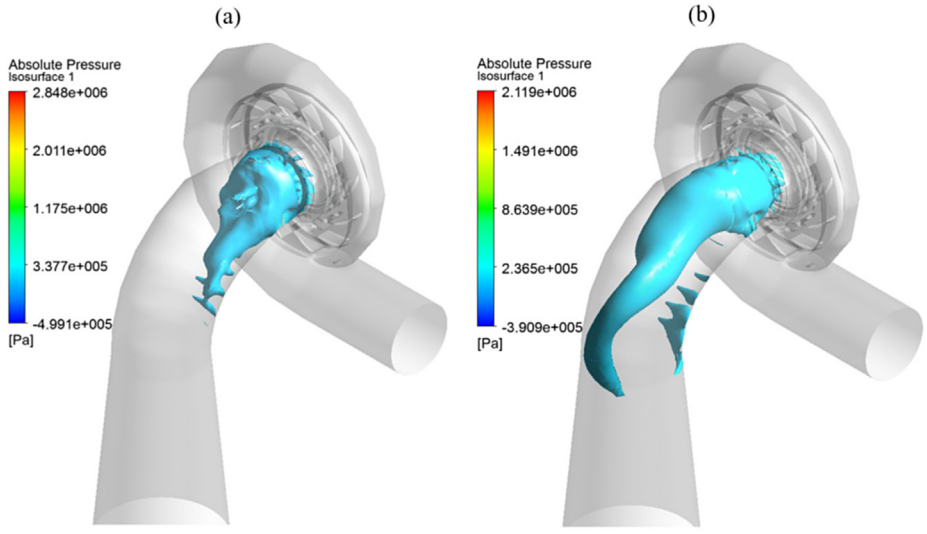

Fig. 7. Pressure in the draft tube (a) optimal operating point (b) partial load.

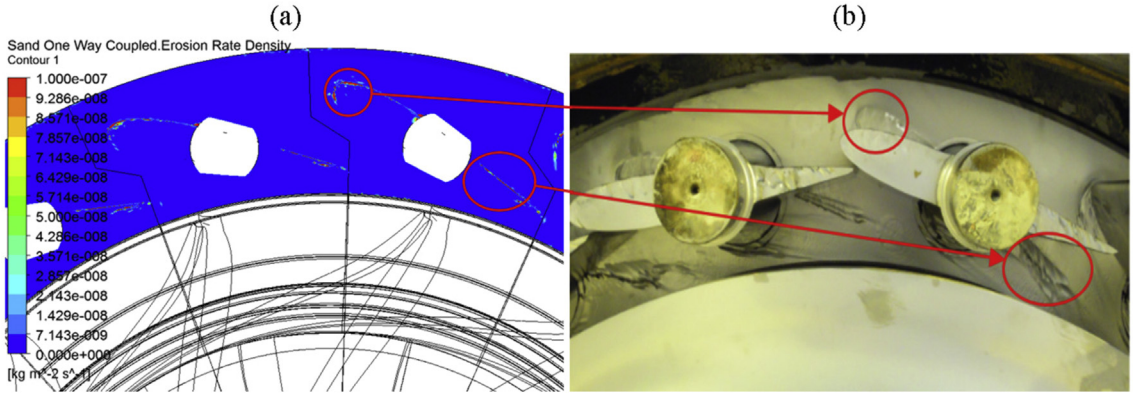

Fig. 8. Qualitative comparison of (a) actual erosive wear and (b) simulated wear in the turbine of the Amaime plant taken from Ref. [28].

cause high wear on these surfaces [29] according with the model presented in Fig. 3.

Furthermore, using LES (large eddy simulation) in the vicinity of the guide vane, a recirculation zone was identified at approximately 75% of the length of the vane, as shown in Fig. 10. The simulation was developed locally using velocity field results from a simulation of the full turbine at the point of maximum efficiency as the boundary condition.

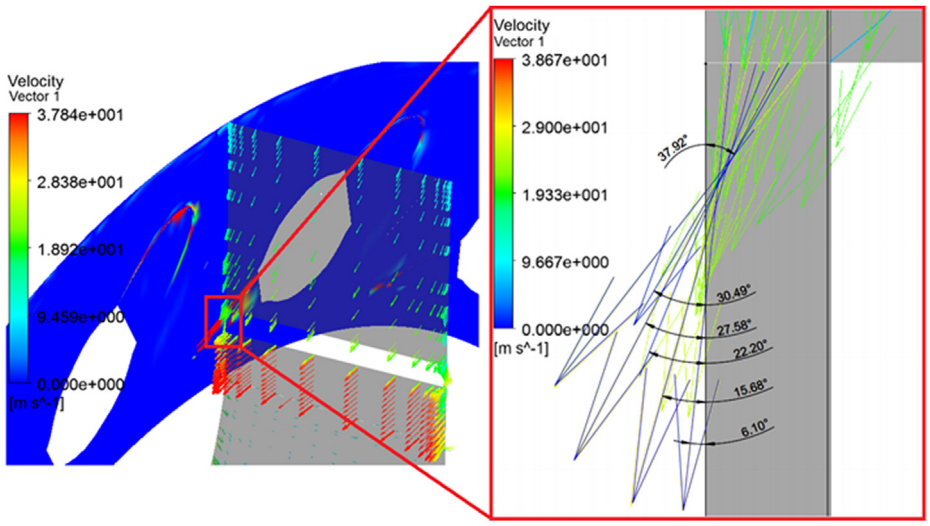

Fig. 9. Angles of attack of the particles on the wear rings calculated by CFD at 10 MW of power.

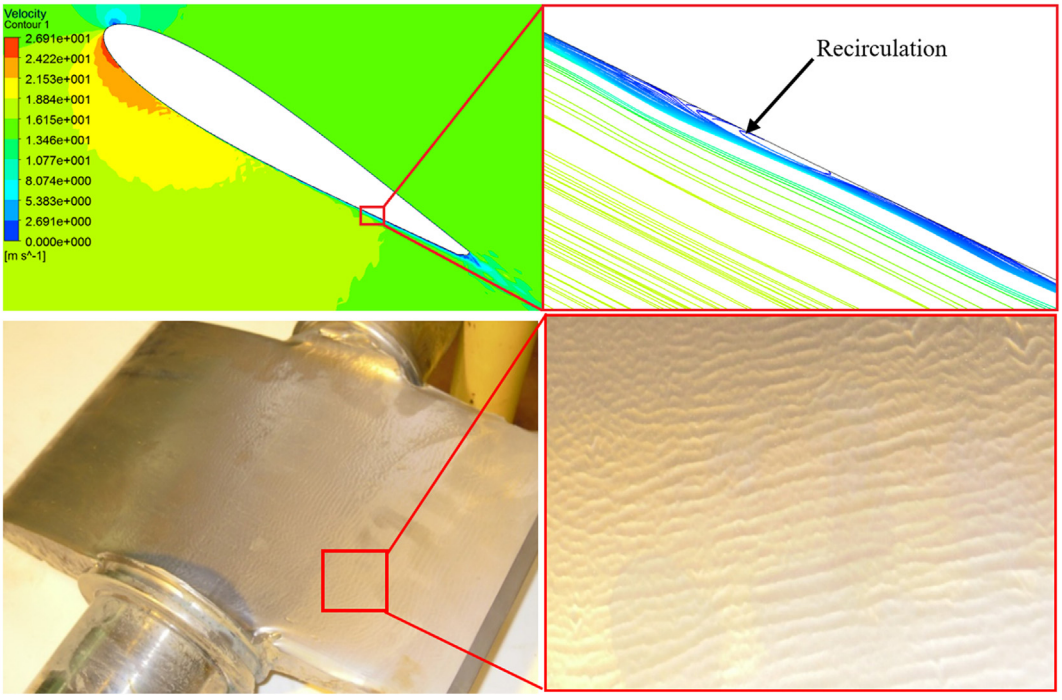

Fig. 10. Small recirculation due to separation of the boundary layer corresponding to the simplified simulation compared with orange peel-type wear in an actual blade.

Such recirculation region, which is actually a separation/reattachment of the boundary layer around the blade, is responsible for the orange peel-type wear pattern [1] and has been identified and confirmed experimentally in worn surfaces in parallel work [4]. Importantly, this pattern could not be observed in the simulation of the complete turbine due to the high cost of the calculation involving an LES simulation and the size of the necessary discretization.

Additionally, as a result of the initial simulation, we were able to identify the wear on the runner caused by recirculation when operating at partial load, which is shown in Fig. 11, where the velocity vectors and the joining area between the band and the blade that presented wear were identified; according to Neopane [1], this is an area susceptible to wear when operating at partial load. It is noted that in this area, the flow changes direction, which gives results in a wide range of angles of attack of the particles that are critical because they accelerate the erosive wear.

Finally, an analysis of the cavitation phenomenon indicates that in both partial load and full load there are zones prone to the occurrence of cavitation (identified in Fig. 12 as iso-surfaces calculated at saturation pressure at 25 °C), which appear only on the trailing edge of the runner blade, whereby generated cavity bubbles are moved downstream and are unable to collapse near surfaces; thus, cavitation erosion does not occur. This behaviour is consistent with the observations of the runner surfaces because no traces of cavitation erosion were found [4].

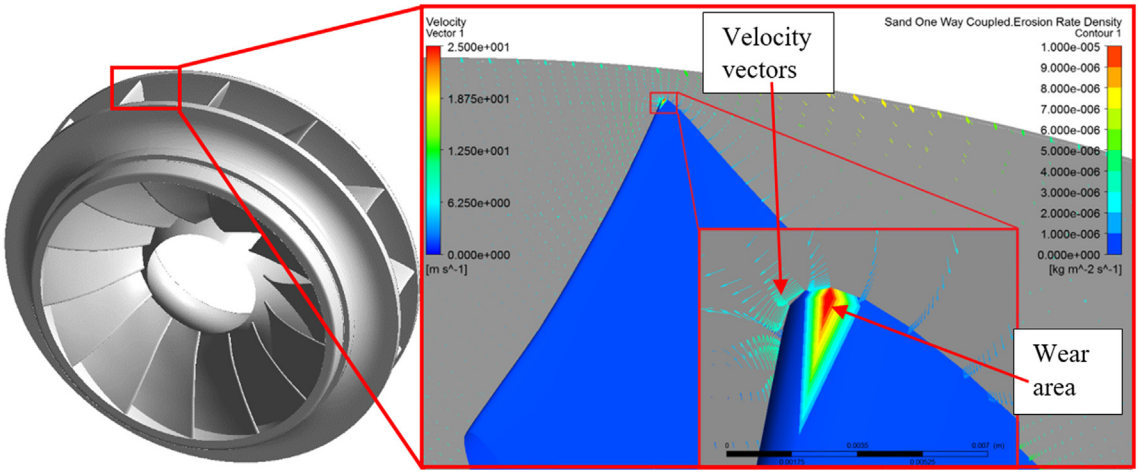

Fig. 11. Velocity vectors and erosive wear areas calculated by CFD at 5 MW of power.

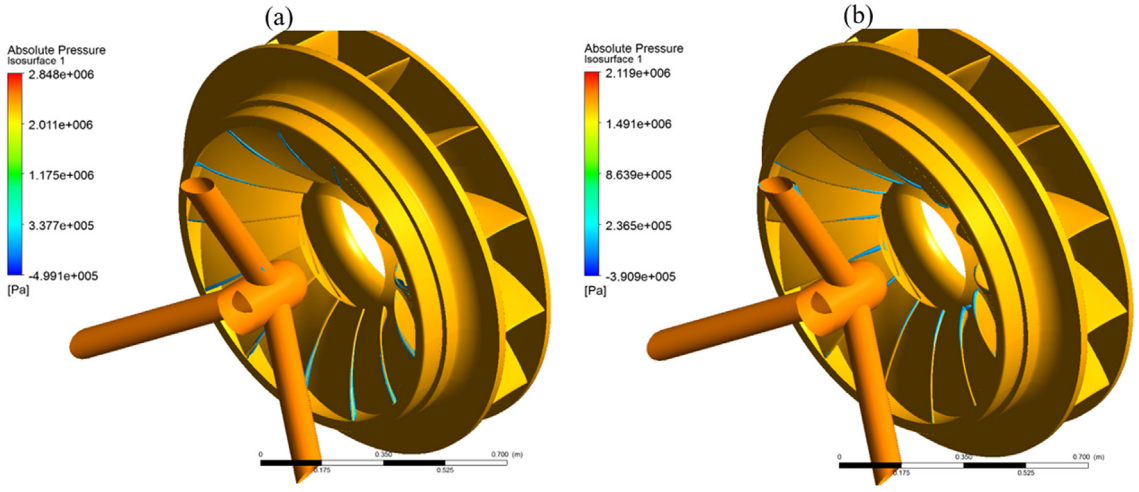

Fig. 12. Verification of cavitation in the turbine, (a) optimum and (b) partial load of 3 MW.

3.3. Numerical determination of the wear rate

Through the CFD simulation, characteristic wear curves for the runner and the anti-wear plates - guide vanes assembly were determined, which are presented in Fig. 13. The numerical wear rate was characterized in terms of the power generation and hard particle concentration in the water.

The behaviour obtained for the wear rate as a function of the generated power can be explained by observing the flow variables around the runner. As the generated power decreases, there is an increase in the wear rate at any concentration with a maximum value of 3 MW in the case of a concentration of 10 ml/l. The decrease of wear rate at 2 MW of power for this same concentration is due to the reduced flow velocity caused by the closure percentage of the guide vanes.

Moreover, when the generated power approaches the optimum turbine design point, the wear rate decreases to a minimum value for an established concentration. If the power continues to increase until the maximum generating capacity, once again, an increase in wear rate is observed, which is consistent with removing the turbine from its point of maximum efficiency.

The wear behaviour of the turbine can be explained by reviewing the fluid velocity field and its streamlines. As shown in Fig. 6 (a), at the optimal design point, the most uniform flow area with low recirculation at the runner inlet causes the sand particles dispersed in the fluid stream to not impact the surface of the blades directly for both the suction side or the pressure side, and therefore, the rate of erosion is low (Fig. 14(a)).

In contrast, at partial load, there are large areas of recirculation at the runner inlet, as shown in Fig. 6, which implies a greater interaction between the sand particles and the surface of the rotor blade in the area near the entrance and middle part of the blade area; therefore, generally, a higher erosion rate and erosion concentration in this region occurs, which is confirmed in Fig. 14(b). Given this behaviour, it is possible to operate the plant according to the available flow rate and the measured concentration to obtain the minimum overall wear rate.

3.4. Operation of the facility depending on the wear of the generator groups

Using the results and wear characteristics curves developed numerically for the installation in question, it follows that whenever there is flow available to generate at the design point, even when using a single group, it is desirable to operate in such a way as to minimize wear on the machine.

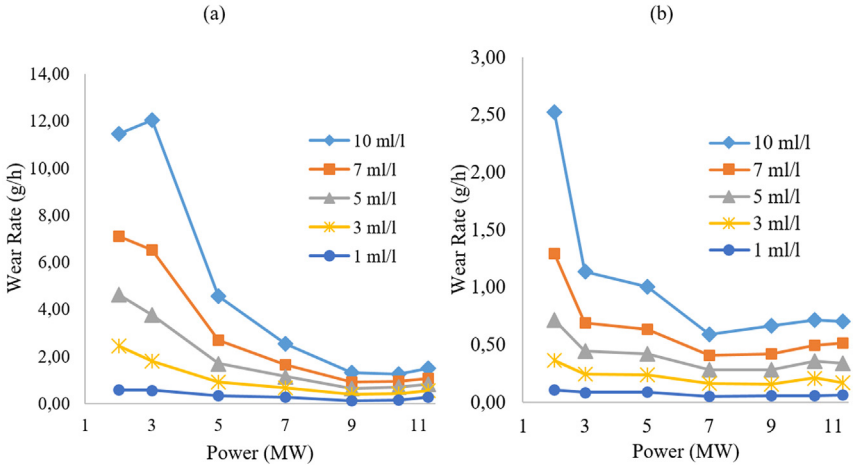

Fig. 13. Wear rate vs. generated power at different concentrations of hard particles in the (a) runner and (b) anti-wear plate–guide vane assembly.

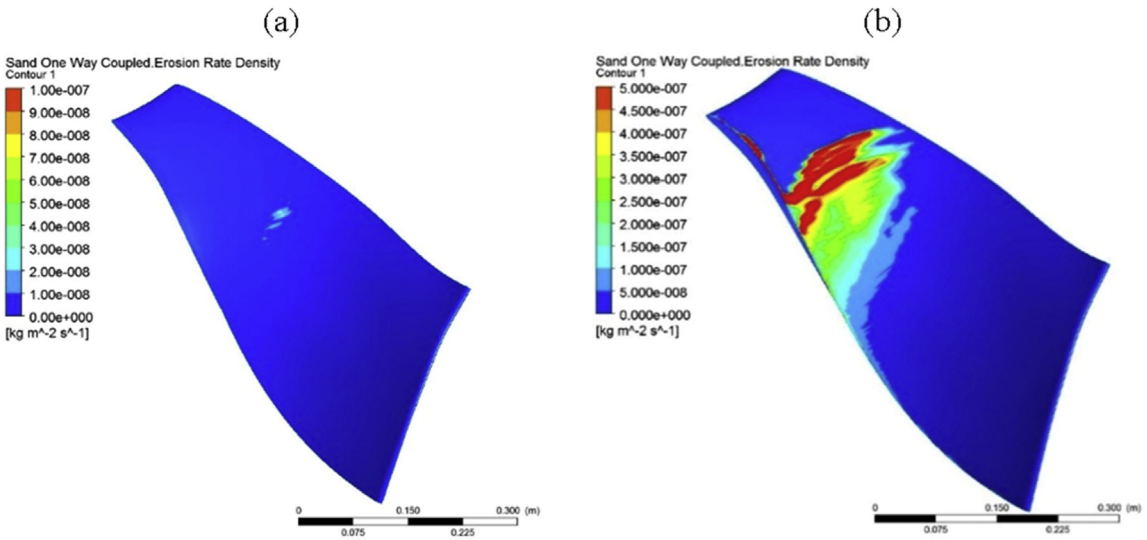

Fig. 14. Erosion at the runner blades and pressure side at the (a) optimum and (b) partial load.

However, for this particular installation, several times, the flow exceeded 6 m^3/s, which is the required value to generate at that point, and the flow will split between the two generating units (turbines) of equal capacity available in Amaime. Therefore, a decision criterion is required that determines which flow to use in the turbines for each group to minimize the cost of generation, which is implicitly associated with the cost of maintenance and repair due to erosive wear of the machine. Analysis of the wear rate as a function of the power generated, based on the simulations, helps generate operation recommendations for the different scenarios that may arise, i.e., according to the available flow and sand concentration in the water to generate operational strategies that minimize wear generated in turbines of the plant.

Fig. 15 shows the overall wear rate, which is the sum of the wear in the generating groups as a function of the turbinated flow in group one when water contains 10 ml/l of sediment; this behaviour is maintained for all concentrations evaluated.

These data support the conclusion that for the lowest total wear, the flow must be allocated by taking into account the following criteria: For low flow rates (less than 6.34 m^3/s of the available total), one must run the plant with only one turbine by making full use of flow available to the other turbine not in operation. For flows between 6.34 m^3/s and 10.34 m^3/s, the available flow is to be divided equally between the turbines. Finally, for a flow rate greater than 10.34 m^3/s, flow must be supplied to a turbine that corresponds to the optimum operating point (5.86 m^3/s), and the remaining flow supply is sent to the other turbine.

So far, the operation criterion only takes into account technical factors of availability and operating conditions, but it is necessary to make a study of the economic factors involving the efficiency losses due to the cumulative wear, the repair costs due to wear, the selling price of energy, among others. Additionally, it is necessary to identify how sensitive are the costs to the variation of any of these factors.

3.5. Wear cost analysis

The following costs are associated with wear: *i*) costs of repairing turbine components, *ii*) cost of efficiency loss due to wear, *iii*) costs associated with the generation loss due to the absence of groups during repair, and *iv)* administrative costs.

Data on lost efficiency (ΔE) presented in Fig. 16 were obtained for each generation time using the following relationship:

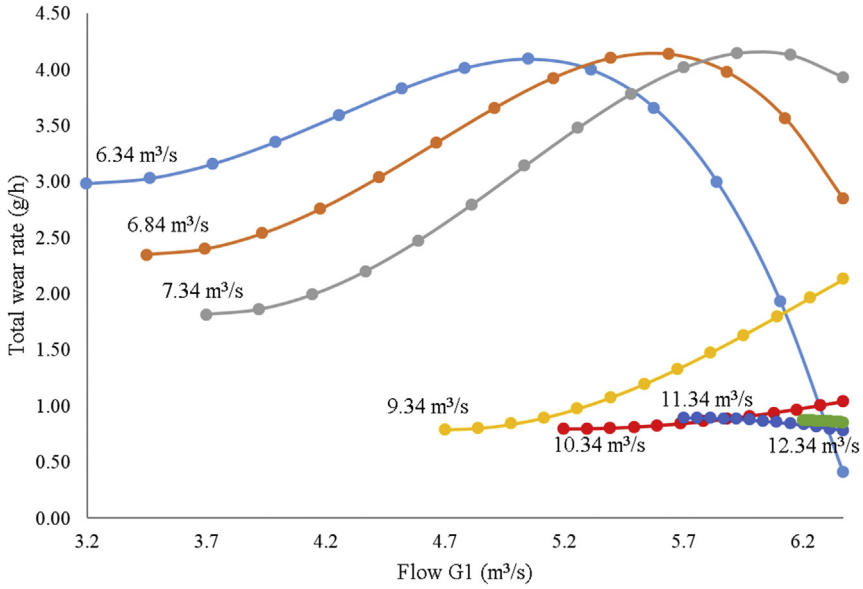

Fig. 15. Total erosion rate according to the turbined flow in generation group 1 (G1) for different total available flow at a concentration of 10 ml/l.

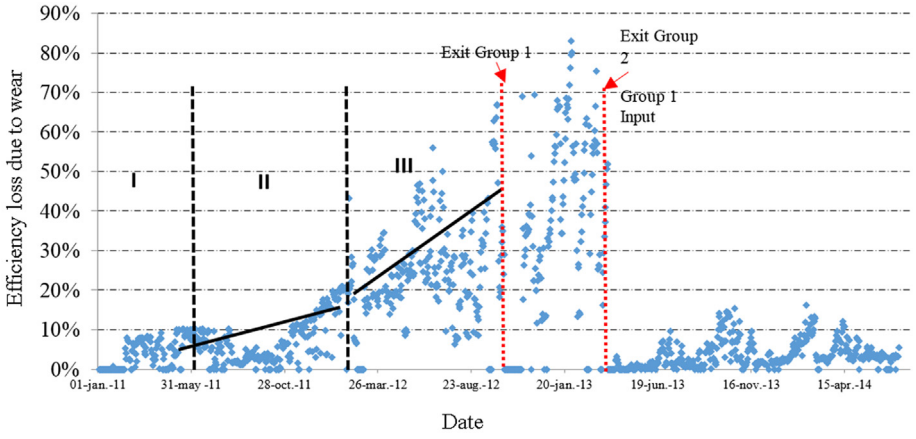

Fig. 16. Daily efficiency loss between 2011 and 2014.

$$\Delta E = 1 - P_r/P_t \tag{8}$$

where P_r is the actual generated power, and P_t is the power that would be generated with the turbine without wear.

Fig. 16 shows how the loss in efficiency increased over time until the year 2012 and the beginning of 2013. In particular, 2012 was a critical year in which there was an accelerated loss of efficiency in contrast to the first year of operation (plant began operation on January 1, 2011), where efficiency remained approximately constant, and losses were at levels near or below 10%.

Between 2011 and 2012, Colombia was affected by *La Niña* phenomenon, which produced the greatest raining period in the history of this country. This event can be related to accelerated wear on the turbines because as shown in Fig. 16, the accelerated loss of efficiency began in late 2011 and continued throughout 2012.

The recovery of the efficiency shown in Fig. 16 is due to the repair of generation group number 1 that occurred on October 16, 2012 (first dotted line) and returned on April 10, 2013. For generation group number 2, the overhaul began April 10, 2013 (second dotted line), i.e., April 10, 2013 begins a new cycle of operation of one repaired machine and therefore, a new cycle of wear.

In the last half of 2013 to July of 2014, the loss of efficiency is maintained at levels near or below 10%. On May 10th of 2013 a control system was implemented to stop the plant's operation whenever the sediment concentration exceeded a critical value of 2 ml of sediment per litre of water, which was measured using the sedimentation method with an Imhoff cone.

While Fig. 16 is not a typical curve of wear, it can be correlated with a curve of this type considering that there are three stages in the wear process: *i*) *running-in* or settling period where the rate of settlement wear is high; *ii*) period of stable or stationary wear where the wear rate is approximately constant; and *iii*) *run-out* or accelerated wear period, where severe accelerated wear and the wear rate increase. Therefore, from Fig. 16, one can make an analogy between the data loss efficiency found for the years 2011 and 2012 and the behaviour of a typical curve wear in a tribo-system with approximately equivalent trends. In fact, the rapid loss of efficiency suffered by the turbines is because the turbine components reached a period of severe wear; currently, it is recommended to perform extensive repair when the turbine exits the stable period.

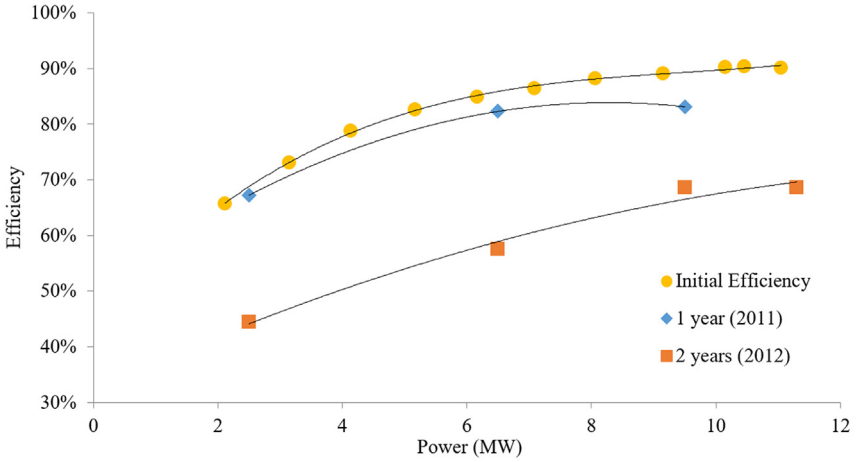

Fig. 17. Efficiency of the EPSA – Amaime generation groups.

To illustrate and demonstrate the dramatic effect that erosive wear has on the efficiency of generating groups, in Fig. 17, the evolution of efficiency curves is shown as a function of power over two years of operation. The fall of efficiency is evident both at the point of maximum efficiency and at partial load, where the effect is more pronounced.

The cost associated with the loss of efficiency was calculated from the difference between the actual power output hour by hour, and the power that could have been generated with the turbine in the initial operating efficiency.

The cost due to the absence of the second machine for repairs was calculated using the power that would be generated with the available turbine flow that was not used due to the absence of the second machine. This cost exists as long as the river flow is above the maximum usable by one machine; due to the absence of the second machine, the surplus was not captured. Historically, the Amaime facility has a plant factor of 0.58 (ratio between the historical average river flow and the maximum flow available for a turbine with two generating units, i.e., 12 m^3/s). As shown in Fig. 18, it can be understood that in many instances, the plant factor was well above the historical value, which explains that when a machine is down due to wear, money is lost by failing to take advantage of the flow peaks that are above average, which explains the money loss when operating with a single turbine.

Given the wear-associated costs mentioned above, Table 5 shows the consolidation of these costs between 2011 and 2014, which considers the start of operation of the two generating units to date when they returned again to operate together (July 11, 2014), due to that, it was not possible to record hour by hour of the sale value, hence, different average sale energy values were used in the cost estimation, as shown in Table 5.

The total cost in Table 5 is due to wear that occurred during the years of analysis, and therefore, the mass loss of the turbines is the primary cause of these costs; the wear rate data that were used for the erosion analysis are presented in Section 3.3, which was used to estimate total mass loss in the period evaluated. The model estimates the loss of mass in grams per hour depending on the concentration and generated power (operating point).

The total mass loss estimated for the runner is 53 kg and 11 kg for rest of elements and the average cost of each gram is worth 101.051 COP (33.68 USD) for sale value 120 COP/kW-h. Fig. 19 shows the money lost by wear in accordance with the flow rate and the sediment concentration in the water, which results from the product between the average cost of the mass loss in grams per

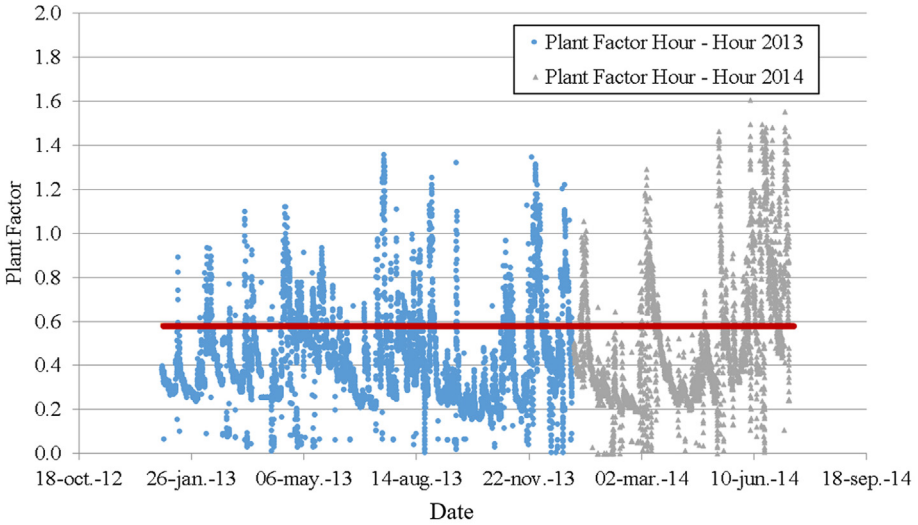

Fig. 18. Plant factor hour–hour 2013 and 2014 compared with the Amaime plant factor corresponding to the average historical flow.

Table 5
Cost associated with the wear of turbines (Exchange rate 3000 COP/USD).

Description	Wear cost for sale value 120 COP/kW-h	Wear cost for sale value 200 COP/kW-h	Wear cost for sale value 500 COP/kW-h	Wear cost for sale value 800 COP/kW-h
Money lost due to efficiency loss	3,784,686,875 COP (1,261,562 USD)	6,307,811,458 COP (2,102,603 USD)	15,769,528,644 COP (5,256,510 USD)	25,231,245,830 COP (8,410,415 USD)
Money lost due to equipment absence (equipment repair time)	1,507,899,659 COP (502,633 USD)	2,513,166,098 COP (837,722)	6,282,915,247 COP (2,094,305 USD)	10,052,664,396 COP (3,350,888 USD)
Equipment repair cost	1,107,048,000 COP (369,016 USD)			
Administrative management	150,000,000 COP (50,000 USD)			
Total	6,549,634,534 COP (2,183,212 USD)	10,078,025,557 COP (3,359,342 USD)	23,309,491,891 COP (7,769,831 USD)	36,540,958,226 COP (12,180,319 USD)

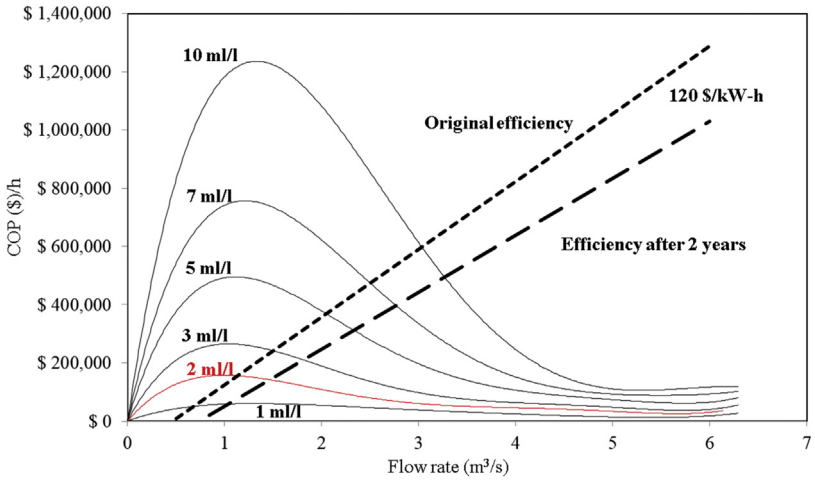

Fig. 19. Plots of wear costs per hour as a function of the flow rate and concentration for sale value 120 COP/kW-h (stop criteria).

hour and the erosion data curves of the turbine obtained computationally and presented in Fig. 13.

Thus, the plots in Fig. 19 represent the money lost per hour when the turbines operate at a certain flow rate (operating point) and a given sediment concentration. Additionally, the dotted lines show the money the plant bills for sale value 120 COP/kW-h with the original efficiency and efficiency after two years.

From above, Fig. 19 can be used to establish a stopping criterion based on technical and economic factors in the operation groups. The area will be profitable when the operating point (flow rate-sediment concentration) of the group is below the area bounded by the selling profit of generation. Otherwise, it is recommended to stop generation. As it is clear, from the data in Fig. 19, the stop criteria depends on the current efficiency of the machine.

On the other hand, the curve corresponding to the concentration of a 2 ml/l suggests that it is not always economically feasible to stop operation when the river is in this condition. Even operating with concentrations of 10 ml/l can be profitable as long as the turbine operates at a flow rate higher than 3 m^3/s for the sale value of 120 COP/kW-h with original efficiency or at flow rate higher than 3.25 m^3/s with the efficiency of the severely worn machine. In fact, using the current stop criterion (stop when the concentration exceeds 2 ml/l), operation halted for 472 h between 14 May 2013 and 29 October 2014. In these 472 h, the billing stopped in approximately 569,281,343 COP (189,760 USD), and the cost that was avoided by wear reached 33,271,270 COP (11,090 USD), i.e., at that time, a total of 536,010,073 COP (178,670 USD) was lost. Thus, for the specific case of the concentration of 2 ml/l, if the provided flow (around 1 m^3/s) is able to generate over 2 MW, it is profitable to operate at this concentration when the machine is not worn (original efficiency).

These analyses have been conducted considering an only one sale value of kW-h, however this value can change. A cost sensitivity analysis could be performed by considering that the sale value of electric generation is very changing and depend on the market [30–32], for instance in Fig. 20 is shown different curves for the money lost by wear and linear lines for money bills at different sale values obtained for the original efficiency and a concentration of 5 ml/l.

The vertical line was plotted to identify the interception between selling price of generation and money lost by wear. According with this result the value of flow rate where interception occurs is little affected by selling price of kW-h and doing this exercise for all concentrations, the results follow the same behaviour. In Fig. 21 is summarized the minimum flow rate of operation at different concentrations to ensure that the generation produces more money than the money lost by wear.

With loss of efficiency, the minimum flow rate to operate increase because the power generation decreases with the same flow rate, therefore, is necessary to increase the flow rate to ensure the operability condition; the situation expressed here is presented in Fig. 21, where can be seen that the minimum flow rate of operation is always higher in the condition of the severely worn machine than the condition without wear, this is with the original efficiency. It is remarkable to establish that the minimum flow rate of operation is slightly affected or slightly sensitive to change of cost of kW-h and depend principally on efficiency of the turbines as shown in Fig. 21.

4. Conclusions

A complete analysis based on computation fluid dynamics and real costs of wear were widely investigated for a small-scale

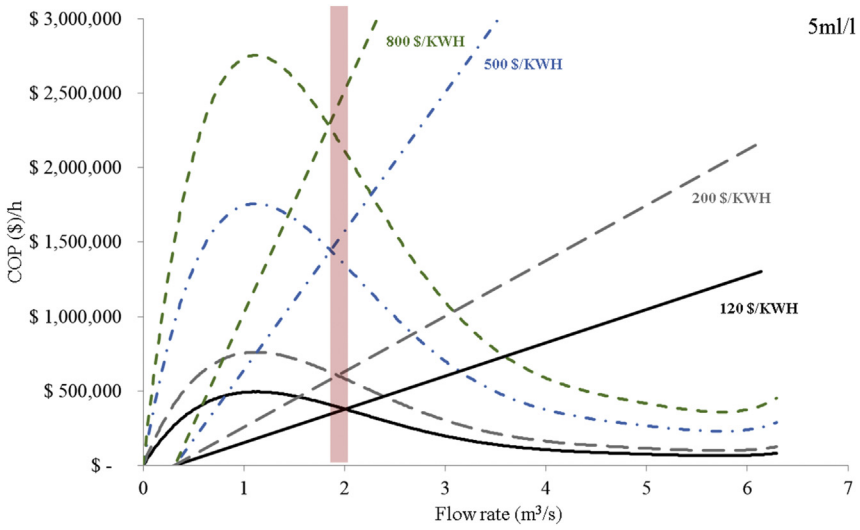

Fig. 20. Plots of wear costs per hour as a function of the flow rate and different sale values of kW-h (stop criteria) for 5 ml/l.

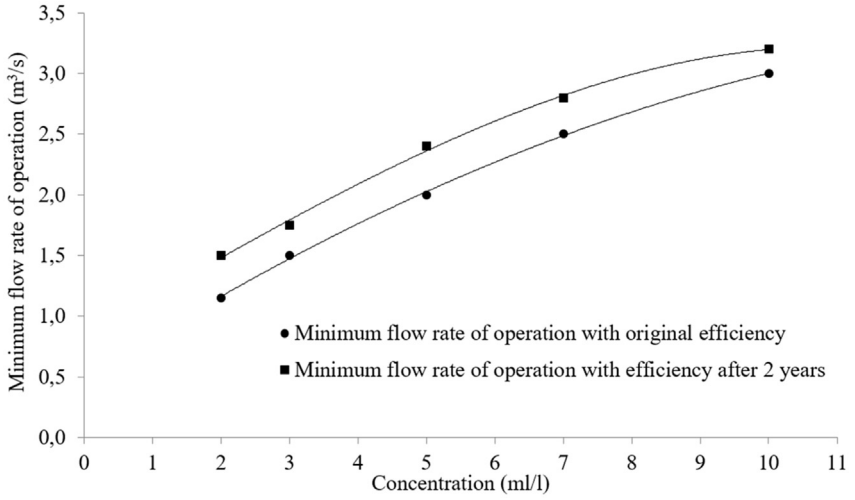

Fig. 21. Minimum flow rate of operation for different concentration at two different efficiencies.

generation plant with two generation groups of 10 MW each. The described methodology can be implemented in different power producing companies.

The present work led to the following conclusions:

- A relationship between wear rate and operating power of the turbine at different concentrations of sediment for critical turbine components that are exposed to erosion was found. A tendency for low wear at the design specifications for the turbine design and high wear at low powers or beyond design specifications is presented. Based on these findings, a new flow distribution methodology for the operation of turbines was established to minimize wear and take full advantage of water resources.
- Loss of power was used as the monitoring variable, which correlated with the level of machine wear; this one registered a mean loss of efficiency around 35% in two years. The change in the rate of efficiency loss defines the *run-out* of the equipment and hence this situation should be avoided.
- A strategy of operation and shutdown was designed, which takes into account the available flow, sediment concentration, and wear level. The implementation of this strategy allows the plant to operate more profitably because it weighs the costs of operation, maintenance, and repair due to wear with potential profits. It was well established that the minimum flow rate of operation is not sensitive to change of cost of kW-h and depend principally on sediment concentration and less of efficiency of the turbines.

Acknowledgements

The authors acknowledge COLCIENCIAS, EPSA E.S.P. A CELSIA Company, and Universidad del Valle for the support obtained through Project no. 110656237170.

References

[1] Neopane HP. Sediment erosion in hydraulic turbines. Glob J Res Eng Mech Mech Eng 2010;11(6).
[2] Singh M, Banerjee J, Patel P, Tiwari H. Effect of silt erosion on Francis turbine: a case study of Maneri Bhali Stage-II, Uttarakhand, India. ISH J Hydraul Eng 2013;19(1):1–10.
[3] Thapa BS, Dahlhaug OG, Thapa B. Sediment erosion in hydro turbines and its

effect on the flow around guide vanes of Francis turbine. Renew Sustain Energy Rev 2015;49:1100–13.
[4] Teran LA, Roa CV, Muñoz-Cubillos J, Aponte RD, Valdes J, Larrahondo F, Rodríguez SA, Coronado JJ. Failure analysis of a run-of-the-river hydroelectric power plant. Eng Fail Anal October 2016;68:87–100. ISSN 1350-6307, http://dx.doi.org/10.1016/j.engfailanal.2016.05.035.
[5] Eltvik M, Dahlhaug OG, Neopane HP. Prediction of sediment erosion in Francis turbines. Conference Prediction of sediment erosion in Francis turbines. IAHR.
[6] Thapa BS, Eltvik M, Gjosaeter K, Dahlhaug OG, Thapa B. Design optimization of Francis runners for sediment handling. In: Water resources and renewable energy development in Asia, Thailand; 2012.
[7] Allen G. Inflation: the value of the pound 1750-2002: house of commons library. 2003.
[8] Jost P. Economic impact of tribology. Proc Mech Fail Prev Group 1976:117–39.
[9] Rabinowicz E. The least wear. Wear 1984;100(1):533–41.
[10] Jost HP. Tribology—origin and future. Wear 1990;136(1):1–17.
[11] Sinatora A. Tribologia: Um resgate histórico e o estado da arte. 2005. Erudição apresentada como parte dos requisitos do concurso para professor titular do departamento de Engenharia Mecânica) Escola Politécnica da Universidade de São Paulo, São Paulo.
[12] Pradhan PMS. Improving sediment handling in the Himalayas. Nepal: OSH research; 2004.
[13] Castro AM. Metodología de apoyo para la programación a corto plazo de la operación de unidades de generación tipo Francis en rangos extendidos. Medellin - Colombia: Universidad EAFIT; 2014.
[14] Christensen LR, Greene WH. Economies of scale in US electric power generation. J Polit Econ 1976:655–76.
[15] Nilsson O, Sjelvgren D. Hydro unit start-up costs and their impact on the short term scheduling strategies of Swedish power producers. IEEE Trans Power Syst 1997;12(1):38–44.
[16] Thompson M, Davison M, Rasmussen H. Valuation and optimal operation of electric power plants in competitive markets. Oper Res 2004;52(4):546–62.
[17] Eltvik M, Thapa BS, Dahlhaug O, Gjosaeter K. Numerical analysis of effect of design parameters and sediment erosion on a Francis runner. Conference Numerical analysis of effect of design parameters and sediment erosion on a Francis runner.
[18] Teran LA, Larrahondo FJ, Rodríguez SA. Performance improvement of a 500-kW Francis turbine based on CFD. Renew Energy 2016;96:977–92.
[19] Laín S, García M, Avellan F, Quintero B, Orrego S. Simulación numérica de turbinas Francis. Medellin, Colombia: Fondo Editorial Universidad EAFIT; 2011.
[20] ANSYS. ANSYS CFX-Solver theory guide. Canonsburg U.S.A.: ANSYS, Inc; 2013.
[21] Menter FR. Two-equation eddy-viscosity turbulence models for engineering applications. AIAA J 1994;32(8):1598–605.
[22] ANSYS. ANSYS CFX-Solver modeling guide. Canonsburg U.S.A.: ANSYS, Inc; 2013.
[23] Grant G, Tabakoff W. An experimental investigation of the erosive characteristics of 2024 aluminum alloy. 1973. DTIC Document.
[24] Romo S, Santa J, Giraldo J, Toro A. Cavitation and high-velocity slurry erosion resistance of welded Stellite 6 alloy. Tribol Int 2012;47:16–24.
[25] Shivamurthy R, Kamaraj M, Nagarajan R, Shariff S, Padmanabham G. Slurry erosion characteristics and erosive wear mechanisms of Co-based and Ni-based coatings formed by laser surface alloying. Metall Mater Trans A 2009;41(2):470–86.
[26] Camacho JL, Marquina-Chávez A, Escalante-Martínez J, Márquez-Vera C, Hernández-Romero I, Galicia-Badillo A. Santes-Bastián MdC. In: An analysis of the solid particle erosion damage caused on AISI 304; 2014.
[27] Clancy LJ. Aerodynamics. Wiley; 1975.
[28] Roa CV, Muñoz J, Teran LA, Valdes JA, Rodríguez SA, Coronado JJ, Ladino A., Effect of tribometer configuration on the analysis of hydromachinery wear failure, Wear, 332–333, May–June 2015, 1164-1175, ISSN 0043-1648, http://dx.doi.org/10.1016/j.wear.2015.01.068
[29] Hutchings IM. Tribology: friction and wear of engineering materials. 1992.
[30] García J, Gaviria A, Salazar L. Determinantes del precio de la energía eléctrica en el mercado no regulado en Colombia. Rev Ciencias Estratégicas 2011;19(26).
[31] Lozano I, Rincón H. Formación de las tarifas eléctricas e inflación en Colombia. Banco de la República; 2010.
[32] Rodríguez AM. Informe de inflación. Corficolombiana; 2016. p. 1–8.

4. ARTICLE 2: COMPUTATIONAL STUDY OF PARTICLE SIZE EFFECT ON JET EROSION WEAR DEVICE

Wear 374-375 (2017) 97–103

Contents lists available at ScienceDirect

Wear

journal homepage: www.elsevier.com/locate/wear

Computational study of the particle size effect on a jet erosion wear device

R.D. Aponte [a,b], L.A. Teran [a,*], J.A. Ladino [a], F. Larrahondo [b], J.J. Coronado [a], S.A. Rodríguez [a,*]

[a] Research Group of Fatigue and Surfaces, Mechanical Engineering School, Universidad del Valle, Cali, Colombia
[b] EPSA E.S.P. A CELSIA Company, Cali, Colombia

ARTICLE INFO

Article history:
Received 3 September 2016
Received in revised form
18 November 2016
Accepted 19 November 2016
Available online 31 December 2016

Keywords:
Computational fluid dynamics
Erosion by hard particle
Particle size
Jet erosion device

ABSTRACT

Computational fluid dynamics (CFD) is a useful tool to predict the erosion behaviour over geometries exposed to conditions of severe erosion wear. This work shows how CFD can be used to virtually characterize the wear behaviour of materials used in several hydraulic components, including turbomachinery systems, in which it is important to consider the effect of particle size. In addition, this work develops a methodology for determination and validation of the constants involved in the well-known Tabakoff-Grant model for erosion prediction using the erosion wear obtained via erosion testing in a jet tribometer reported in the literature as a reference. From the experimental data, an optimization algorithm was performed to determine the optimal values of Tabakoff-Grant model constants for ASTM A743 grade CA6NM martensitic stainless steel. The simulated erosion rate agrees with the experimental data for the material analysed in jet erosion simulations with impact angles ranging from 15° to 90°. The change of the angle of maximum erosion rate for small particles, which has been reported in the literature via experimentation, was explained satisfactorily. The results showed that the erosion rate with smaller particles is affected by fluid flow, since small particles tend to follow the flow streamlines, while larger particles move according to the conditions imposed by the jet at its outlet. The effective impingement angle against the surface for small particles is lower than the impingement angle for large particles; therefore, the angle of maximum erosion rate, measured between the jet and the sample's surface, for small particles increases.

1. Introduction

Erosive wear due to sand particles is one of the most important problems that must be taken into account at the design stage for hydraulic turbines, particularly for run-of-the-river facilities. Wear conditions are influenced by the river's water conditions and local hydrological conditions during the operation period. This is the case for several plants located at Los Andes and the Himalayas that, have been affected by erosive wear via sand particles [1–5] with severe damage to the machines' components, causing premature loss of efficiency and increasing corrective maintenance and subsequent economic losses.

During the past decades, computational fluid dynamics (CFD) has become an important tool to design hydraulic machinery under several operational conditions, including sand wear erosion. One of the well-known models for erosion behaviour in ductile materials due to hard particles is the Tabakoff-Grant model [6]. However, literature regarding the erosion model's constants that define the interaction between different hard particles and materials is limited. To obtain this information, it is necessary, but not sufficient, to perform experimental tests in which variables such as concentration, particle velocity, impingement angle, particle size and particle shape can be related to the material's erosion rate. Next, this information must be processed and the constants of the model obtained for implementation within the CFD software.

In general, erosion caused by hard particles exhibits a different behaviour in ductile and brittle materials. In the case of ductile materials, the ductility of the surface allows the absorption of the particle energy when it impinges the surface at near normal angles; however, when the particle hits the surface with lower angles, the surface tends to lose material by cutting. According to Hutchings [7], in ductile materials, the angles that exhibit major losses of material are in a range of 15–30°, while in brittle materials, the angle for maximum mass loss is 90°.

Experimental results obtained by Romo et al. [8] include a comparison of the slurry erosion resistance of a Stellite 6 coating and 13Cr-4Ni stainless steel. They performed tests of slurry erosion

* Corresponding authors.
E-mail addresses: leoatell04@gmail.com, leonel.teran@correounivalle.edu.co (L.A. Teran), sara.rodriguez@correounivalle.edu.co (S.A. Rodríguez).

http://dx.doi.org/10.1016/j.wear.2016.11.042
0043-1648/

at several impact angles defined between the sample and the jet, obtaining the characteristic curves for erosion interactions between sand and the tested materials. Using a particle size of 300 μm, they observed a behaviour in accordance with the general statement explained previously, with an angle for maximum erosion of approximately 45° for both materials. Shivamurthy et al. [9] evaluated the resistance to slurry erosion of Stellite 6 relative to the base material 13Cr-4Ni stainless steel at particle sizes of 100 μm and 375 μm and several impact angles between the sample and the jet. Their analysis showed that for largest particles, the 13Cr-4Ni Stainless steel exhibits a similar behaviour as that found by Romo, while the Stellite 6 coating undergoes maximum erosion rate at an angle of 60°. For the smallest particles, the Stellite 6 coating maximum erosion angle is 90°, while in the 13Cr-4Ni steel, it is 60°; however, they do not provide an explanation of the cause of the change in this angle with the particle size. In addition, in their analysis about wear mechanisms, they found that for both materials, i.e., Stellite 6 coating and 13Cr-4Ni steel, there is evidence of micro cutting, plastic deformation with chip fracture, crater lips and plowing marks in all tested angles; generally, these mechanisms are associated with ductile behaviour.

Although 13Cr-4Ni stainless steel is currently the most common material used in the manufacturing of hydraulic turbines and although experimental data regarding erosion are available, the coefficients of the erosion models have been neither obtained nor used in CFD simulations of these machines. Eltvik et al. [10] used CFD to investigate erosion problems in a Francis turbine constructed from 13Cr-4Ni steel using the Finnie and the Tabakoff-Grant erosion models with AISI 304 stainless steel constants. They found that the Tabakoff-Grant model provides more reliable erosion predictions than Finnie's model since it uses five constants that relate the erosion to the particles and the surface properties; in contrast, Finnie's model employs only two constants. The obtained results were qualitatively verified by inspecting a worn Francis turbine at Cahua power plant in Peru.

Others authors, such as Mansouri et al. [11] combined CFD results with experimental data obtained from a normal impinging jet test submerged in water using slurry with sand particles on AISI 316 stainless steel specimens to develop an equation that allows for erosion prediction. They used CFD simulations with low Stokes number (in this condition the particles tend to follow the streamlines of the fluid) to characterize the particle impact velocity, impingement angle on the surface, which is affected by the fluid flow, and frequency at specific locations on the specimen. The obtained data were correlated with the measured erosion depth of the specimen subjected to the impingement jet tests to obtain the correlation.

In this work, CFD analysis is performed to predict erosion by hard particles of CA6NM stainless steel, which is equivalent to 13Cr-4Ni stainless steel. To achieve this goal, experimental results reported in the literature were used to determine the coefficients for the Tabakoff-Grant erosion model [6]. The methodology used in determining the coefficients is explained with the aim of helping with the model's use for other materials using experimental data. The coefficients are validated and used to perform a computational study of the particle size effect of the erosion behaviour of CA6NM stainless steel.

2. Materials and methods

2.1. Erosion model

The effect of particles on the wear of a ductile material surface is modelled via CFD coupled with the erosion model developed by Tabakoff and Grant [6,12]. The model consists of a solid dispersed phase (particles) immersed, transported and diffused in a continuous incompressible fluid (water) phase, and evolved in a Lagrangian way. Simulations can be performed using either one-way or two-way coupling. In one-way coupling, the effect of the particles on the fluid is ignored. In two-way coupling, the effect of particles on the fluid is modelled with momentum source terms in the Navier Stokes equations [13]. The dimensionless erosion rate E is determined from the Tabakoff-Grant model:

$$E = k_1 f(\gamma) V_p^2 \cos^2\gamma\left[1 - R_T^2\right] + f(V_{PN}) \tag{1}$$

$$f(\gamma) = \left[1 + k_2 k_{12} \sin\left(\gamma \frac{\pi/2}{\gamma_0}\right)\right]^2 \tag{2}$$

$$R_T = 1 - k_4 V_p \sin\gamma \tag{3}$$

$$f(V_{PN}) = k_3 (V_p \sin\gamma)^4 \tag{4}$$

$$k_2 \begin{cases} 1.0 \; if \; \gamma \le 2\gamma_0 \\ 0.0 \; if \; \gamma > 2\gamma_0 \end{cases} \tag{5}$$

where the dimensionless variable E corresponds to the ratio of the mass loss due to erosion to the particle's mass, V_p is the impact velocity of the particle, γ is the angle of impact, γ_0 is the angle of maximum erosion, R_T is the tangential restitution ratio and k_1, k_{12}, k_3, and k_4, are constants that depend on the particle properties (e.g., hardness, shape) and the surface material. The constants define the reference speeds V_1, V_2, and V_3 implemented in the CFD software:

$$V_1 = \frac{1}{\sqrt{k_1}} \quad V_2 = \frac{1}{\sqrt[4]{k_3}} \quad V_3 = \frac{1}{k_4} \tag{6}$$

The constants are obtained through an adjustment of the experimental data (Section 3.1). The erosion rate of an arbitrary surface is calculated as follows:

$$E_r = E * \dot{N} * m_p \tag{7}$$

where E_r is the erosion rate due to a particle, m_p is the average of one particle mass, and $\dot{N}$ is the particle number rate, which is a representative value of the particle concentration in the medium [13]. The shape factor is an indication of the roundness of the particle: a particle with a shape factor value of 1.0 is spherical, while a particle with a shape factor of 0.1 is an irregular particle with sharp edges, which generally causes more damage to a surface than a spherical particle. In the CFX solver, the shape factor is related to the drag forces on the particle, while the effect of this factor on the surface wear is related to the experimental constants of Tabakoff-Grant model. The data are normalized with the goal of transforming the numerical and experimental values to a suitable scale for comparison with the erosion model. The transformed values are defined as follows:

$$N_E = \frac{E_r}{V_j A_o \rho_{H_2O}\left(\frac{C}{1-C}\right)} \tag{8}$$

where N_E is the dimensionless normalized erosion, E_r is the erosion rate in kg/s, V_j is the average jet velocity in m/s, A_o is the cross-sectional area of the jet's outlet, C is the sand concentration or mass fraction and ρ_{H_2O} is the water density in kg/m^3.

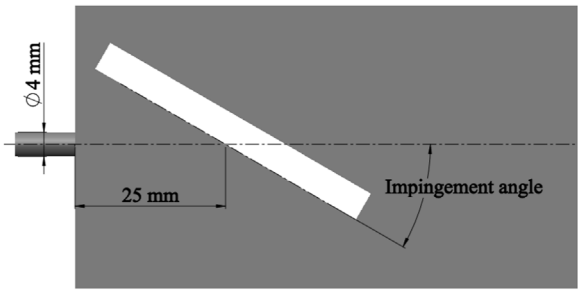

Fig. 1. Fluid domain of the simulated geometry.

2.2. CFD configuration

The fluid domain for this study, which was adapted from [8], corresponds to a jet erosion bench and is shown in Fig. 1. Six impingement angles were simulated (15°, 30°, 45°, 60°, 75° and 90°).

The model was discretized using a structured mesh (Fig. 2), and refined near the zone of the specimen surface affected by hard particle erosion.

To reach a numerically independent result, convergence analysis of both the mesh size and the number of representative particles was developed (Section 2.1). The monitor variable was the erosion rate over the entire plate surface. Fig. 3a and b show the results of the independence study with respect to the number of particles and the number of nodes, respectively, for a representative impingement angle of 45°. In all cases, the erosion rate difference between the last two results is less than 2%; in fact, the difference between the smallest and the largest number of particles is less than 2%, showing that the erosion rate variable is not significantly affected by the particle number.

Particle characteristics are presented in Table 1. Following the recommendation of the solver modelling guide [13], to capture the effect of the particles in the fluid with the minimum use of CPU, the particles were one-way and fully coupled to the continuous phase, which is liquid water at standard conditions. In the one-way-coupled case, 100,000 representative particles were established to calculate the erosion rate; in the fully coupled case, 12,500 particles were established to calculate the effect of particles on the fluid. Verification between one-way and fully coupled erosion rates showed a difference less than 0.6%; therefore, in all simulations, only one-way-coupled results were evaluated. Particle sizes of 30 μm, 100 μm and 300 μm with a shape factor of 0.78 were simulated.

All simulations were steady-state simulations using the $k-\omega$ shear stress transport (SST) turbulence model [14] and the Tabakoff-Grant erosion model [6]. The RMS residuals for mass, momentum and particle tracks were set at 1×10^{-4} as the convergence criteria. The CFD platform used was ANSYS CFX®, which is widely used in turbomachinery and erosion simulations [4,10,15,16].

The boundary conditions used in the model were based on the experimental configuration reported by Romo et al. [8] and are presented in Fig. 4. In this case, water and particles are added through the inlet with a velocity of 25 m/s and a sand concentration of 0.1 wt%. The slurry jet hits the sample surface and then leaves the domain through the surfaces defined as an opening where the pressure is the standard atmospheric pressure.

3. Results and discussion

3.1. Adjustment of the constants of the Tabakoff-Grant model

To adjust the experimental curve of the Tabakoff-Grant erosion model, experimental results taken from Romo et al. [8] were employed. They used the test parameters listed in Table 2, and their results are based on the interaction between sand and CA6NM stainless steel. This table also lists the parameters used in the experiment of Shivamurthy [9] that will be used to validate the results obtained from the adjustment process. The shape factors, in Romo and Shivamurthy's experiments, were verified and calculated from particles' pictures that they present their manuscripts using the Eq. (9) [7].

$$F = \frac{4\pi A}{P^2} \tag{9}$$

where A is the plain area of the particle and P is its perimeter.

With the normalized data N_E from Eq. (8), a simple polynomial fit with 10 terms and R^2 of 0.998 was developed. Next a Nelder-Mead simplex algorithm [17], embedded the in MATLAB® optimization library, was applied to find a first approximation of the constants of the Tabakoff-Grant model used in the CFD simulations. The algorithm minimizes an "error function" resulting from the difference between the data obtained with the Tabakoff-Grant model and the data obtained with the polynomial function. The algorithm changes the constant values of the erosion model in such a way that best fits with the polynomial curve, in the sense of minimizing an error function. The constants obtained with this process were used to obtain the curve via CFD simulations; however, the curve slightly deviated from the experimental results. Therefore, to refine the values of the constants, three additional CFD simulations for each impingement angle were performed, multiplying all constants by a unique factor to move the curve up

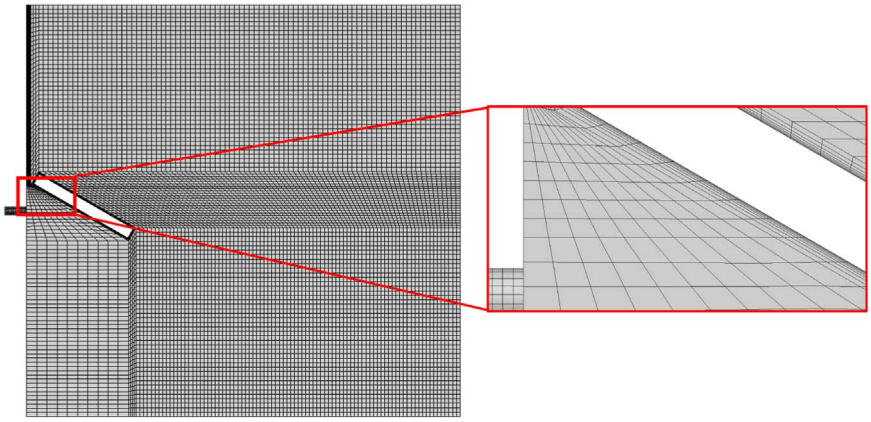

Fig. 2. Mesh used in the CFD model.

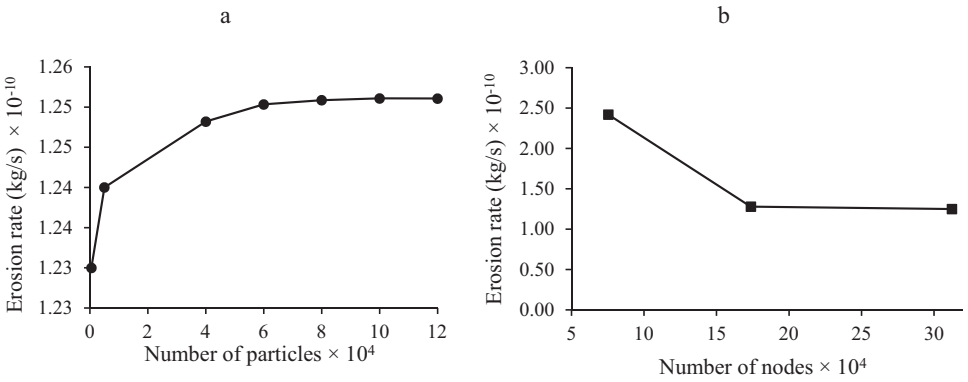

Fig. 3. Example of independence study of (a) number of particles and (b) mesh size, for erosion simulation with particles of 100 μm, 0.1% concentration and 45° impingement angle.

Table 1
Particle characteristics.

Variable	Case 1	Case 2	Case 3
Size	300 μm	100 μm	30 μm
Material	Quartz		
Density	2650 kg/m^3		
Shape factor	0.78 ± 0.02		
Minimum diameter	150 μm	38 μm	9.3 μm
Maximum diameter	425 μm	212 μm	55 μm
Mean diameter	359.9 μm	93 μm	33.2 μm
Standard deviation	84.2 μm	87 μm	12 μm

Table 2
Parameters of test rig configuration.

Parameter	Romo's experiment [8]	Shivamurthy's experiment [9]	
Angle of impingement (deg.)	15, 30, 45, 60, 75, 90	30, 45, 60, 90	
Jet velocity (m/s)	25	12	
Impinging medium	H_2O+SiO_2 (0.1 wt. %) submerged in water	H_2O+SiO_2 (1 wt%) in air	
Sand flow (g/min)	18.8	205.6	
Shape factor	0.78 ± 0.02	0.62 ± 0.07	0.72 ± 0.06
Particle size	300 μm	100 μm	375 μm

or down to obtain the best fit shown in Fig. 5, where the comparison between the experimental and the CFD results using the obtained constants is presented. It can be seen that the CFD data are inside of experimental confidence interval. The final fitting constants are presented in Table 3.

Using the obtained constants of the erosion model corresponding to the interaction between sand and CA6NM stainless steel, simulated results were obtained and are presented in Fig. 6. In the figure, erosion patterns are shown; the shapes of the wear marks, presented as contours of the erosion rate density obtained through simulation, are consistent with the experimental results obtained by Romo et al. [8] at each impingement angle.

3.2. Particle size assessment

Fig. 7 shows a comparison of the erosion behaviour with particles sizes of 30 μm, 100 μm and 300 μm (cases 1, 2 and 3 of Table 1). The jet angle for maximum erosion rate is found to increase for smaller particles. This phenomenon occurs because smaller particles tend to follow the fluid, while larger particles (because of their higher inertia) follow a path defined by the jet at the outlet, as shown in Fig. 8, i.e., the particle impact angle and the particle velocity are influenced by the flow characteristics. Thus, when the angle between the specimen and the jet is 75°, small particles tend to follow the fluid flow, thereby causing the impact angle of the particles to approach 45°. The last situation can be validated with experimental data obtained by Shivamurthy et al. [9] in which the jet angle for maximum erosion changes from 40° to 60° when the particle size is reduced from 375 μm to 100 μm. This interaction between fluid and particles is characterized by the non-dimensional Stokes number and has

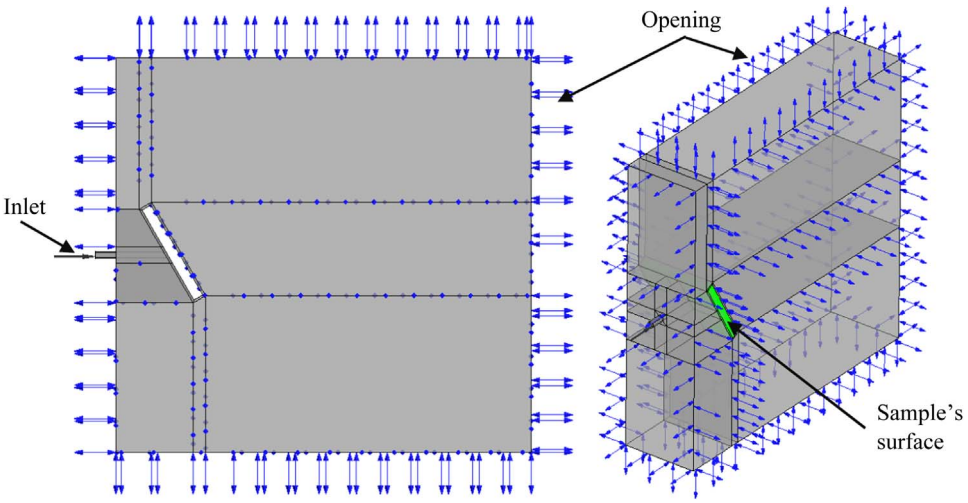

Fig. 4. Boundary conditions.

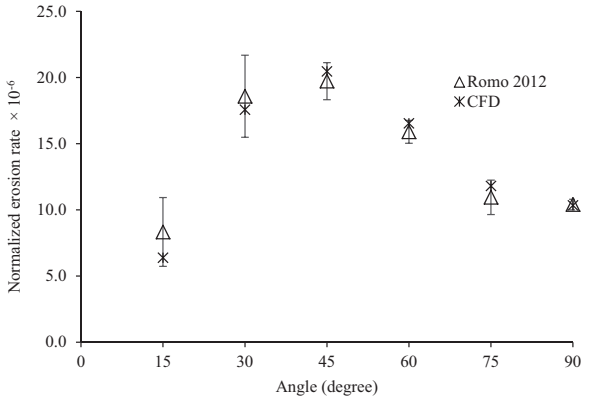

Fig. 5. Comparison of the experimental and CFD results.

Table 3
Fitting constants of the erosion model for CA6NM stainless steel.

Constant	Value
k_{12}	0.407
V_1 (m/s)	67.63
V_2 (m/s)	58.46
V_3 (m/s)	135.8
γ_0	45°

been widely analysed in terms of erosion processes by Solnordal et al. [18]. They found that particle velocities and impact angles are not affected by the fluid flow if the particle sizes are larger than 32.5 μm, where the Stokes number approaches 10 in a flow of air at 60 m/s and above. Thus, when the Tabakoff-Grant erosion model constants are adjusted based on experimental results obtained with jet erosion tests, it is important to verify that the

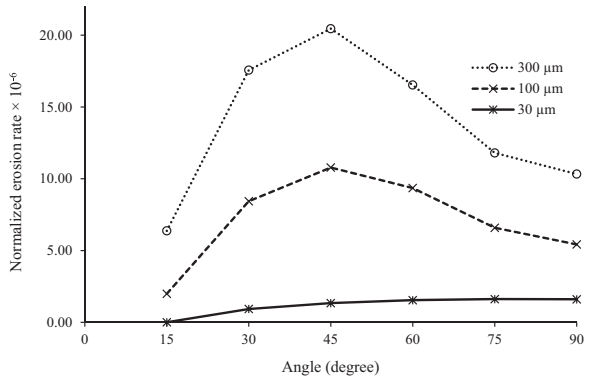

Fig. 7. Erosion rate behaviour for different particle sizes.

particle size is sufficiently large to follow the angle imposed by the jet.

In Fig. 9, a comparison is made between the CFD results using the obtained constants of the erosion model in Table 3, and the experimental data from Shivamurthy et al. [9] using the test rig configuration with the parameters shown in Table 2. The simulation provides an erosion rate at the same order of magnitude over the entire evaluated range, despite the Tabakoff-Grant model constants being obtained from a very different experimental configuration. It can be observed that maximum erosion angles between the jet and the specimen are predicted very well for both sizes 100 and 300 μm. Moreover, the CFD data follows the same pattern of the experimental data and the minimum erosion rate is obtained at the same angle. The minimum and maximum deviations for 100 μm are 42% and 80% respectively, while for 300 μm these deviations are 78% and 82% respectively. These discrepancies can be attributed to the differences in particles and surfaces materials, since Romo use a treated 13-4 stainless steel, which hardness is 280 $HV_{62.5}$, while Shivamurthy used an untreated

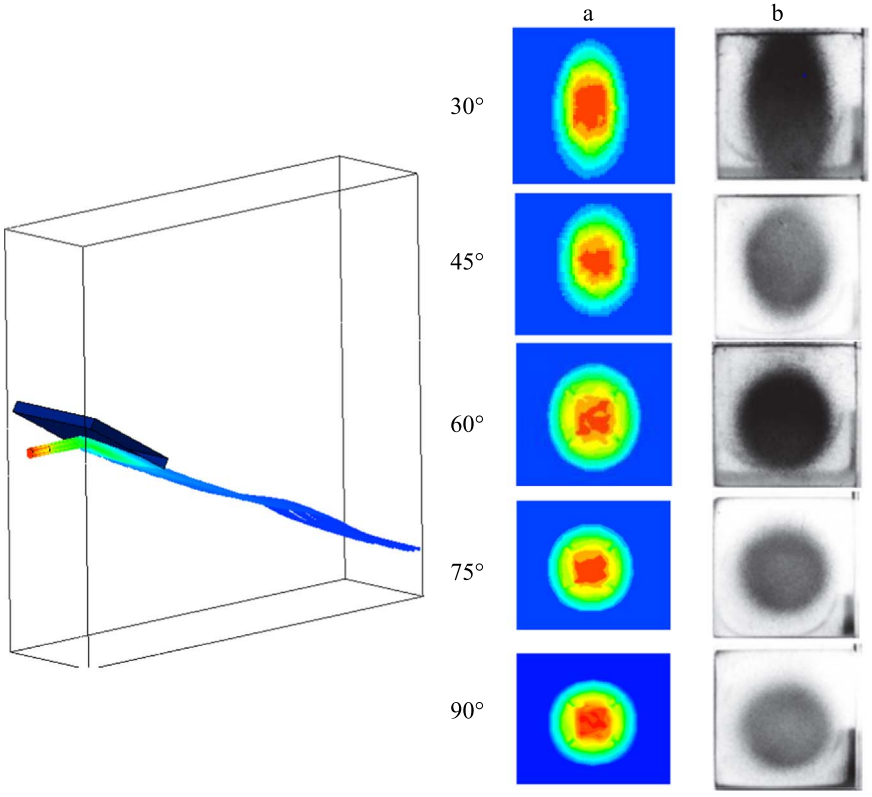

Fig. 6. (a) Erosion rate density contours obtained by CFD compared with (b) specimens' actual marks reported in [8].

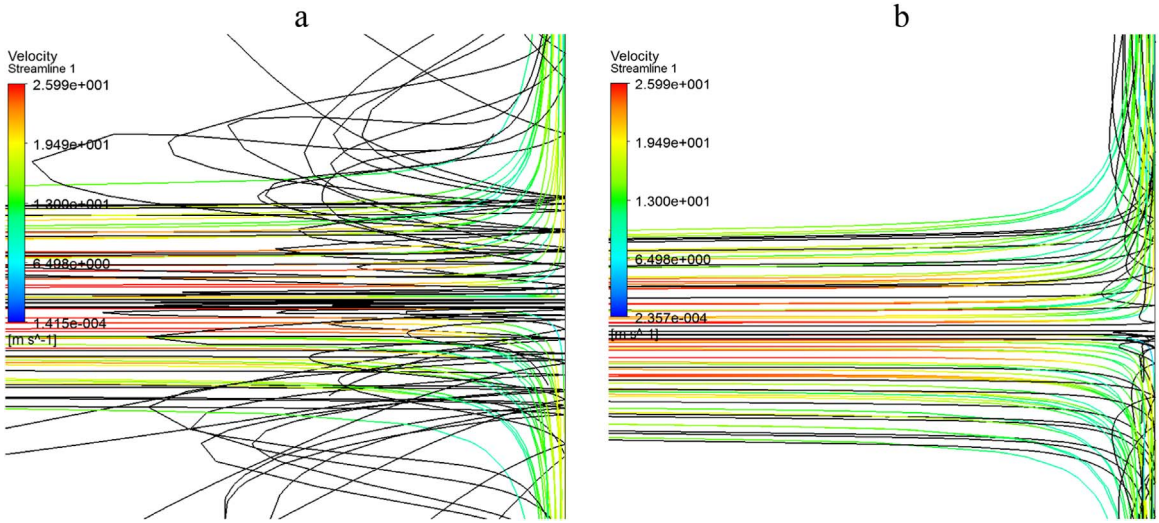

Fig. 8. CFD results at 90° showing that the effective impact angle of the particles decreases with small particles; particle tracks are represented by black lines, and the jet's streamlines are represented by coloured lines: (a) 300 μm and (b) 30 μm. (For interpretation of the references to color in this figure legend, the reader is referred to the web version of this article.)

material, which hardness is 240 HV_{100}. Moreover, the shape factor has a significant effect on the erosion rate. This factor changes with particle sizes, as was showed by Coronado [19], that is, experimentally it is difficult to obtain large and small particles with the same shape factor. Additionally, the CFD solver takes into account the shape factor as a function of the drag force of the fluid on the particles but not their cutting capacity on the material; this effect is accounted in the computed constants since it is known that particles with lower shape factor have higher capability of erosive wear [20,21]. The described situations made that the fitting constants of the Tabakoff-Grant model changed between both experiments. On the other hand, the experimental deviations of this kind of tests are very large, as can be seen in Fig. 5, where the deviation is 31%, this means that some data could be inside of the experimental deviation. Another reason for these discrepancies is the limitation of CFX solver to represent the differences in the experimental setup: while Romo uses a submerged slurry jet; Shivamurthy uses a slurry jet in air, which is a three phase configuration that the CFX solver is unable to reproduce. In the case of hydraulic machinery, like Francis turbines or pumps, subjected to erosion by hard particles and considering that there is no cavitation, only two phases exist (solid particles and liquid). This configuration is the one used in Romo's experiment and can be simulated in CFX solver.

With the methodology used to obtain the constants of a model implemented in the CFD solver, several materials used in hydraulic machines can be evaluated through simulation, for operating conditions involving erosion by hard particles. This methodology will be helpful when modifying geometries in such a way that the erosion rate is minimized and the maintenance costs reduced.

4. Conclusion

A methodology that uses experimental results to determine the constants of an erosion model implemented in CFD simulation was developed. The model constants for CA6NM stainless steel were found and validated. The assessment of the particle size showed that the erosion rate with smaller particles is affected by fluid flow since small particles tend to follow the flow streamlines while larger particles move according to the conditions imposed by the jet at its outlet. The effective impingement angle against the surface for small particles, whose trajectory is affected by the fluid behaviour, is lower than the impingement angle of large particles; therefore, the angle of maximum erosion rate for small particles increases. It is important to account for this effect when the experimental constants of the Tabakoff-Grant model are adjusted, i.e., it is necessary to confirm that the particle size is sufficiently

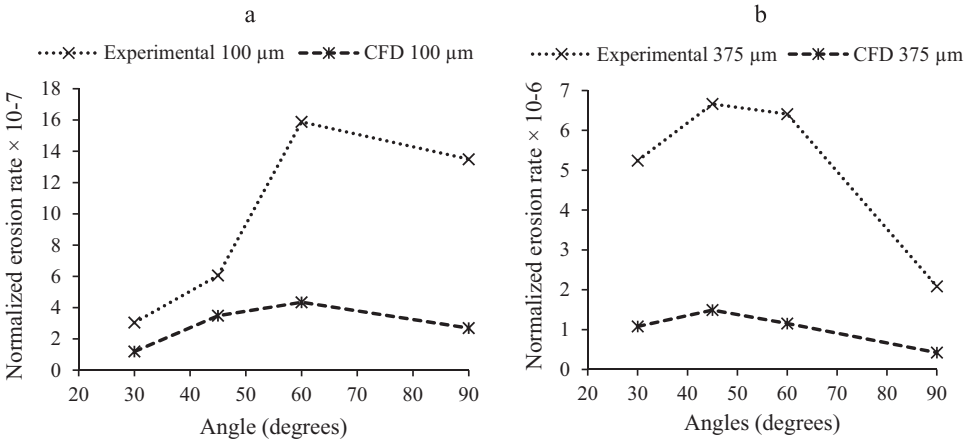

Fig. 9. Comparison of maximum erosion rate angle obtained by CFD and experimental data reported in [9].

large to follow the angle and velocity conditions imposed in the jet test rig.

The validation with the experimental results showed that the CFD model predicted very well the angles where minimum and maximum erosion rate occur, for two particle sizes. However, the quantitative wear rate results were deviated between 42% and 82% this due to differences in materials, limitations in simulation, and experimental deviations.

Acknowledgements

The authors acknowledge COLCIENCIAS, EPSA - CELSIA and Universidad del Valle for support that was obtained through Project no. 110656237170.

References

[1] H.P. Neopane, Sediment erosion in hydro turbines, Faculty of Engineering Science and Technology, Norwegian University of Science and Technology, 2010.
[2] M. Singh, J. Banerjee, P. Patel, H. Tiwari, Effect of silt erosion on Francis turbine: a case study of Maneri Bhali Stage-II, Uttarakhand, India, ISH J. Hydraul. Eng. 19 (2013) 1–10.
[3] L. Teran, C. Roa, J. Muñoz-Cubillos, R. Aponte, J. Valdes, F. Larrahondo, S. Rodríguez, J. Coronado, Failure analysis of a run-of-the-river hydroelectric power plant, Eng. Fail. Anal. 68 (2016) 87–100.
[4] L.A. Teran, R. Aponte, J. Muñoz, C.V. Roa, J.J. Coronado, J.A. Ladino, F. Larrahondo, S.A. Rodríguez, Analysis of economic impact from erosive wear by hard particles in a run-of-the-river hydroelectric plant, Energy 113 (2016) 1188–1201.
[5] B.S. Thapa, O.G. Dahlhaug, B. Thapa, Sediment erosion in hydro turbines and its effect on the flow around guide vanes of Francis turbine, Renew. Sustain. Energy Rev. 49 (2015) 1100–1113.
[6] G. Grant, W. Tabakoff, An experimental investigation of the erosive characteristics of 2024 aluminum alloy, DTIC Doc. (1973).
[7] I.M. Hutchings, Tribology: Friction and Wear of Engineering Materials, 1992.
[8] S. Romo, J. Santa, J. Giraldo, A. Toro, Cavitation and high-velocity slurry erosion resistance of welded Stellite 6 alloy, Tribology Int. 47 (2012) 16–24.
[9] R. Shivamurthy, M. Kamaraj, R. Nagarajan, S. Shariff, G. Padmanabham, Slurry erosion characteristics and erosive wear mechanisms of Co-based and Ni-based coatings formed by laser surface alloying, Metall. Mater. Trans. A 41 (2009) 470–486.
[10] M. Eltvik, O.G. Dahlhaug, H.P. Neopane, Prediction of sediment erosion in Francis turbines, in: 4th International Meeting on Cavitation and Dynamic Problems in Hydraulic Machinery and Systems, IAHR, 2011.
[11] A. Mansouri, H. Arabnejad, S. Shirazi, B. McLaury, A combined CFD/experimental methodology for erosion prediction, Wear 332 (2015) 1090–1097.
[12] ANSYS, ANSYS CFX-Solver Theory Guide, ANSYS, Inc., Canonsburg U.S.A., 2013.
[13] ANSYS, ANSYS CFX-Solver Modeling Guide, ANSYS, Inc., Canonsburg U.S.A., 2013.
[14] F.R. Menter, Two-equation eddy-viscosity turbulence models for engineering applications, AIAA J. 32 (1994) 1598–1605.
[15] M.Eltvik, B.S.Thapa, O.Dahlhaug, K.Gjosaeter, Numerical analysis of effect of design parameters and sediment erosion on a Francis runner, in: Proceedings of the Fourth International Conference on Water Resources and Renewable Energy Development in Asia, Thailand, 2012.
[16] B.S. Thapa, M. Eltvik, K. Gjosaeter, O.G. Dahlhaug, B. Thapa, Design Optimization of Francis Runners for Sediment Handling, Water resources and Renewable energy Development in Asia, Thailand, 2012.
[17] J.C. Lagarias, J.A. Reeds, M.H. Wright, P.E. Wright, Convergence properties of the Nelder–Mead simplex method in low dimensions, SIAM J. Optim. 9 (1998) 112–147.
[18] C.B. Solnordal, C.Y. Wong, A. Zamberi, M. Jadid, Z. Johar, Determination of erosion rate characteristic for particles with size distributions in the low Stokes number range, Wear 305 (2013) 205–215.
[19] J.J. Coronado, Abrasive size effect on friction coefficient of AISI 1045 steel and 6061-T6 aluminium alloy in two-body abrasive wear, Tribology Lett. 60 (2015) 1–6.
[20] G.R. Desale, B.K. Gandhi, S.C. Jain, Effect of erodent properties on erosion wear of ductile type materials, Wear 261 (2006) 914–921.
[21] G. Stachowiak, G. Stachowiak, The effects of particle characteristics on three-body abrasive wear, Wear 249 (2001) 201–207.

5. ARTICLE 3: MINIMIZING EROSIVE WEAR THROUGH A CFD MULTI-OBJECTIVE OPTIMIZATION METHODOLOGY FOR DIFFERENT OPERATING POINTS OF A FRANCIS TURBINE

Elsevier Editorial System(tm) for Energy
Manuscript Draft

Manuscript Number:

Title: Minimizing erosive wear through a CFD multi-objective optimization methodology for different operating points of a Francis turbine

Article Type: Full length article

Keywords: Erosion wear; Computational Fluid Dynamics; Francis turbines; Optimization; Genetic Algorithms; Artificial Neural Networks

Corresponding Author: Mr. Ruben Dario Aponte Nuñez,

Corresponding Author's Institution: Universidad del Valle

First Author: Ruben Dario Aponte Nuñez

Order of Authors: Ruben Dario Aponte Nuñez; Leonel Alveyro Teran Llorente; Juan Fernando Grande Gil; John Jairo Coronado Marin; Jair Alexander Ladino Ospina; Francisco Jose Larrahondo Cobo; Sara Aida Rodriguez Pulecio

Abstract: Erosive wear has been a serious concern mainly in run-of-the-river medium and small Francis turbines from both economic and technical point of view. With the aim to find ways of mitigation of erosive wear, this paper proposes a methodology to obtain, via optimization approach, geometries that maximize the resistance to erosive wear by hard particle and cavitation of the internal components (runner, guide vanes and cover labyrinths). This improvement was done to reduce the time and costs of corrective maintenance and to maximize the machines availability and energy generation profits. The methodology used Computational Fluid Dynamics and optimization techniques such as design of experiments of factorial type, artificial neural networks and genetic algorithms, with a multi-point and multi-objective approach, simultaneously erosive wear by hard particle and cavitation damage as well as efficiency. A new geometry was obtained for the turbine, 35% more resistant to erosive wear by hard particle and cavitation damage for the different operating points, maintaining efficiency close to the original value throughout the operating range. With the optimized geometry, a mechanical check was performed using finite element simulations to validate that the optimal geometries had the required strength.

Suggested Reviewers: Saurabh Sangal
er.saurabh.sangal@gmail.com

Biraj Singh Thapa
bst@ku.edu.np

Ole Gunnar Dahlhaug
ole.g.dahlhaug@ntnu.no

July 25, 2018

Energy,

this work develops an optimization methodology to couple the CFD models using a two-phase fluid-particle model with an erosion model, with multi-point (operation at optimum point of operation and under partial load) and multi-objective (performance increase in efficiency, resistance to erosive wear by hard particle and by cavitation) optimization algorithm to solve the problem in Amaime's facility. The optimization methodology was implemented based on studies using Computational Fluid Dynamics (CFD), genetic algorithms (GA), artificial neural networks (ANN) and design of experiments (DOE). A new geometry was obtained for the turbine, 35% more resistant to erosive wear by hard particle and cavitation damage for the different operating points, maintaining efficiency close to the original value throughout the operating range. With the optimized geometry, the verification process of the new design was continued, and mechanical strength analysis, modal analysis and fatigue verification were performed using finite element simulations to validate that the optimal geometries had the required strength.

The authors,

Ruben Dario Aponte
Leonel Alveyro Teran
Juan Fernando Grande
John Jairo Coronado
Jair Alexander Ladino
Francisco Larrahondo
Sara Aida Rodríguez

Highlights

- CFD, optimization and machine learning were combined to improve a Francis turbine.
- A new improved geometry of the runner blades, guide vanes was obtained.
- A mechanical verification of the optimized components was performed.

Minimizing erosive wear through a CFD multi-objective optimization methodology for different operating points of a Francis turbine

R.D. Aponte[1 2], L.A. Teran[1], J.F. Grande[1], J.J. Coronado[1], J.A. Ladino[1], F.J. Larrahondo[2], S.A. Rodríguez[1]

[1]*Research Group of Fatigue and Surfaces, School of Mechanical Engineering, Universidad Del Valle, Cali, Colombia*

[2]*EPSA E.S.P. A CELSIA Company*

1. Abstract

Erosive wear has been a serious concern mainly in run-of-the-river medium and small hydro power facilities from both economic and technical point of view. With the aim to find ways of mitigation of erosive wear, this paper proposes a methodology to obtain, via optimization approach, geometries that maximize the resistance to erosive wear by hard particle and cavitation of the internal components (runner, guide vanes and cover labyrinths). As application case, Francis turbines data from Amaime hydraulic power plant, operated by the CELSIA E.S.P. Company in southwestern Colombia are used. This improvement was done to reduce the time and costs of corrective maintenance and to maximize plant availability and energy generation profits. The methodology used to achieve this goal uses Computational Fluid Dynamics (CFD) and optimization techniques such as design of experiments of factorial type, artificial neural networks and genetic algorithms, with a multi-point and multi-objective approach, since were considered different points of operation, simultaneously erosive wear by hard particle and cavitation damage as well as efficiency. A new geometry was obtained for the turbine, 35% more resistant to erosive wear by hard particle and cavitation damage for the different operating points, maintaining efficiency close to the original value throughout the operating range (differences smaller than 3%). With the optimized geometry, the verification process of the new design was continued, and mechanical strength analysis, modal analysis and fatigue verification were performed using finite element simulations to validate that the optimal geometries had the required strength.

2. Introduction

Amaime hydraulic power plant, which has a total generation capacity of 19.9 MW, is a run-of-the-river facility with two Francis turbines of 9.95 MW each one, that is, they don't have a dam before the penstock pipe. The main characteristics of each turbine are shown in Table 1. This plant started operations in 2011 and after 5 months of operation, turbine units began to show signs of low performance and wear on the runner, cover labyrinths and guide vanes, which was revealed by the high temperature in the thrust bearing. These damages cost the company over the first 2-year period $ 400,000, due to repairs, and the efficiency of the machines decrease up to 25% due to severe wear [1, 2]. The high concentration of solid particles in the water striking over the components largely generates this erosive wear. In addition, the water availability which varies according to the time of year, makes not possible to operate at the Best Efficiency Point (BEP) due to the low flow rate during summers and in the rainy seasons operation is restricted due to the high amount of

sediments in the river, causing an operation regime at partial load. This partial load generates high pressure gradients and as a consequence of this, recirculation profiles appears downstream the blades and the appearance of the cavitation wear , increases the total wear of their components [2].

Particle and cavitation wear are common issues specially in reaction turbines run-of-the-river installations. Those issues have been mitigated around the world with different strategies such as sediment monitoring [3], operation strategies to reduce the wear cost [2], study of desanders [4], turbines geometric optimization [5-15] and improvement of the materials used in the turbine components [16-24].

Table 1. Main characteristics of Amaime´s hydraulic power plant turbine.

	Value
Length of Inlet pipe [m]	4865
Net Head [m]	195.98
Nominal Speed [rpm]	720
Capacity [MW]	10
Design Flow Rate [m^3/s]	6

One of the first studies that evaluates the effect of erosion wear specifically in Francis turbines with a CFD approach was made by Neopane in 2010 [7], where were performed a two-phase CFD study of a Francis turbine where not only different hydraulic characteristics of the turbine were evaluated, but also the effect of erosive wear by hard particles immersed in the water was considered. As a result of his research he concluded that operating the turbine at maximum load not only generates low efficiency but also high turbulence intensities and inlet relative velocities greater than the output of the runner generating swirling flows. With respect to erosion wear, he found that the implemented CFD model agrees with experimental tests and the erosion rate increases when the turbine is operating outside the BEP. Also, in 2011 Lain *et. al* [6], as a part of a global analysis of CFD simulations of Francis turbines, estimated the effect of operating a 10MW Francis turbine out of the BEP with different problematic operation conditions such as erosion wear, cavitation, hydraulic losses and fatigue. They found an increment of 200% in erosion wear when turbine is operating out the BEP compared with the erosion damage at its BEP. The last is due to vortex formation by high pressure gradients near the hub and shroud of the runner. However, in that research, no optimization studies were developed, only CFD studies of actual operating conditions were performed.

In the optimization process of a Francis turbine by means of a CFD studies, Derakhshan et al. [9] used a multi-objective optimization method based on artificial neural networks, genetic algorithms and CFD package to solve the Navier - Stokes 3D equations. The objective of this research was to increase the overall efficiency of the turbine at BEP by changing the profile of the runner blades keeping the net head as a constrain. The maximum error in efficiency computed numerically was 0.22% compared measured data. As a result of the optimization process, a 1.8% increment in efficiency was achieved compared with the initial geometry.

Considering the previous approaches, in 2014 Terán et al [10] used CFD in the development of a new geometry that increased the efficiency of a Francis turbine (designed

and built more than one hundred years ago) to a value close to recent turbines. Due to the complexity of the geometry, they implemented a methodology that combines a factorial design of experiments, artificial neural networks and optimization by genetic algorithms. Modifications were made in the runner blades and covers focused to reduce recirculation on the runner blade and keeping to the minimum the phenomenon of main cavitation which cause wear at the runner outlet. Finally, with the modifications obtained and after the implementation an increase in efficiency of 14.77% at BEP was achieved, which managed to increase energy production to 16.4%.With the objective to evaluate erosion wear in the runner of the turbine, Thapa et al. in 2012 [8] performed an optimization study by means of "KHOJ" in house software and complemented with CFD simulations comparing different shapes of runner blades that allowed to reduce the recirculation and relative speeds and a consequent erosion reduction confirmed with the *a posteriori* CFD simulations. In fact, CFD results showed that the shape with warp blades has a significant effect on the velocity distribution and therefore over the erosion rate, reducing this effect by 33% with respect to the original model. Therefore, this work develops an optimization methodology to couple the CFD models using a two-phase fluid-particle model with an erosion model, exposed in the previous literature review, with multi-point (operation at optimum point of operation and under partial load) and multi-objective (performance increase in efficiency, resistance to erosive wear by hard particle and by cavitation) optimization algorithm to solve the problem in Amaime's facility. The optimization methodology was implemented based on studies using Computational Fluid Dynamics (CFD), genetic algorithms (GA), artificial neural networks (ANN) and design of experiments (DOE).

3. Materials and methods

The process to optimize the turbine components, began with the geometric modelling by means of Computer Aided Design (CAD) base on manufacturing drawings and 3D scanning to runner blades and guide vanes reconstruction. A complete CFD model implemented in ANSYS CFX was made to capture all the hydrodynamic features and variables (i.e. efficiency, power, flow rate, net head) and a simplified CFD model consisting of a section of guide vanes, runner and cover labyrinths to quickly compute the erosion phenomena. Mesh convergence, results and validation analysis were deeply developed and standardized in [2] and applied in this work. Also, the Tabakoff and Grant erosion model implemented in ANSYS CFX was validated with experimental data reported in [25, 26] and a CFD simulation of those experiments to find calibration constants for the quartz-CA6NM-steel interaction [27]. The optimization process followed a sequential procedure: First, the guide vanes optimization was performed, followed by the runner blades and finally the analysis of labyrinths, in order to reduce computational effort to achieve convergence in the optimization process.

An analysis of variance (ANOVA) was implemented, with the main objective to see the effect of changing the geometry of the cover labyrinths in places where the change of fluid direction takes place by mean of chamfers (a total of 5 parameters were analyzed), this analysis led to no significant changes in the erosion rate for both generator side, cover labyrinths and suction side cover labyrinths. This is due to the restrictions in the geometry that only allow changes in places where the fluid directions change, i.e, in the labyrinths

corners where chamfers were proposed. This analysis is not presented in this paper due to it did not lead to significant changes.

3.1. Parametrization and objective function

The approach for the model parametrization was made for the two objects of reference, i.e. the guide vanes and runner.

Guide vanes: These have a constant section profile as they do not have twist angle, so they were parametrized by a 2D Bezier function defining the angle z of the camber line in Figure 1 which initial geometry is based on manufacturing drawings. The polynomial function form of 5 parameters is given as:

$$z = A(1-y)^3 + (B - Cx^2)(1-y)^2 + (1-y)(D - Ex^3) + 16.2 \quad (1)$$

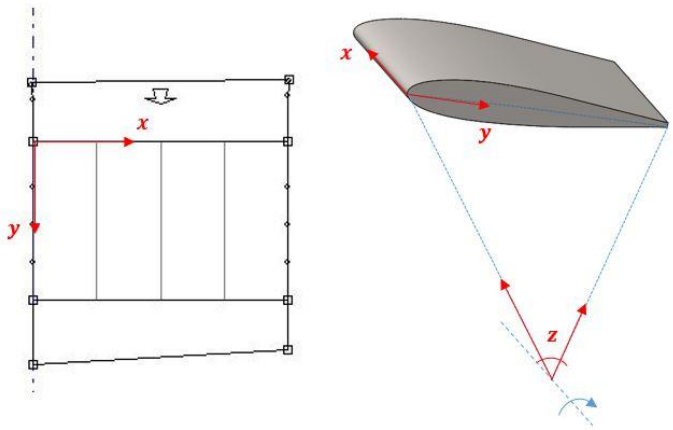

Figure 1.Guide vane parametrization.

Although the clearance between the guide vanes and the wear ring is directly correlated with the wear rate in that area [28], it remained at 0.2 mm, which is the minimum value allowed for mounting.

Runner: After the 3D scan and CAD modelling, the runner blade surface was characterized by surface function of a third order polynomial, with calibration constants obtained by mean of least squares algorithm. The equation of 9 parameters is:

$$z = Ay + Bx + Cy^2 + Dyx + Ex^2 + Fy^3 + Gy^2x + Hyx^2 + Ix^3 \quad (2)$$

In both equations (1) and (2), x and y represents the spatial coordinate over the blade surface, and z is the angular position of a point in the blade's mean surface defined by the camber lines. Coefficients A to I are the calibration parameters of the blade, which change in the optimization process (See Figure 1 and Figure 2). Finally, the thickness for both guide vanes and runner blades, which is defined as a function of the camber line, remained the same as in the original design.

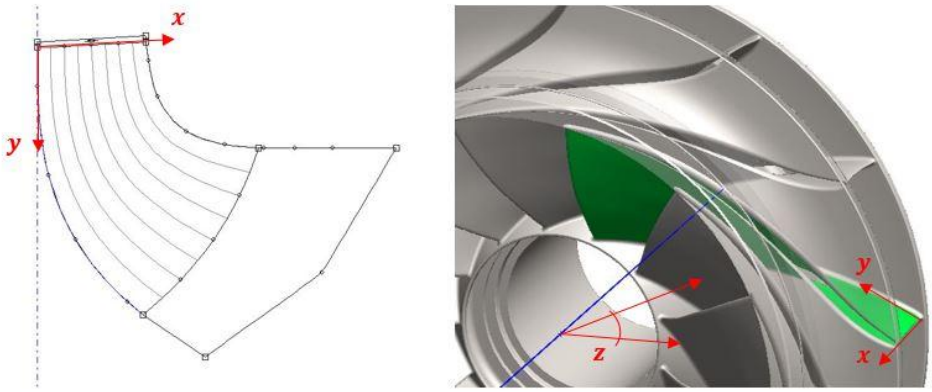

Figure 2. Runner blade parametrization.

Objective function: *Terán et. al.* [2] based on the historical operation data of the facility, showed that there are two points of high operation frequency which are 10 MW (at the BEP) and 3MW (at partial load). That is why the objective function was chosen to be multi-point and multi-objective, in which the blades profiles could have an optimal performance in both points. For the guide vanes and runner blades, the objective function is:

$$OF_T = (OF_{@3MW}) + (OF_{@10MW}) \tag{3}$$

Where OF_T is the global objective function defined as the superposition of an objective function for each operating point, which is given by:

$$OF_{@} = w_\eta \left(\frac{\eta_{req} - \eta}{\eta_{req}}\right)^2 + w_e \left(1 - Log\left(\frac{ER}{ER_{req}}\right)\right)^2 + w_h \left(\frac{H_{req} - H}{H_{req}}\right)^2 + w_c \left(\frac{A_{req} - A}{A_{req}}\right)^2 \tag{4}$$

Where η_{req} , ER_{req} , H_{req} and A_{req} are required efficiency, erosion rate, net head and cavitated surface (is the area of an isosurface obtained at the value of vapor pressure of water at work temperature, which encloses the region were cavitation can appear) respectively. In the same way, η , ER , H and A are the efficiency, erosion rate, net head and cavitated surface obtained from the CFD simulation. Each term of the Equation 4 represents the relative error between the value obtained in each iteration and the desired objectives. Also, w represents the weight of each term in order to define which variable is more important, giving bigger relevance to the erosion rate, which is expressed in logarithm form due to its small value. The values of w_η, w_e, w_h and w_c are 10, 10, 1 and $1x10^{-5}$ respectively.

3.2. Design of experiments, artificial neural networks and genetic algorithm

Fractional factorial design of experiments was used to obtain the most relevant aspects from the runner blades, guide vanes and labyrinths parameters, in order to train the neural network efficiently in a shorter simulation time [5]. In this process, high and low values for the parameters were used; and an initial database was built with 32 individuals for the runner blades (factorial design 2^{n-k}, with $k = 4$) and 32 individuals for the guide vanes (factorial design 2^n). Each individual (geometries) was simulated using a CFD simplified model to obtain efficiency, wear rate, net height and cavitation area and the corresponding value of the objective function, as describe in [2].

With the built database as input, artificial neural network (ANN) was used to obtain an output solution field of the objective function as function of the parameters. The learning capability of the ANN allows the prediction of the objective function of a new geometry candidate as the database grows in the iterative process of the optimization. This makes the optimization process shorter as it is not necessary a CFD simulation. That is, no solution of flow equations is needed to obtain an objective function for each candidate as the ANN predict them from the actual database.

Finally, genetic algorithm (GA) analyzes all the database in an evolutionary process of selection, recombination and mutation of each database individual, to create a candidate with the characteristics that minimizes the objective function. Without the use of ANN, the GA needs to evaluate each candidate with CFD simulation which implies a large amount of CPU time. When a candidate is chosen, the proposed geometry is simulated using CFD and it becomes part of the database, making it to grow and focus on the most relevant characteristics that make the objective function be minimized: This is the learning optimization process. The process in graphical for of DOE-ANN-GA integrated optimization process is shown in Figure 3. Also, it is important to note that the overall optimization process described above, follows the approaches made by [5, 9, 10] and the corresponding schematic block diagram is shown in Figure 4.

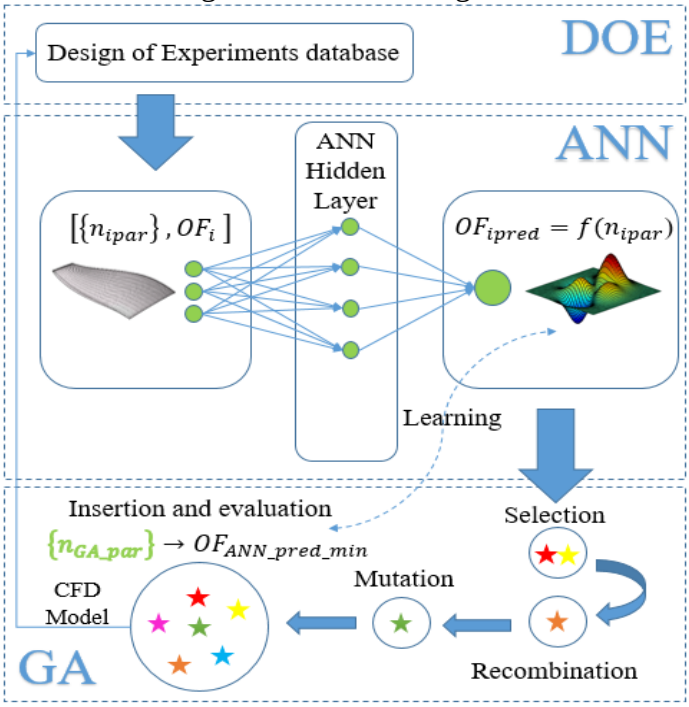

Figure 3. Schematic process of integrated DOE-ANN-GA optimization.

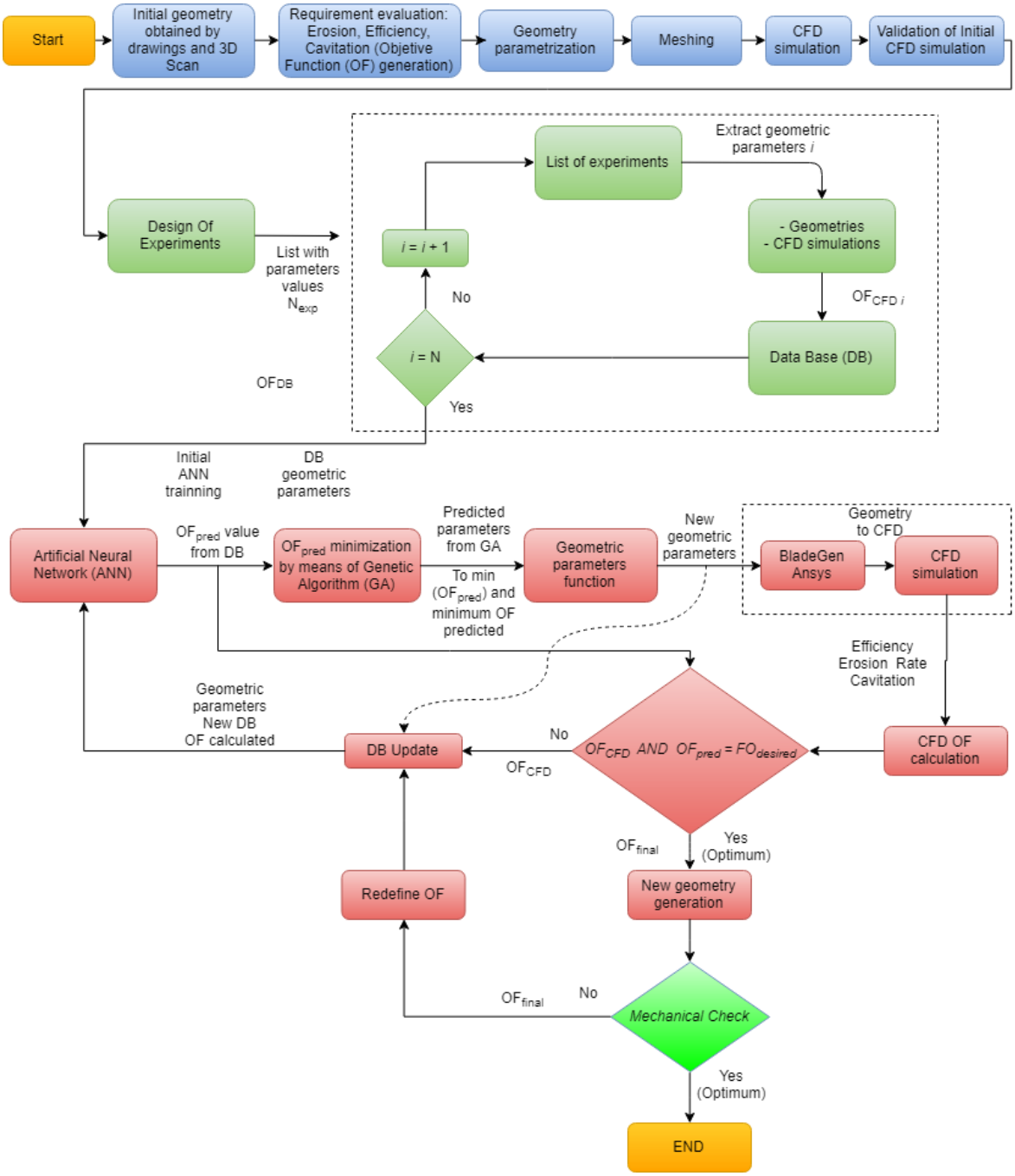

Figure 4. Schematic block diagram of the overall turbine optimization process.

3.3. Guide vane structural integrity analysis

In order to perform a comprehensive integrity analysis, high resolution unsteady CFD simulations around the guide vanes were made in order to capture high frequency trailing edge vortices, their behavior and their influence in unsteady pressure loads. The frequencies of the pressure and load fluctuations around the guide vane for the new optimized geometry

were evaluated by means of modal analysis and compared with the frequencies for the original geometry and with guide vane natural frequency.

Also, a study of the geometry at the trailing edge that best behaves in terms of the frequency of pressure fluctuations was also carried out. In the Figure 5, β and d are the chamfer angle and chamfer offset and were evaluated from 15 to 60 degrees and 0 to 3.5 mm respectively.

For static structural analysis, pressure distribution was imported from the 3D CFD analysis as load conditions and cylindrical support were set on the guide vane shaft. On the other hand, trailing edge vortices analysis used a 2.5D CFD approach with Large Eddy Simulation (LES) as turbulence model (see Figure 5b); No induced vortices were considered in this analysis. The complete setup definition of the three simulations approach is described in Table 2. For all simulations, the mesh convergence studies gave differences up to 1% in the reference variables between the two finest meshes.

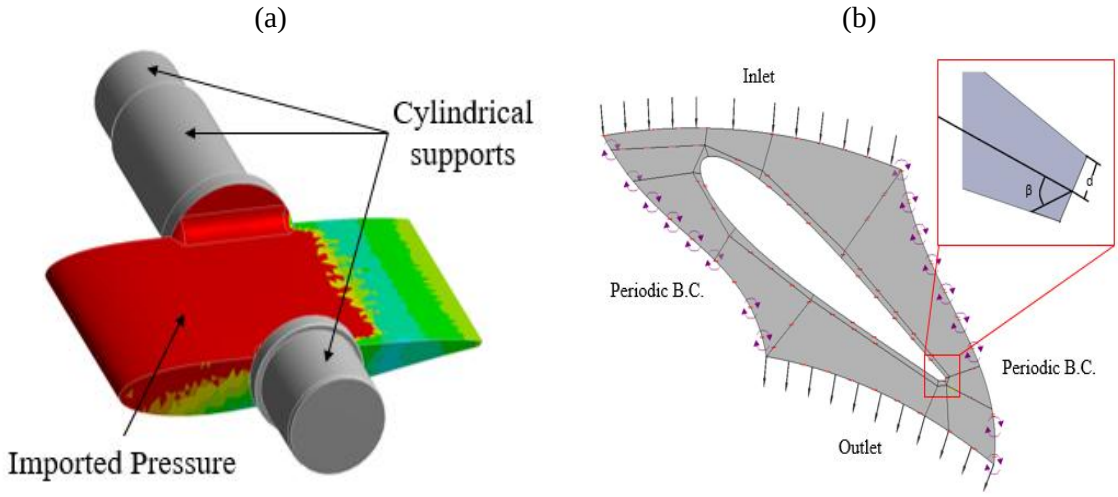

Figure 5. Boundary conditions for the guide vane at (a) 3D structural analysis and (b) Von Karman 2D LES analysis.

Table 2. Definition of simulations and models used for the guide vanes.

	FEA Structural Analysis 3D	**CFD 3D**	**LES Analysis CFD 2.5D**	**Modal Analysis 3D**
Mesh type	Tetrahedral	Tetrahedral	Structured hexahedral	Tetrahedral
Number of elements	68.596	499.482	274.606	82.813
Simulation type	Linear static	Stationary	Transient	Modal
Turbulence model	N/A	N/A	LES Smagorinsky	N/A
Total simulated time	N/A	N/A	0.05 s	N/A
Time step	N/A	N/A	1×10^{-5} s	N/A

3.4. Runner structural verification

A Finite Element Analysis (FEA) was performed to verify the structural integrity of the runner after the optimization process. In the same way as the guide vanes, a static structural simulation was made, using the pressure distribution obtained in the CFD analysis as loads and the nominal rotational frequency in a case and overspeed. Also, a transient CFD simulation where developed to obtain the pressure fluctuation throughout the runner, and with the aim of compare the excitation frequency with the natural frequency obtained in a modal check for the runner-shaft-flywheel-rotor group. Also, the transient simulation leads to obtain the pressure distribution that carry to the minimum and maximum stress for a fatigue analysis (See Figure 6). The complete setup definition of the two simulations approach is described in Table 3. For all the simulation the mesh convergence was 5%.

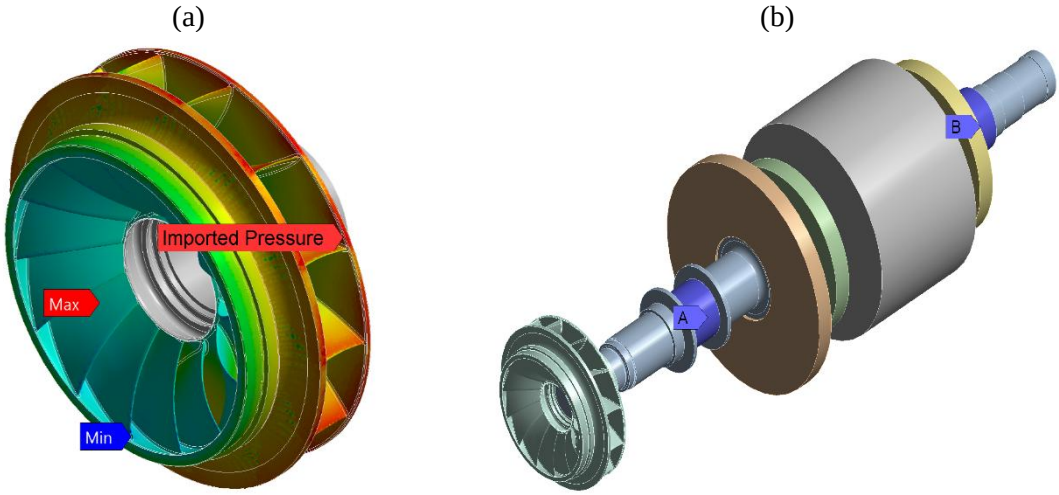

Figure 6. Boundary conditions for the runner at (a) 3D structural analysis and (b) 3D modal analysis.

Table 3. Definition of simulations and models used for the runner.

	FEA Structural Analysis	**CFD 3D**	**Modal Analysis**	**Transient Analysis**
Mesh type	Tetrahedral	Structured hexahedral	Tetrahedral	Structured hexahedral
Number of elements	588.371	2.359.043	676.368	2.359.043
Simulation type	Linear static	Steady State	Modal	Transient
Turbulence model	N/A	N/A	N/A	SST
Total simulated time	N/A	N/A	N/A	0.25 s
Time step	N/A	N/A	N/A	2.31×10^{-4} s

4. Results

4.1. Guide vane optimization

The complete optimization process for the guide vanes ended in the 167th iteration with an ANN prediction error below than 7%, as shown in Figure 7.

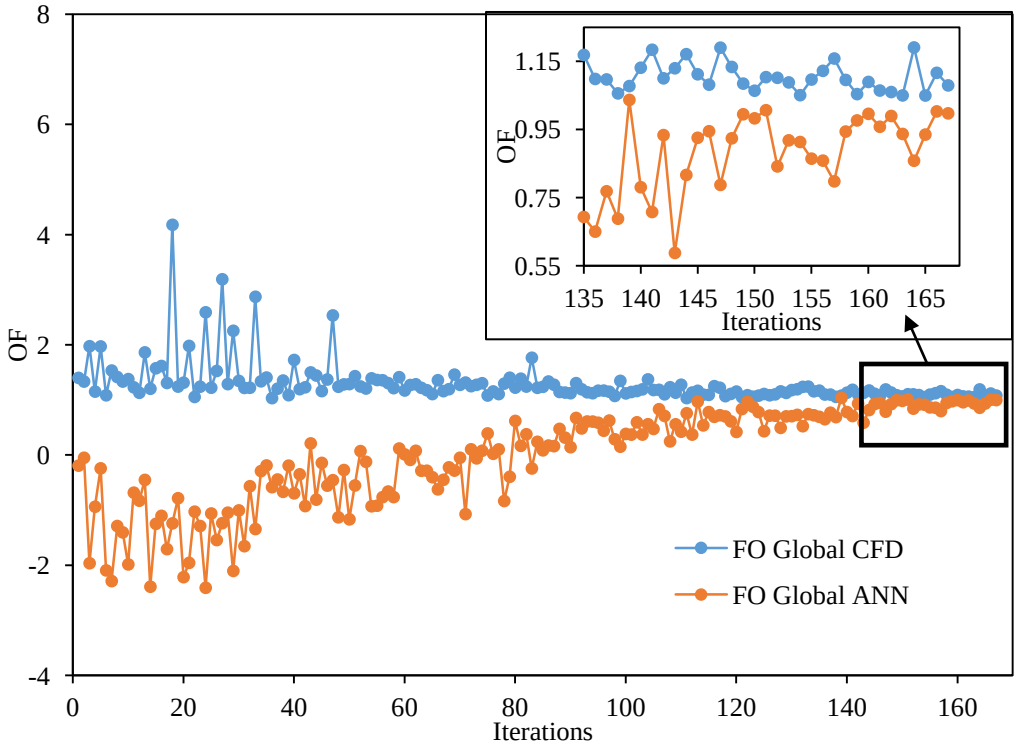

Figure 7. Guide vane optimization convergence.

In Table 4 are shown the efficiency and the erosion rate of original and optimized guide vane and it can be seen that there is not a significant change in the efficiency itself in both operation points (less than 2%); but in the erosion rate there is a decrease up to 24%.

Table 4. Guide vane erosion and efficiency comparison between original and optimized blade shape.

	Original	Optimized	Difference
Efficiency @ 3MW [%]	83.58	83.57	-0.01
Efficiency @ 10MW [%]	91.62	89.84	-1.78
Erosion Rate @ 3MW [x 10^{-8} Kg/s]	12.80	9.83	-23%
Erosion Rate @ 10MW [x 10^{-8} Kg/s]	4.69	3.55	-24%

On the other hand, the blade profile slightly changed, where the optimization process leaded to reduce the clearance leakage flow by driven towards a non-symmetric profile, which reduces the formation of horseshoe vortex and vortex filaments at the guide vane inlet and outlet respectively. A similar strategy was recommended by Lain *et. al* [6] and

Chitrakar [29]. The Figure 8 shows the optimized profile above the original and also the reduction of the erosion rate density is shown in Figure 9.

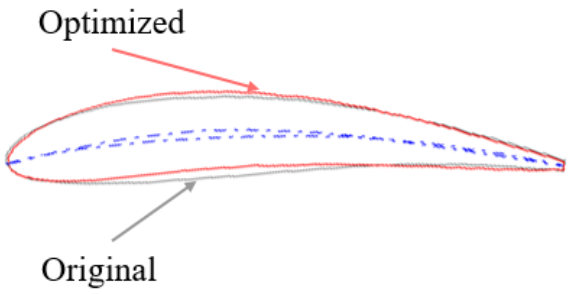

Figure 8. Guide vane profile optimization.

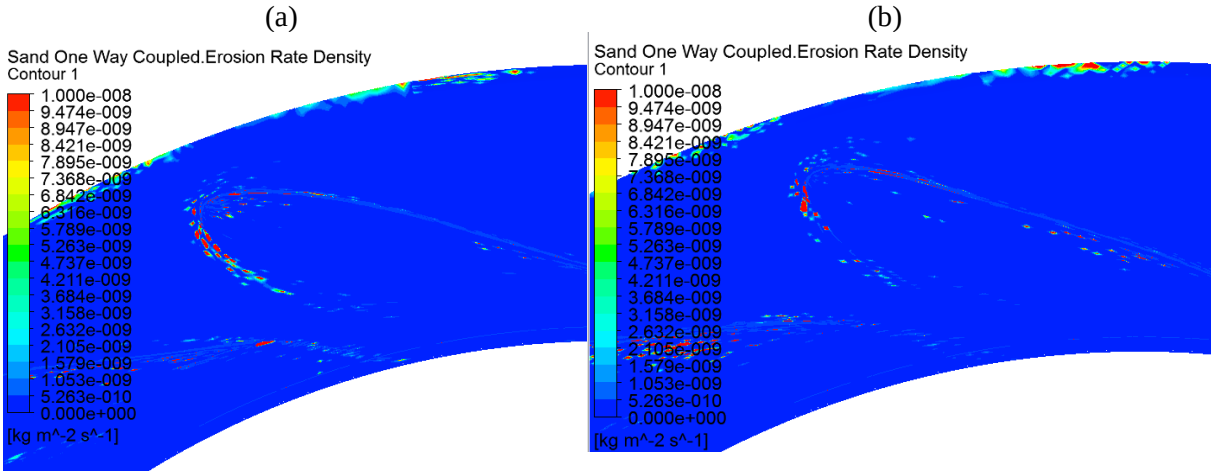

Figure 9. Erosion rate density on the covers at the clearance between guide vane and cover for(a) original guide vane (b) Optimized guide vane

As described in section 3.3, Von Karman vortex generation leads to a modal structural check in which the Von Karman vortex generation frequency could have an important effect in the structural stability; it was found that the shape of the trailing edge had a direct relationship with this frequency in the same wat as reported in [29]. At the beginning of the optimization, the blade profile does not had a chamfer in the trailing edge as the original profile had. Therefore, in orden to obtain a permisible modal safety factor, the best size of the chamfer was determined.

The Figure 10.a shows the Von Karman vortex generation in the guide vane with chamfer which frequency is 1070 Hz and the first mode of vibration at 1415 Hz is shown in Figure 10.b. The maximum difference between those frequencies is 24%, which is considered to be in a safety zone according to [30], and it is found where $\beta = 60º$ and $d = 0$.

(a) (b)

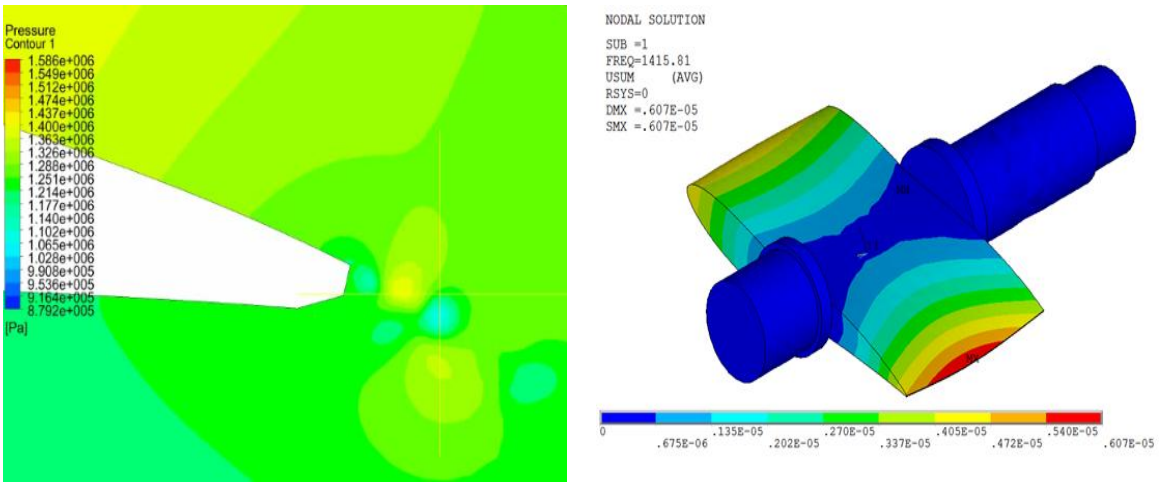

(c)

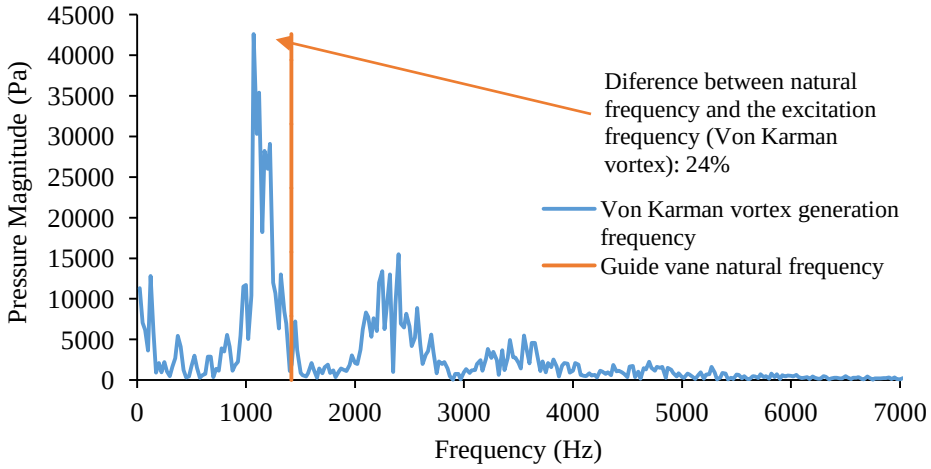

Figure 10. Guide vane modal analysis (a) Von Karman vortex generation $\beta = 60º$ $d = 0$ ((b) Guide vane natural 1st mode frequency and (c) frequency comparison.

4.2. Runner optimization

For the runner, the complete optimization process ended in the 120th iteration with and ANN prediction error below than 15%, as shown in Figure 11.

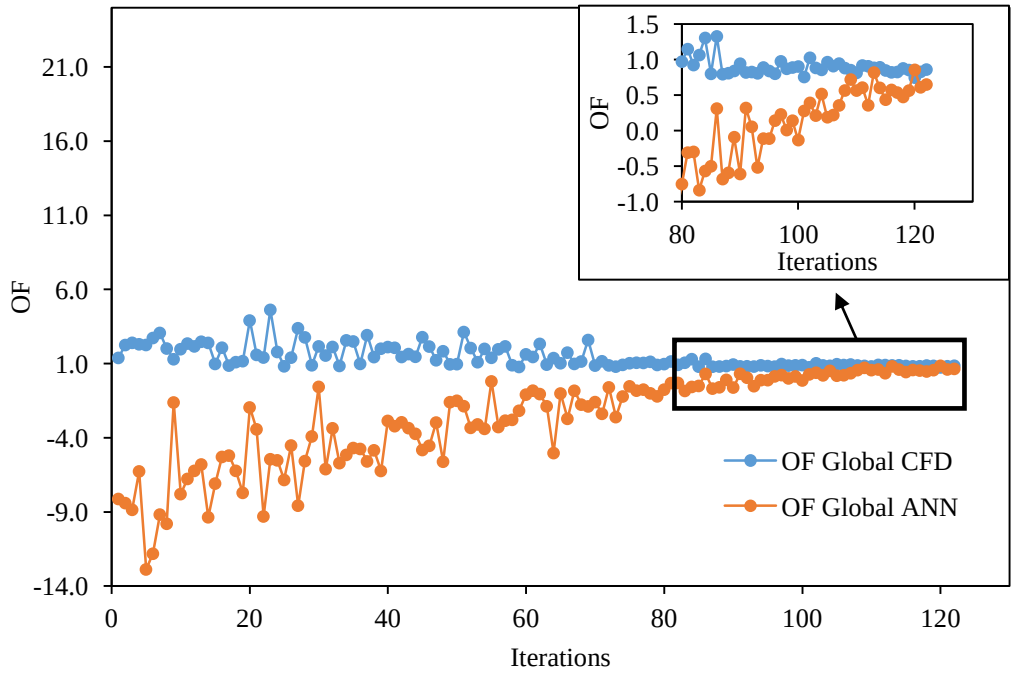

Figure 11. Runner optimization convergence

In Table 5 are presented the efficiency and erosion rate at 3MW and 10 MW for both the original and optimized runner geometries. Analyzing the efficiency and the erosion rate, it can be seen that there is not a significant change in the efficiency itself in both operation points (less than 2%); but in the erosion rate there is a decrease up to 75%. The Figure 12 shows the optimized profile compared with the original geometry and reduction of the erosion rate density is shown in Figure 13 and Figure 14.

Table 5. Runner comparison.

	Original	**Optimized**	**Difference**
Efficiency @ 3MW [%]	83.58	83.57	-0.01
Efficiency @ 10MW [%]	91.62	89.84	-1.78
Erosion Rate @ 3MW [x 10^{-8} Kg/s]	86.52	21.77	-75%
Erosion Rate @ 10MW [x 10^{-8} Kg/s]	21.25	17.41	-18%

(a) (b)

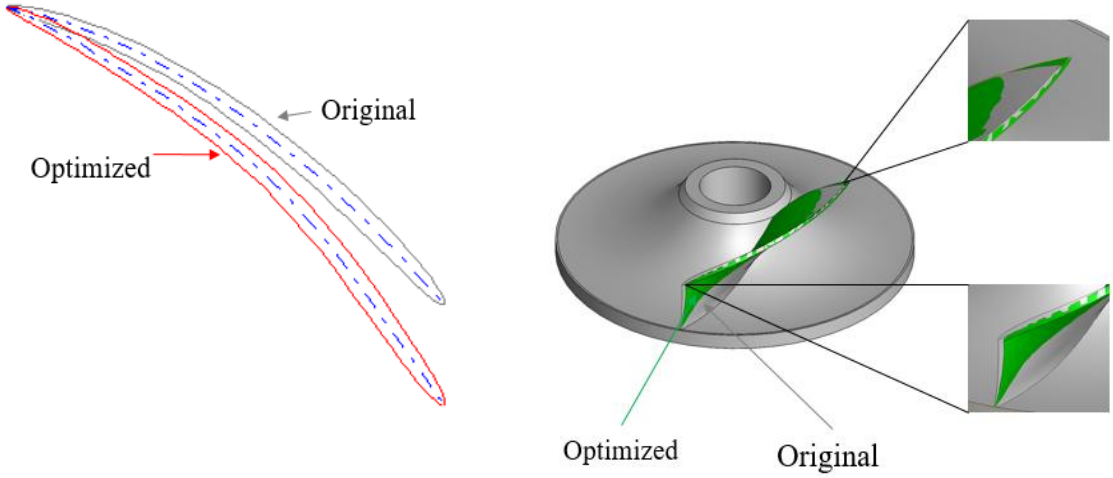

289 *Figure 12. Runner optimized profile above the original (a) meridional section (b) 3D superposition*

(a) (b)

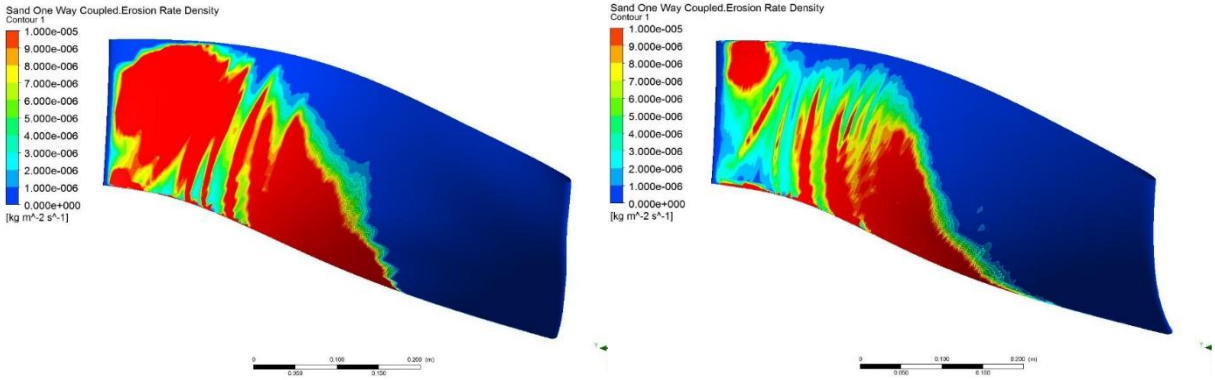

290 *Figure 13. Erosion rate density in suction side for 3MW blade in (a) original runner profile and (b) optimized runner*
291 *profile.*

(a) (b)

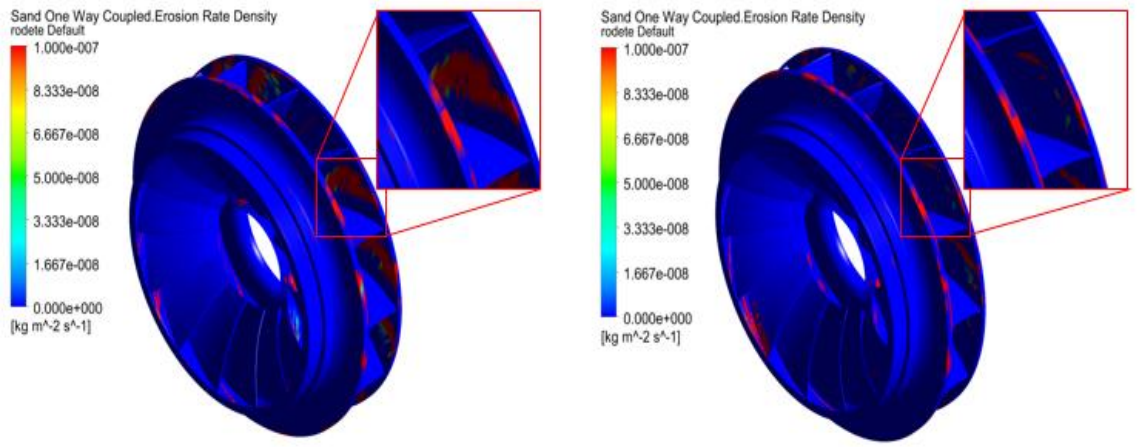

Figure 14. Runner overall erosion rate density at 3MW in (a) Original runner geometry and (b) Optimized runner geometry

(a) (b)

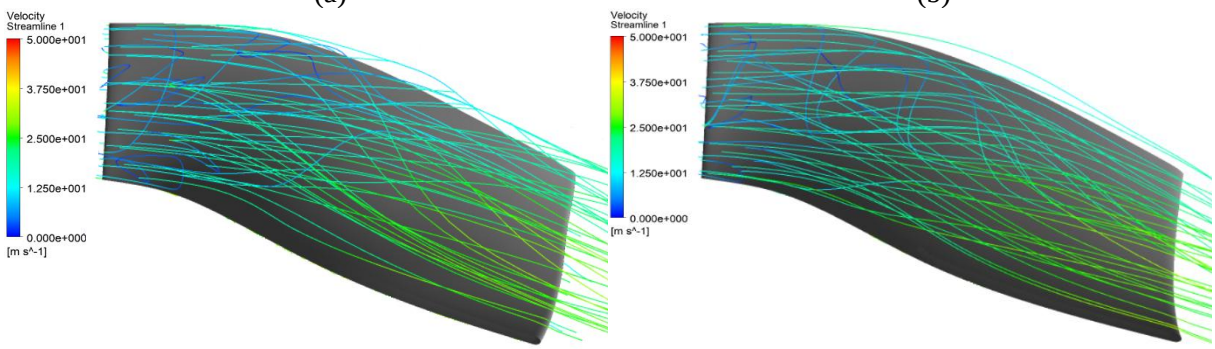

Figure 15. Streamlines around the blade for 3 MW (a) original profile and (b) optimized profile.

Figure 15 shows a reduction of the recirculation around the first half of the blade and between blades with a consequent reduction of erosion wear was observed. Similar results were obtained by [6, 31] where the increase in erosion is attributed to the formation of vortices caused by the increase in relative velocities. The Figure 16 shows the normalized blade angle distribution relative to inlet angle at 50% blade span for in the optimization process for the original shape and the optimized blade and with another optimum candidate (shape 116), these last two, with a more smoothed distribution and a consequent decrease in the relative velocities.

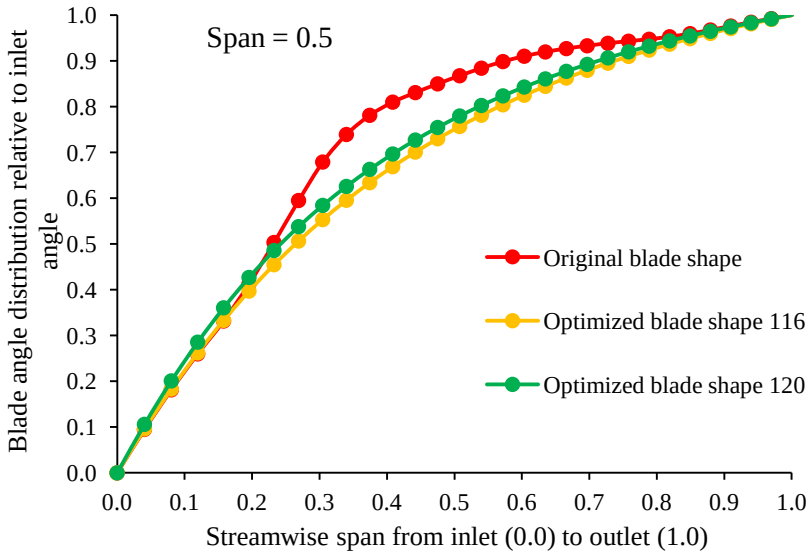

Figure 16. Blade angle distribution shape comparison during optimization process.

4.3. Mechanical strength analysis

For the pressure distribution given by the stationary CFD analysis, the maximum equivalent Von Mises stress was 72.75 MPa at 10MW in the guide vane, located in the root of the guide vane support, as the guide vanes materials is an ASTM A743 grade CA6NM (S_y = 550 MPa, S_{ut} = 755 MPa and E = 200 GPa [32]) which leads to a value of 10.1 for the static safety factor (see Figure 17).

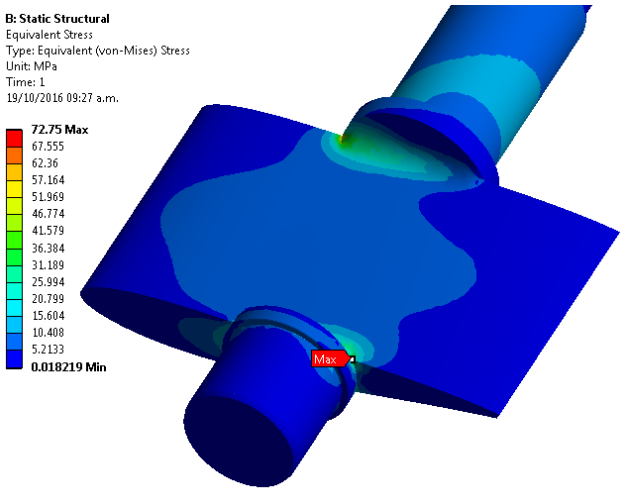

Figure 17. Guide vane static structural analysis at 10 MW.

With a transient CFD simulation, the variation of the pressure was obtained in the pressure side surface on the guide vanes (Figure 18a). the fatigue safety factors for the different operating powers were calculated and it was concluded that the power which could generate more fatigue damage is 10MW with a safety factor of 2.08 for $1x10^{10}$ cycles corresponding to 31 years of operation. The S_e value was estimated using the

recommendations made by [33], applying correction factors for shape, roughness, reliability and coating surface type for the resistance to 10^6 cycles and extrapolating the life curve.

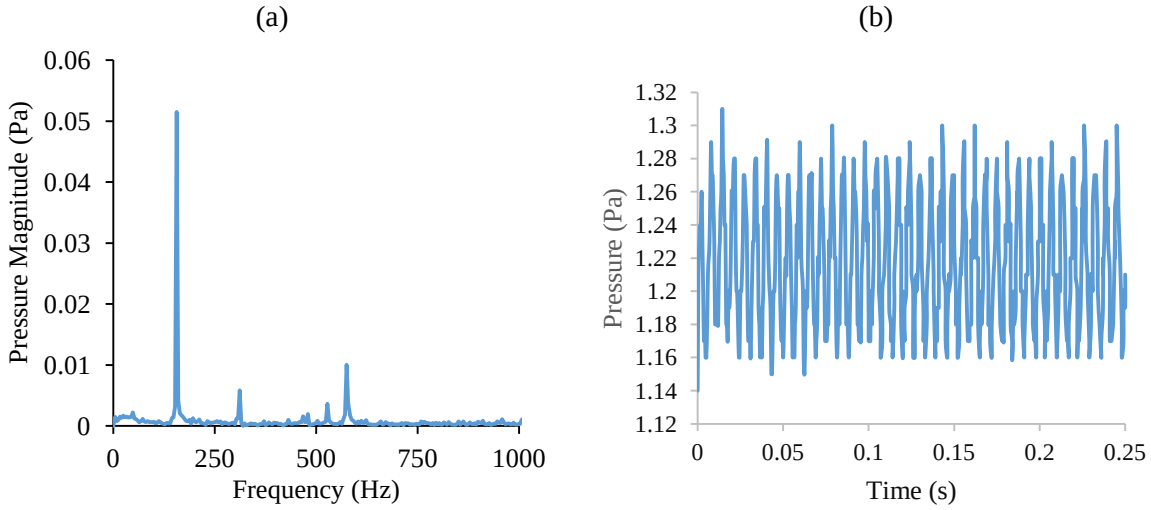

Figure 18. Guide vane dynamic analysis (a) frequency domain pressure and (b) time domain pressure.

The maximum stress is located in the blade root trailing edge in the Francis turbines and is higher at high powers [6], therefore the static structural analysis of the runner was made at the BEP and for two speed points, i.e., synchronic speed with electrical load at 10 MW and overspeed. Figure 19 shows the Von Mises stress comparison for the original and optimized runner at 10 MW @ 720 rpm.

Knowing that the material of the runner is a stainless-steel ASTM A743 grade CA6NM and although both the stresses and the displacements for the optimized runner were greater than those on the original runner in 26% and 9% respectively, it keeps quite reliable static safety factors so that the optimized blades against static loads remains resistant, even at overspeed regime. (See Table 6).

(a) (b)

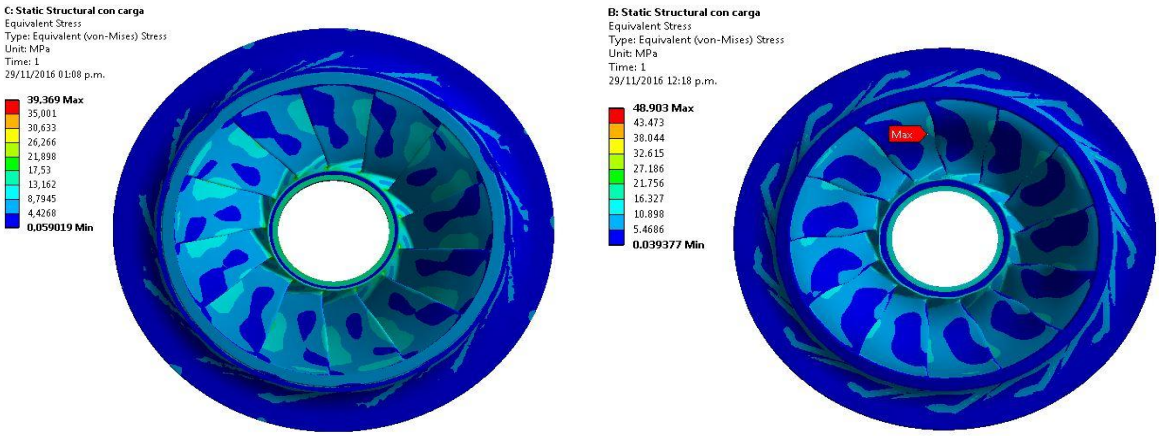

Figure 19. Von Mises stress for the 10 MW (a) original and (b) optimized runner.

Table 6. Runner static stresses and displacements for 10 MW.

	With load @ 720 rpm	Without load @ 1440 rpm
Maximum von Mises stress (MPa)	39	165
Static Safety factor	11.25	3.33
Displacements (mm)	0.1	0.34
Radial Displacements (mm)	0.09	0.35

The modal and dynamic check for the runner was made based on the rotor-stator interaction at the outlet of the guide vanes and the inlet of the runner. The Figure 20 shows the pressure fluctuation in this part of the turbine.

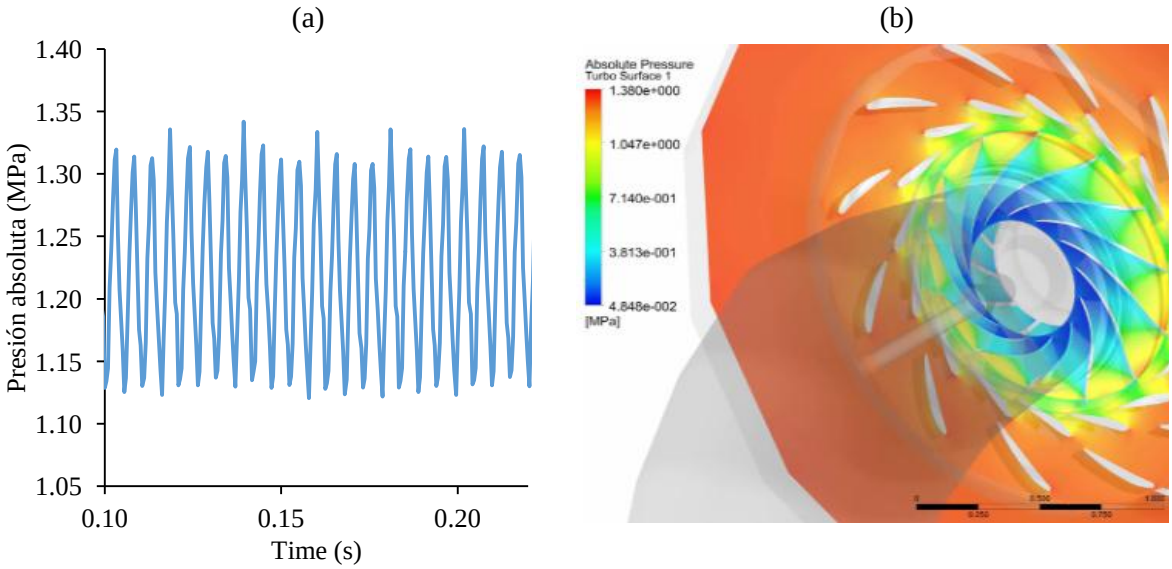

Figure 20. Runner dynamic check (a) pressure fluctuation (b) pressure distribution in the turbine.

As well as in the guide vanes, the fatigue safety factor was obtained by means of the pressure fluctation in the rotor-stator interface. In this case, the fatigue safety factor is 2.28 for $1x10^{10}$ cycles corresponding to 31 years of operation as shown in Figure 21b. The modal check leads to a 78% difference between natural fequency and exitation frequency, confirming that the runner works in a safe frequency zone [30] (see Figure 21c).

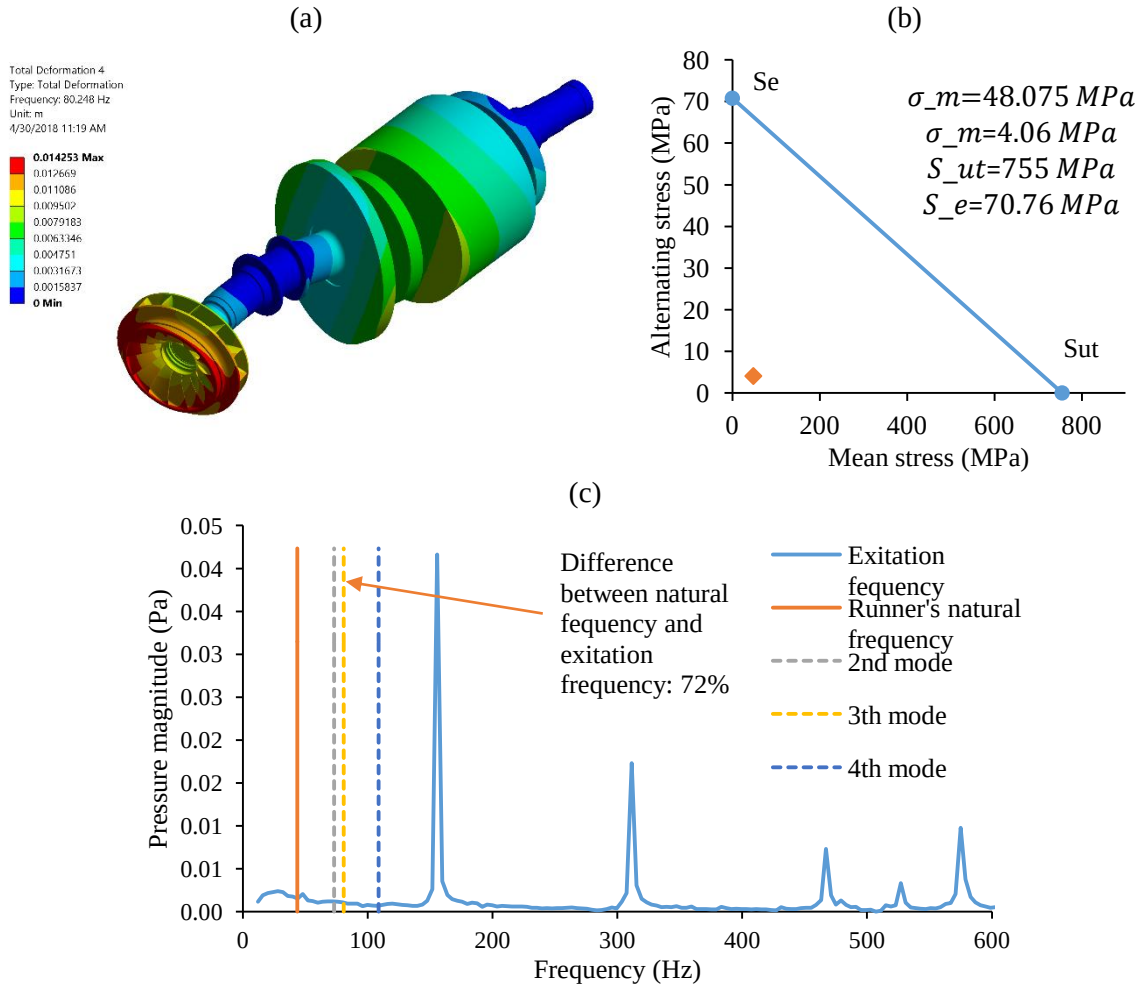

Figure 21. Runner's dynamic and modal analysis (a) 4th natural frequency (b) dynamic check and (c) frequency comparison.

4.4. Turbine overall improvement

After the optimization process ended, where the optimum geometry reached the desired characteristics, it could be observed that, for the hydrodynamic variables such as the power and efficiency, no important differences were observed between the original and optimized shapes, i.e., a maximum reduction in the efficiency of the turbine was 0.9 points at 10 MW (Figure 22). However, in the case of wear rate, a considerable reduction between the original shape and the optimized shape was found, decreasing this up to 73% at 3 MW as shown in Figure 23.

Making a projection with this finding and appliying it to the operational data record in the Amaime plant from May 2013 to October 2014 [1, 2] it was estimated that the loss of

material of the turbine was 49.38 Kg for the original shapes and for the optimized shape would be 13.42 Kg.

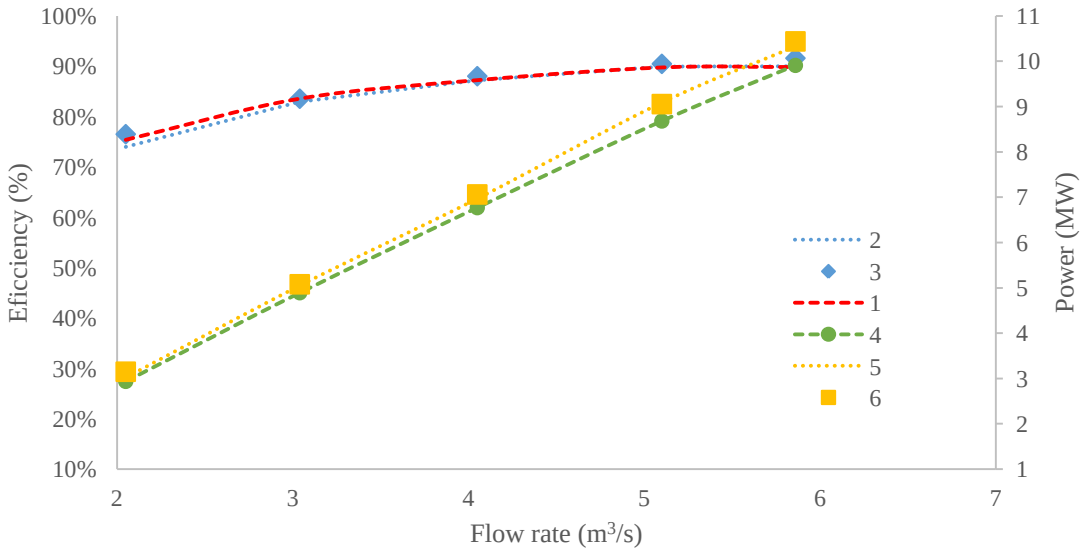

Figure 22. Comparison between turbine hydrodynamic variables 1) Simulated efficiency of the optimized turbine shape 2) Simulated efficiency of the original turbine shape 3) Experimental efficiency of the original turbine shape 4) Simulated power of the optimized turbine shape 5) Simulated power of the original turbine shape and 6) Experimental power of the original turbine shape

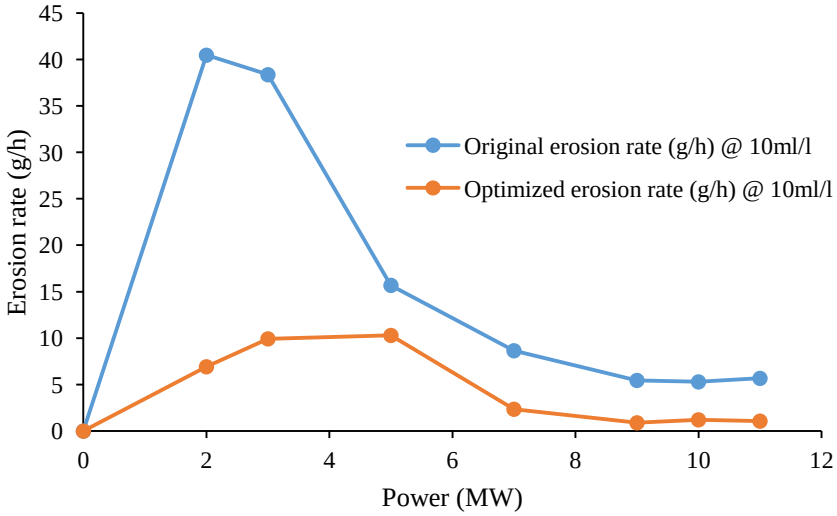

Figure 23. Turbine wear rate of the turbine as a function of the generated power.

5. Conclusions

The use of design of experiments, artificial neural networks, genetic algorithms and CFD, allowed a multi-objective and multipoint optimization process to obtain a better geometry of the main components of a Francis turbine. The methodology developed and implemented in this work, resulted in a decrease in erosion rate in the turbine by 35% with no significant change in the hydraulic performance as the overall turbine efficiency decrease only 0.9

points and the mechanical verification showed permissible safety factors that validates the reliability of the turbine optimized components.

6. Acknowledgments

The authors acknowledge COLCIENCIAS, EPSA-CELSIA and Universidad del Valle for the provided support through project number 110656237170 and CI - 2896.

7. References

[1] L. Teran *et al.*, "Failure analysis of a run-of-the-river hydroelectric power plant," *Engineering Failure Analysis*, vol. 68, pp. 87-100, 2016.

[2] L. Teran *et al.*, "Analysis of economic impact from erosive wear by hard particles in a run-of-the-river hydroelectric plant," *Energy*, vol. 113, pp. 1188-1201, 2016.

[3] S. Sangal, M. K. Singhal, and R. P. Saini, "Hydro-abrasive erosion in hydro turbines: a review," *International Journal of Green Energy*, vol. 15, pp. 232-253, 2018.

[4] G. De Cesare, J. M. Ribeiro, S. A. Kantoush, and M. Federspiel, "River intake and desander efficiency testing on a physical model using UVP and LSPIV," in *Proceedings of the 7th International Symposium on Ultrasonic Doppler Methods for Fluid Mechanics and Fluid Engineering*, 2010, no. EPFL-CONF-148516, pp. 47-50.

[5] K. Kostrewa, Z. Alsalihi, and R. Van den Braembussche, "Optimization of radial turbines by means of design of experiment," VKI-PR-2003-172003.

[6] S. Lain, M. Garcia, F. Avellan, B. Quintero, and S. Orrego, F. E. U. EAFIT, Ed. *Simulación numérica de turbinas Francis*. 2011.

[7] H. P. Neopane, "Sediment erosion in hydro turbines,," Faculty of Engineering Science and Technology, NTNU, 2010.

[8] B. S. Thapa, B. Thapa, M. Eltvik, K. Gjosater, and O. G. Dahlhaug, "Optimizing runner blade profile of Francis turbine to minimize sediment erosion," in *IOP Conference Series: Earth and Environmental Science*, 2012, vol. 15, no. 3, p. 032052: IOP Publishing.

[9] S. Derakhshan and A. Mostafavi, "Optimization of GAMM Francis turbine runner," *World Acad. Sci. Eng. Technol*, vol. 59, pp. 717-723, 2011.

[10] L. Teran, F. Larrahondo, and S. Rodríguez, "Performance improvement of a 500-kW Francis turbine based on CFD," *Renewable Energy*, vol. 96, pp. 977-992, 2016.

[11] M. Eltvik, "Sediment Erosion in Francis Turbines," ed: NTNU, 2013, p. 147.

[12] R. A. Van den Braembussche, "Numerical optimization for advanced turbomachinery design," in *Optimization and computational fluid dynamics*: Springer, 2008, pp. 147-189.

[13] Y. Enomoto, S. Kurosawa, and H. Kawajiri, "Design optimization of a high specific speed Francis turbine runner," in *IOP Conference Series: Earth and Environmental Science* vol. 15, ed: IOP Publishing, 2012, p. 32010.

[14] S. Galván, C. Rubio, J. Pacheco, C. Mendoza, and M. Toledo, "Optimization methodology assessment for the inlet velocity profile of a hydraulic turbine draft tube: part I—computer optimization techniques," *Journal of Global optimization*, vol. 55, no. 1, pp. 53-72, 2013.

[15] E. Flores, L. Bornard, L. Tomas, J. Liu, and M. Couston, "Design of large Francis turbine using optimal methods," in *IOP Conference Series: Earth and Environmental Science* vol. 15, ed: IOP Publishing, 2012, p. 22023.
[16] L. A. Espitia and A. Toro, "Cavitation resistance, microstructure and surface topography of materials used for hydraulic components," *Tribology International,* vol. 43, pp. 2037-2045, 2010.
[17] J. Santa, L. Espitia, J. Blanco, S. Romo, and A. Toro, "Slurry and cavitation erosion resistance of thermal spray coatings," *Wear,* vol. 267, no. 1-4, pp. 160-167, 2009.
[18] B. S. Mann and V. Arya, "Abrasive and erosive wear characteristics of plasma nitriding and HVOF coatings: their application in hydro turbines," *Wear,* vol. 249, pp. 354-360, 2001.
[19] A. N. Allenstein, C. M. Lepienski, A. J. A. Buschinelli, and S. F. Brunatto, "Improvement of the cavitation erosion resistance for low-temperature plasma nitrided Ca-6NM martensitic stainless steel," *Wear,* vol. 309, pp. 159-165, 2014.
[20] T. Manisekaran, M. Kamaraj, S. M. Sharrif, and S. V. Joshi, "Slurry Erosion Studies on Surface Modified 13Cr-4Ni Steels: Effect of Angle of Impingement and Particle Size," *Journal of Materials Engineering and Performance,* vol. 16, pp. 567-572, 2007.
[21] H. S. Grewal, H. S. Arora, H. Singh, and A. Agrawal, "Surface modification of hydroturbine steel using friction stir processing," *Applied Surface Science,* vol. 268, pp. 547-555, 2013.
[22] B. Kishor, G. P. Chaudhari, and S. K. Nath, "Cavitation erosion of thermomechanically processed 13/4 martensitic stainless steel," *Wear,* vol. 319, pp. 150-159, 2014.
[23] B. S. Mann, "High-energy particle impact wear resistance of hard coatings and their application in hydroturbines," *Wear,* vol. 237, pp. 140-146, 2000.
[24] R. C. Shivamurthy, M. Kamaraj, R. Nagarajan, S. M. Shariff, and G. Padmanabham, "Influence of microstructure on slurry erosive wear characteristics of laser surface alloyed 13Cr–4Ni steel," *Wear,* vol. 267, pp. 204-212, 2009.
[25] S. Romo, J. Santa, J. Giraldo, and A. Toro, "Cavitation and high-velocity slurry erosion resistance of welded Stellite 6 alloy," *Tribology International,* vol. 47, pp. 16-24, 2012.
[26] R. Shivamurthy, M. Kamaraj, R. Nagarajan, S. Shariff, and G. Padmanabham, "Slurry erosion characteristics and erosive wear mechanisms of Co-based and Ni-based coatings formed by laser surface alloying," *Metallurgical and Materials Transactions A,* vol. 41, no. 2, p. 470, 2010.
[27] R. D. Aponte, L. A. Teran, J. A. Ladino, F. Larrahondo, J. J. Coronado, and S. A. Rodríguez, "Computational study of the particle size effect on a jet erosion wear device," *Wear,* vol. 374-375, 2017.
[28] B. S. Thapa, O. G. Dahlhaug, and B. Thapa, "Flow measurements around guide vanes of Francis turbine: A PIV approach," *Renewable Energy,* vol. 126, pp. 177-188, 2018.
[29] A. D. A. Neto and F. Saltara, "Study of stay vanes vortex-induced vibrations with different trailing-edge profiles using CFD," *International Journal of Fluid Machinery and Systems,* vol. 2, no. 4, pp. 363-374, 2009.

[30] T. C. Vu, B. Nennemann, P. Ausoni, M. Farhat, and F. Avellan, "Unsteady CFD prediction of von Kármán vortex shedding in hydraulic turbine stay vanes," *Proceedings of Hydro2007, Granada,* 2007.
[31] M. Eltvik, B. S. Thapa, O. Dahlhaug, and K. Gjosaeter, "Numerical analysis of effect of design parameters and sediment erosion on a Francis runner," in *Fourth International Conference on Water Resources and Renewable Energy Development in Asia, Thailand*, 2012.
[32] B. L. da Silva, F. de Oliveira, J. L. de Almeida Ferreira, and J. A. Araújo, "Characterization of ASTM A743 CA6NM alloy steel used in hydrogenator components," in *21th International Congress of Mechanical Engineering*, 2011.
[33] E. Haibach, *Analytical Strength Assessment of Components in Mechanical Engineering: FKM-Guideline*. VDMA, 2003.

APPENDIX

5.1. Appendix 1: DOE-ANN-GA optimization code

```
clear
close all
clc
tic
Ip=xlsread('Population.xlsx');
InPop=Ip(:,1:9);
S=size(Ip);
PopSize=S(1);
global net
A=Ip(:,1);
B=Ip(:,2);
C=Ip(:,3);
D=Ip(:,4);
E=Ip(:,5);
F=Ip(:,6);
G=Ip(:,7);
H=Ip(:,8);
I=Ip(:,9);
FunO=Ip(:,10);
inputs=[A,B,C,D,E,F,G,H,I]';
targets=FunO';
net = feedforwardnet(20);
net = configure(net,inputs,targets);
net = init(net);
net.trainParam.epochs=5000;
net.trainParam.min_grad=1e-20;
net.trainParam.mu_max=1e20;
net.trainFcn = 'trainlm';
reg=0;
while 1
    R=reg;
    if R>0.7
    break
    end
    [net,tr] = train(net,inputs,targets);
    outputs = net(inputs);
    reg=regression(targets,outputs);
end
options = gaoptimset('PopulationSize',PopSize,...
    'Vectorized','on',...
    'Generations',5000,...
    'InitialPopulation',InPop,...
    'PlotInterval',1,...
    'PlotFcns', @gaplotbestf,...
    'TolFun',1e-100);
ub=[14.254375   4.704125    67.8755 4.77825 -1.729375   -1.270125...
   19.9845  -0.149125   -0.03275];
lb=[9.165625    2.735875    29.2045 2.78175 -2.930625   -1.969875...
   9.7555   -1.650875   -0.98725];
A=eye(9,9);
b=ub;
[x, fval] = ga(@ObjectiveFunction,9,A,ub,[],[],lb,ub,[],[],options);
toc
R
x
fval
```